RICE UNIVERSITY

Modulating Gold Nanoparticle in vivo Delivery for Photothermal Therapy Applications Using a T Cell Delivery System

by

Laura Carpin Kennedy

A THESIS SUBMITTED
IN PARTIAL FULFILLMENT OF THE
REQUIREMENTS FOR THE DEGREE

Doctor of Philosophy

APPROVED, THESIS COMMITTEE:

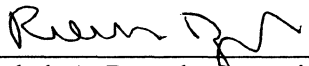

Rebekah A. Drezek, Committee
Chair, Professor of Bioengineering

Jennifer L. West, Isabel C. Cameron
Professor of Bioengineering

Jason H. Hafner, Associate Professor
Physics & Astronomy

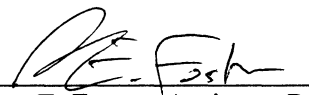

Aaron E. Foster, Assistant Professor
Pediatrics-Hematology/Oncology
Center for Cell and Gene Therapy
Baylor College of Medicine

HOUSTON, TEXAS
AUGUST 2011

ABSTRACT

Modulating Gold Nanoparticle in vivo Delivery for
Photothermal Therapy Applications Using a T Cell Delivery System

by

Laura Carpin Kennedy

This thesis reports new gold nanoparticle-based methods to treat chemotherapy-resistant and metastatic tumors that frequently evade conventional cancer therapies. Gold nanoparticles represent an innovative generation of diagnostic and treatment agents due to the ease with which they can be tuned to scatter or absorb a chosen wavelength of light. One area of intensive investigation in recent years is gold nanoparticle photothermal therapy (PTT), in which gold nanoparticles are used to heat and destroy cancer. This work demonstrates the utility of gold nanoparticle PTT against two categories of cancer that are currently a clinical challenge: trastuzumab-resistant breast cancer and metastatic cancer. In addition, this thesis presents a new method of gold nanoparticle delivery using T cells that increases gold nanoparticle tumor accumulation efficiency, a current challenge in the field of PTT. I ablated trastuzumab-resistant breast cancer in vitro for the first time using anti-HER2 labeled silica-gold nanoshells, demonstrating the potential utility of PTT against chemotherapy-resistant cancers. I next established for the first time the use of T cells as gold nanoparticle vehicles in vivo. When incubated with gold nanoparticles in culture, T cells can internalize up to 15000 nanoparticles per cell with no detrimental effects to T cell viability or function (e.g.

migration and cytokine secretion). These AuNP-T cells can be systemically administered to tumor-bearing mice and deliver gold nanoparticles four times more efficiently than by injecting free nanoparticles. In addition, the biodistribution of AuNP-T cells correlates with the normal biodistribution of T cell carrier, suggesting the gold nanoparticle biodistribution can be modulated through the choice of nanoparticle vehicle. Finally, I apply gold nanoparticle PTT as an adjuvant treatment for T cell adoptive transfer immunotherapy (Hyperthermia-Enhanced Immunotherapy or HIT) of distant tumors in a melanoma mouse model. The results presented in this thesis expand the potential of gold nanoparticle PTT from only chemotherapy-sensitive or localized cancers to chemotherapy-resistant non-localized cancers that currently defy conventional therapies.

ACKNOWLEDGMENTS

I would first like to thank my advisor, Dr. Rebekah Drezek, for her research and professional insights and for her willingness to nurture new and off-the-wall ideas. I would also like to thank my thesis committee, Dr. Jennifer West, Dr. Jason Hafner, and Dr. Aaron Foster, for their assistance in working through the thesis process.

I especially thank my fellow laborers in the lab: Adham Bear, the patient collaborator and T cell wrangler, Joseph Young, the nanoparticle synthesis extraordinaire, and Jean Kim, the faithful undergraduate. These projects would have never been finished without you. I would also like to thank the other members of the Drezek lab who contributed their time, insights, and ideas over the course of my time in the lab, and Germaine Agollah, who synthesized the gold-silica nanoshells for the trastuzumab-resistance project.

I would like to thank my husband, Chris, and my parents for their loving support throughout this long process --- these projects would have never been finished without you either! This thesis is dedicated to my Dad, the first scientist I ever knew, and Dr. Alfred Sciuto, my first true research mentor.

Therefore, since we are surrounded by such a great cloud of witnesses, let us throw off everything that hinders and the sin that so easily entangles. And let us run with perseverance the race marked out for us, fixing our eyes on Jesus, the pioneer and perfecter of faith. For the joy set before him he endured the cross, scorning its shame, and sat down at the right hand of the throne of God. Consider him who endured such opposition from sinners, so that you will not grow weary and lose heart. (Hebrews 12:1-3)

TABLE OF CONTENTS

CHAPTER 1

INTRODUCTION

This thesis combines the use of immunotherapy and gold nanoparticle photothermal therapy (PTT) for the treatment of cancer. First, we ablate trastuzumab-resistant breast cancer cells with gold nanoparticle PTT, showing for the first time that gold nanoparticle PTT is applicable to chemotherapy-resistant cancers. We next demonstrate for the first time increased gold nanoparticle delivery efficiency to a tumor by using T cells as gold nanoparticle delivery vehicles instead of depending on the enhanced permeability and retention (EPR) effect. Finally, we mitigate distant tumor progression in mice with bilateral tumors by using gold nanoparticle PTT as an adjuvant for T cell adoptive transfer immunotherapy. By combining gold nanoparticle PTT with immunotherapy, we extend the treatment limits of gold nanoparticle PTT from localized, conventional treatment responsive cancers to widespread, conventional-treatment resistant cancers.

Motivation for Combining Immunotherapy with Gold Nanoparticle PTT

In 2010, the NIH estimates that more than 1.5 million new cases of cancer are expected to be diagnosed in the United States, with an overall cost of $263.8 billion.[1] Cancer is the second highest cause of death in the United States behind heart disease.[2] Improvements in early diagnosis and cancer treatment have increased the 5 year survival rate of a patient diagnosed with cancer in the United States from 50% in 1975 to 68% in

1999.[1] Although this is an improvement, it is a small increase compared to the billons of dollars that have been spent on research and the millions of lives that continue to be affected.

One reason that overall survival remains below 80% is the lack of effective treatments against advanced cancers. There are several cancers that have very subtle or symptomless beginnings that allow the cancer to progress unnoticed until it is fairly widespread. Ovarian and pancreatic cancer are good examples of two cancers that lack prominent symptoms until advanced disease. The 5-year survival rates for these two cancers between 1975 and 2005 have remained below 50% for ovarian cancer and at less than 10% for pancreatic cancer (**Table 1-1**).[1] In the case of pancreatic cancer, even with early detection, the 5 year survival rate is only 22%.[1] These statistics highlight the need for effective treatments of metastatic disease.

Conventional treatments for cancer include surgery, chemotherapy, and radiation

Table 1-1. Relative Survival Rates for Common Cancers in the United States Based on Stage of Diagnosis (adapted from SEER Stat Fact Sheets [3]

Cancer	5-Year Relative Survival for Regional Spread (Positive Lymph Nodes)	5-Year Relative Survival Distant Spread (Metastatic)
Breast	83.8%	23.4%
Prostate	100%	28.8%
Colon and Rectal	69.2%	11.7%
Lung and Bronchus	24.2%	3.6%
Melanoma	61.4%	15.3%
Ovarian	71.7%	27.2%
Pancreatic	8.6%	1.8%

that are used alone or in combination depending on the type and stage of cancer. Surgery is generally performed to completely remove a localized cancer or to debulk a large tumor to improve patient quality of life and to improve the efficacy of chemotherapy. This is generally effective, particularly in localized cancers such as breast or prostate. However, this is a macroscopic method of treatment for a microscopic disease. Removal of all the diseased tissue is important, and cancers like pancreatic highlight the dangers of leaving microscopic disease behind in the patient. This is also an invasive method of treatment and has potential risks, such as infection and blood loss. Patients that have lymph nodes that are positive for cancer or tumors that are too large or complicated to remove surgically typically receive chemotherapy.

Chemotherapy is a cancer treatment regimen that uses a drug or combination of drugs to target rapidly proliferating cells in the patient. This is a systemic treatment, and it is generally administered intravenously or intrathecally depending on the tumor location. While the general adminstration makes chemotherapy ideal for treating advanced or metastatic cancers, it does result in systemic side effects. Malignant or tumor cells are not the only cells in the body that proliferate quickly; in fact, many healthy tissues such as skin and the intestines replace cells on a daily basis. Symptoms such as nausea, mucositis, alopecia, and myelosuppression can all be caused by the untargeted nature of chemotherapy.[4] These side effects are often distressing and uncomfortable for the patient, and in some cases they can be life-threatening. The side effects of treatment must be carefully weighed by the clinician against potential risks of having cancer. In addition, it is not uncommon for the cancer undergoing treatment to develop resistance to the chosen therapy.

Radiation therapy is another untargeted conventional therapy that is used for the debulking of tumor and treatment of metastases. Radiation targets rapidly prolierating cells using high energy x-rays, gamma rays, or other charged particles to cause breaks in the tumor cell DNA or to generate free radicals that will kill the tumor cells.[5] Like chemotherapy, radiation therapy has side effects due to its non-specific nature.

Rationale for Hyperthermia-Enhanced Immunotherapy (HIT)

Gold nanoparticle photothermal therapy has advantages over conventional treatments because of its ability to target cancerous cells and minimize its effects on healthy tissue. However, this technology has been limited to localized cancers because of limitations in the penetration of near-infrared (NIR) light, discussed in more detail in Chapter 2, and concerns about shielding organs that receive very high doses of gold after nanoparticle intravenous injection. The combination of immunotherapy with gold nanoparticle PTT could mitigate these concerns.

Immunotherapy covers several different categories of pharmaceuticals and cell vaccines. For the purposes of this thesis, we will focus on two particular therapies: trastuzumab (Herceptin®) or anti-HER2, a humanised antibody that targets the ErbB2 tyrosine kinase commonly overexpressed in breast cancer, and adoptive T cell transfer therapy. Immunotherapy could benefit gold nanoparticle PTT in several ways. For one, immunotherapy agents such as trastuzumab could potentially increase the specificity of gold nanoparticles for the tumor cells, potentially increasing gold nanoparticle delivery and retention by the tumor *in vivo*. Although this semi-passive technique has been tried by several groups with modest success,[6, 7] a more active targeting technique could be

using T cells as gold nanoparticle delivery vehicles. T cells often accumulate within the tumor site naturally, and are able to migrate actively through tissue. This could certainly improve gold nanoparticle delivery into the tumor over more passive accumulation via the enhanced permeability and retention (EPR) effect, which is dependent on the sieve-like angiogenic tumor vasculature to allow gold nanoparticles to diffuse into the tumor.

Immunotherapies have also demonstrated clinical success against metastatic cancer, particularly melanoma.[8-10] One disadvantage to the current methods with adoptive T cell transfer is the use of systemic interleukin-2 (IL-2) and/or lymphodepletion chemotherapy regimens to bolster T cell response. Both of these treatments have significant and potentially serious side effects that limit the administration of adoptive T cell transfer. However, there have been studies showing that hyperthermia may augment dendritic cell activation, which ultimately leads to improved T cell activation. This is discussed in detail in the introduction of Chapter 7. Gold nanoparticle PTT may be able to serve as an adjuvant treatment for adoptive T cell transfer, decreasing the need for the addition of systemic IL-2 and lympodepletion regimens during therapy. The ability of gold nanoparticle PTT to debulk the tumor via ablation may also be valuable when combined with adoptive T cell transfer because the T cells will be more effective against smaller lesions. The combination of PTT and T cell adoptive transfer, or hyperthermia-enhanced immunotherapy (HIT), may create a more effective treatment for metastatic cancers.

This thesis will illustrate the benefits of combining immunotherapy with gold nanoparticle PTT. Chapter 2 will discuss gold nanoparticle photothermal therapy, the types of gold nanoparticles that have been developed for therapy, the different irradiation

modalities and their strengths and limitations, and the strategies that have been devised and studied to date for improving gold nanoparticle tumor delivery and biodistribution. Next, we will introduce in Chapter 3 some basic concepts of T cell immunology, the tumor microenvironment and its defense mechanisms against the immune system, and the clinical accomplishments of adoptive T cell transfer to date. In Chapter 4, we will ablate trastuzumab- and lapatinib-resistant HER2+ breast cancer cells using anti-HER2 targeted gold-silica nanoshells. We will then transition to Chapter 5, which will use T cells to deliver gold nanoparticles to tumors more efficiently than the EPR effect-driven delivery of freely injected gold nanoparticles. Chapter 6 will extend on Chapter 5's work by transitioning this technology to antigen-specific murine T cells bearing NIR-resonant hollow gold nanoshells to melanoma tumors. Finally, we will slow the progression of distant non-ablated secondary tumors using a combination of gold nanoparticle PTT and adoptively transferred pmel T cells.

CHAPTER 2[a]

GOLD NANOPARTICLE PHOTOTHERMAL THERAPY FOR THE TREATMENT OF MALIGNANCY

Introduction

In 2010, the National Institutes of Health estimates that more than 1.5 million new cases of cancer will be diagnosed in the United States, with an overall projected cost of $263.8 billion.[1] Development of new approaches to improve screening, diagnosis, and treatment of cancer is an area of intensive research spending and has generated numerous innovations that have enhanced the 5-year survival rates of cancer patients.[1] However, these new and innovative treatments can also contribute to the rising costs of healthcare.[11] To justify these increasing expenses, new cancer treatments should have enhanced efficacy, decreased invasiveness, and fewer side effects than current cancer therapies. Gold nanoparticle photothermal therapies meet these criteria: a single intravenous injection of gold nanoparticles followed by laser irradiation of the tumor is able to induce full tumor regression with a minimum of side effects in mice. The ability of this therapy to provide localized and tumor-specific treatment is because of the special properties of the gold nanoparticles used to convert light to heat.

The wide-ranging utility of gold nanoparticles for biomedical applications is based on the unique and highly tunable optical resonance of gold nanomaterials. When

---

[a] Adapted from: Kennedy LC, Bickford LR, Lewinski NA, Coughlin AJ, Hu Y, Day ES, West JL, Drezek RA, "A New Era in Cancer Treatment: Gold Nanoparticle-Mediated Thermal Therapies"; *Small (Weinheim an der Bergstrasse, Germany)*, 7(2):169-183 (2011).

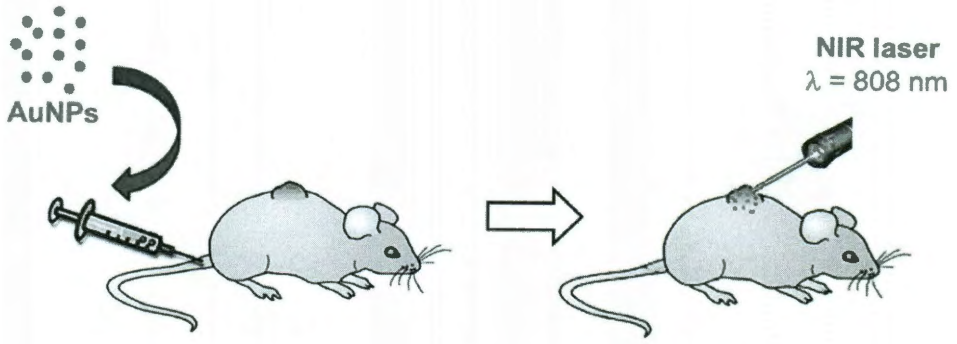

Figure 2-1. Scheme for gold nanoparticle photothermal therapy. The tumor-bearing mouse is intravenously injected with gold nanoparticles tuned to the near-infrared region of light. The gold nanoparticles passively accumulate within the tumor over the course of 6-48 hours. The tumor is then treated with a near-infrared laser. The gold nanoparticles absorb the light energy and convert it to heat, resulting in tumor ablation.

metallic nanoparticles are exposed to light at their resonant wavelength, the conduction band electrons of the nanoparticle generate a synchronized oscillation that ultimately terminates in either light scattering or light absorption. By carefully designing the size, shape, and composition of gold nanoparticles, the proportion of light scattering relative to light absorption can be optimized for the intended application. Gold nanoparticles are currently being studied for use as imaging contrast agents,[12, 13] absorptive heating agents,[14] and as dual imaging and therapeutic agents.[15, 16]

Of these potential applications, gold nanoparticle-mediated hyperthermia has been extensively developed and is currently being studied in early clinical trials.[17] To treat a tumor, gold nanoparticles are systemically administered to the subject and allowed to passively localize to the tumor via the sieve-like tumor vasculature.[18] The tumor is then exposed to an exciting energy source, such as near-infrared (NIR) laser light,[14] radiowaves,[19] or an alternating magnetic field.[20] The gold nanoparticles absorb the incident energy and convert it to heat, which raises the temperature of the tissue and disrupts the cell membrane of the cancerous cells.[21] The most common form of these hyperthermia therapies is gold nanoparticle photothermal therapy (PTT), which uses a

NIR laser as the energy source. **Figure 2-1** depicts the basic process of gold nanoparticle PTT. At the molecular level, hyperthermic effects can be seen as changes in cytoskeletal structure, cell membrane rupture, protein denaturation, impairment of DNA and RNA synthesis, and programmed apoptosis.[22, 23] The long term success of the tumor ablation is dependent on all of the tumor cells being destroyed during treatment.

The first step in performing gold nanoparticle PTT is selecting the gold nanoparticle variant. A diverse range of gold nanoparticles have been explored for use in ablation-based therapies. In the following section, we will discuss the development of the gold nanoparticle variants used for therapy, including gold-silica nanoshells, gold nanorods, and gold colloidal nanospheres. We will also discuss gold nanoparticle options that have a smaller diameter while still being tunable to the near-infrared (NIR); these options include gold nanocages, gold-gold sulfide nanoparticles, and hollow gold nanoshells.

Gold Nanoparticle Variants Used in Photothermal Therapy

Gold-Silica Nanoshells

In 2003, Hirsch *et al.* were the first to demonstrate photothermal therapy using gold-silica nanoshells.[14] Gold-silica nanoshells, composed of silica cores with a thin overlay of gold, were the first gold nanoparticles easily tunable to the NIR. Gold-silica nanoshell fabrication is based on seed-mediated growth, where 'seeds' of gold colloid are attached to the silica cores, and additional gold is added for completion of the shell. By varying the size of the silica core and the thickness of the gold shell, the resonance of

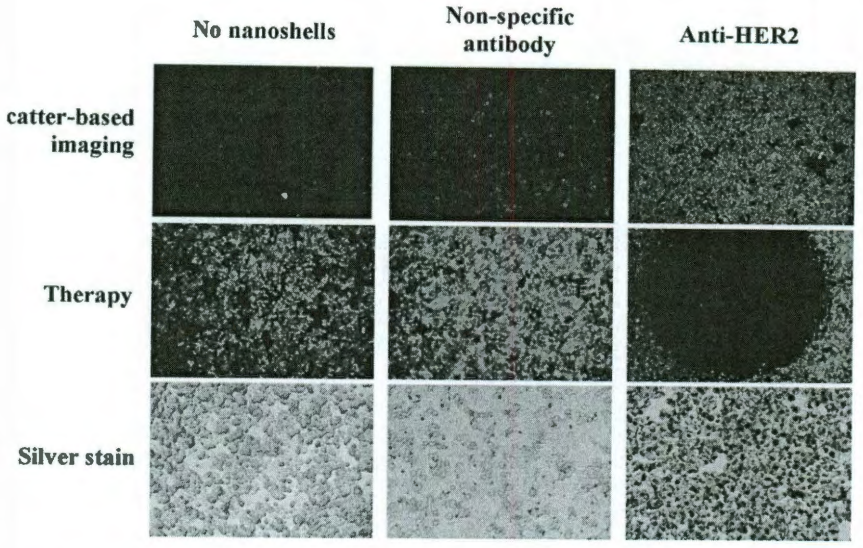

Figure 2-2. *In vitro* therapy of HER2+ breast cancer cells using anti-HER2-conjugated silica-gold (SiO_2) nanoshells. The top row is darkfield imaging of each group, the middle row is a calcein stain of the cells after irradiation with NIR light, and the bottom row is silver staining to show nanoshell binding. Surface modification with a tumor marker-specific antibody increases the specificity of the nanoshell binding *in vitro*.[24]

these nanoshells can span from the visible to the near infrared.

The flexibility of gold-silica nanoshell tuning permits nanoshell use as an imaging contrast agent for darkfield microscopy,[13, 19] two-photon microscopy,[25, 26] reflectance confocal microscopy,[27] and optical coherence tomography (OCT).[15] Additionally, by fabricating nanoshells that are strong absorbers, these particles can be used for photothermal therapy (**Figure 2-2**), and have been tested *in vitro* against human breast, [13, 28, 29] prostate,[30, 31] brain,[32] and liver[33] cancer cell lines. Further studies extended the use of nanoshell-mediated photothermal therapy to *in vivo* use against xenografted subcutaneous colon carcinoma in mice and allografted brain tumors in dogs.[34, 35] The combination of gold-silica nanoshells' ability to scatter and absorb light presents the possibility of both imaging and treating a tumor with the same particles. However, the large size of gold-silica nanoshells presents a challenge to *in vivo* delivery. An alternative gold nanoparticle, gold nanorods, were developed during the same period

as gold-silica nanoshells. They are generally smaller than nanoshells, which may give an advantage for delivery *in vivo*, and they present a slightly enhanced absorption profile per particle, an advantage for therapy.

Gold Nanorods

Like gold-silica nanoparticles, gold nanorods are also easily tuned to the NIR region by simple manipulation of their aspect ratio (length/width) and have been extensively studied for cancer therapy applications. Nanorods have the advantage of small size (on the order of 10 x 50 nm^2), high absorption coefficients, and narrow spectral bandwidths. Owing to their distinctive rod shape, gold nanorods have two absorption peaks corresponding to the longitudinal and transverse resonance. The transverse resonance occurs at around 520 nm, while longitudinal resonance can span from the visible to the NIR wavelengths. Like gold-silica nanoshells, nanorods can also be designed to function as imaging probes, and have been used to enhance imaging contrast in darkfield microscopy[36] and two-photon microscopy.[37] Nanorods have also demonstrated success as photothermal therapy agents *in vivo* against subcutaneous oral squamous cell carcinoma and colon cancer xenografts in mice.[38, 39]

A major concern about the use of gold nanorods for photothermal therapy is their susceptibility to reshaping into gold nanospheres under intense laser illumination, resulting in a loss of the longitudinal NIR resonance (**Figure 2-3**). Without the longitudinal NIR resonance, there would be insufficient heating to ensure an adequate tumor ablation. However, an *in vitro* study by Didychuk and colleagues evaluated the impact of nanorod reshaping on photothermal therapy by embedding polyethylene glycol

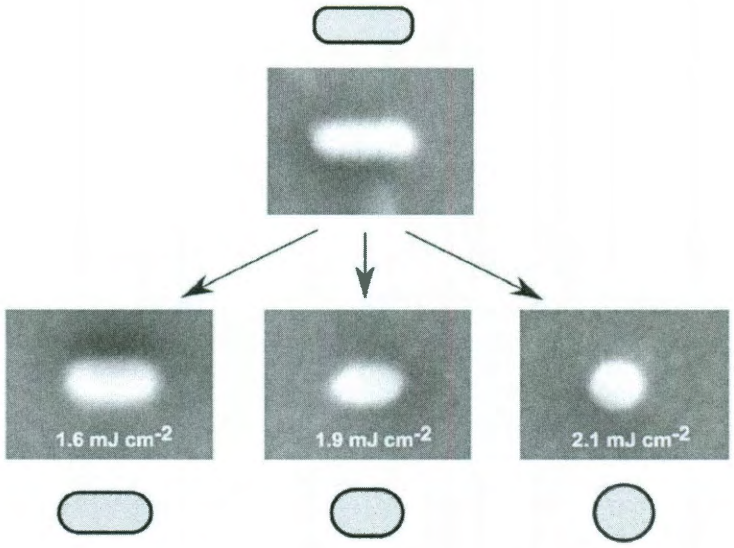

Figure 2-3. Nanorod reshaping under laser illumination. Top box depicts gold nanorods in its native conformation, and the bottom boxes depict nanorod shape after exposure to different laser powers. At the highest power, the nanorod becomes spherical. All SEM images are 200 x 150 nm.[40]

(PEG)-coated nanorods in a tissue phantom gel and irradiating with an 800 nm laser.[41] Their results indicated that at the laser fluence threshold for gold nanorod conversion, photothermal therapy would still be effective for tumors within 10 mm of the illuminated region. This correlates with the *in vivo* limitations of NIR laser penetration, and suggests that photothermal reshaping will not impair tumor ablation.

Additional studies by other groups also suggest that nanorod reshaping can be mitigated by the choice of nanorod surface coating. Chon *et al.* implemented a simple heat-diffusion model to estimate the heat relaxation time of gold nanorods encased in silica shells, and found that heat dissipation in the silica shell was much faster than the gold nanorod reshaping process, resulting in inhibition of nanorod reshaping.[40, 42] In contrast, Horiguchi *et al.* reported an opposite effect on cetyl trimethylammonium bromide (CTAB) bilayer-coated gold nanorods, as CTAB enhanced heat isolation and caused the nanorods to reshape.[43] Based on these results, photothermal therapy is not likely to be impaired by nanorod reshaping within the limitations of NIR laser

penetration, and any concerns about reshaping could be alleviated by coating the nanorods with silica or another coating that rapidly dissipates heat.

Recent studies have compared the photothermal heating efficiencies among NIR-absorbing gold nanoparticles such as gold-silica nanoshells, gold nanorods, and gold-gold sulfide nanoparticles. Both theoretical and experimental results have shown that nanorods offer a superior absorption cross-section versus gold-silica nanoshells when normalizing for particle size differences. In addition, gold nanorods heat at least 6 times faster than gold-silica nanoshells on a per gram of gold basis.[44-46] However, gold-silica nanoshells have a significantly larger photothermal transduction cross-section when compared to gold nanorods on a per particle basis.[44] Despite superior conversion of light to heat, the advantage of gold-silica nanoshells may be lost *in vivo* due to the low delivery yield of these nanoparticles to the tumor. Both gold-silica nanoshells and gold nanorods have poor *in vivo* delivery, with only a small percentage of the injected dose typically accumulating in the tumor. In the case of the gold-silica nanoshells, this is likely due to the large dimensions of the nanoparticle (>100 nm diameter). In the case of the nanorods, the poor delivery could partially be due to the shape of the nanoparticle. To address this problem, smaller particles that are tunable to the NIR region are being applied to photothermal therapy applications. In the next subsection, we discuss the development of gold-gold sulfide nanoshells, gold nanocages, and hollow gold nanoshells as an improved second generation of therapeutic nanoparticles.

Small NIR-Tunable Gold Nanoparticles

The smaller size of gold-gold sulfide (GGS) nanoparticles, gold nanocages, and hollow gold nanoshells (HAuNS) gives a perceived delivery advantage for *in vivo*

photothermal ablation over larger gold nanoparticles. The first example of these smaller gold nanoparticles is gold-gold sulfide nanoparticles that have a total diameter as small as 25 nm (**Figure 2-4**). In addition to their smaller size, which may give a delivery advantage, Gobin *et al.* calculated that gold-gold sulfide nanoparticles have a predicted absorption efficiency that is nearly 30% greater than that seen with gold-silica nanoshells,[47] potentially giving these nanoparticles a heating advantage. To synthesize gold-gold sulfide particles, a reduction of chloroauric acid using sodium sulfide or sodium thiosulfate is used. After this single step fabrication, extensive washing is required to remove contaminating gold colloid from the product. There is some controversy over the exact structure of these particles;[48-50] some groups describe the nanoparticle as a gold sulfide core coated with a thin gold outer shell, while other groups describe these nanoparticles as aggregates of gold. Despite this controversy, these gold nanoparticles have NIR absorbance that has been utilized for ablative therapy.

Gobin *et al.* applied gold-gold sulfide nanoparticles as a photothermal therapy mediating agent against prostate cancer *in vitro* and *in vivo*.[47] Using gold-gold sulfide particles with a core diameter ranging from 30-40 nm and a shell thickness of 3-6 nm,

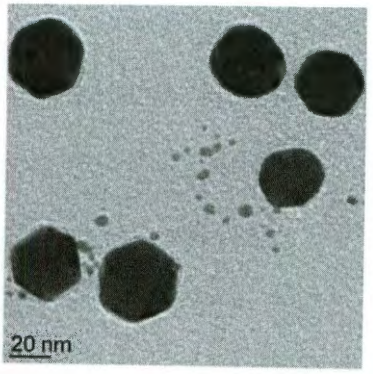

Figure 2-4. TEM image of gold-gold sulfide nanoparticles. Adapted from [47].

cancer cells and tumors were successfully ablated. Gobin and colleagues compared the survival of mice treated with gold-gold sulfide nanoparticles to the survival of mice treated with gold-silica nanoshells. When nanoparticles were allowed to accumulate in the tumors for 24 hours post injection prior to laser treatment, approximately 71% of the mice in the gold-gold sulfide group survived for the duration of the study (8 weeks post-injection), while ~82% of mice from the gold-silica nanoshell group survived for the duration of the study. However, if gold-gold sulfide nanoparticles were allowed to accumulate in tumors for 48 hours prior to laser treatment, the survival of the mice in the gold-gold sulfide treatment group increased to 82% for the duration of the study. This suggests that gold-gold sulfide nanoparticles have longer circulation times than gold-silica nanoshells, resulting in gold-gold sulfide nanoparticles having an optimal timepoint of 48 hours while gold-silica nanoshells have an optimal tumor accumulation time of 24 hours. Quantification of the gold content in the tumor using neutron activation analysis showed that the amount of gold that accumulated in the tumor at 24 hours was approximately the same between the gold-gold sulfide nanoparticle and gold-silica nanoshell group. However, the blood gold content for the gold-gold sulfide nanoparticle group was significantly higher than the gold-silica nanoshell group at 24 hours, indicating that the blood half life for gold-gold sulfide nanoparticles was greater than the blood half life of gold-silica nanoshells. This supports the gold-gold sulfide nanoparticles having maximal tumor accumulation at a timepoint later than 24 hours. However, despite the gold-gold sulfide nanoparticles having a longer half life in circulation, the survival of the mice treated at 48 hours by gold-gold sulfide nanoparticles was not greater than the survival of mice treated at 24 hours by gold-silica nanoshells.

Another type of gold nanoparticle explored for potential cancer therapy is the hollow gold nanoshell (HAuNS). As the name implies, these particles consist of a hollow center with a thin gold shell and can have a total diameter on the order of 30 nm. Hollow gold nanoshells are fabricated by first creating cobalt or silver template nanoparticles. After the addition of chloroauric acid, the template material is oxidized while a thin shell of gold is reduced onto the template surface, resulting in a hollow shell of gold.[51, 52] The hollow core of these nanoshells can be used as a reservoir for drugs or enzymes, giving this nanoparticle a potential role as a dual drug delivery and photothermal agent.[53] The utility of these nanoparticles for photothermal therapy was tested *in vitro* and *in vivo* by Li and colleagues. They conjugated HAuNS to anti-EGFR antibodies and ablated EGFR-overexpressing cells *in vitro*.[7] They subsequently used HAuNS conjugated to a peptide targeting melanocyte-stimulating hormone to target xenografted subcutaneous murine melanoma tumors *in vivo*.[6] In contrast to the gold-gold sulfide nanoparticles, where the smaller size resulted in a longer half life in the blood, Li and colleagues elected to perform laser treatment 4 hours post injection. Blood levels of gold were still high at the 4 hour timepoint, suggesting that a later timepoint would have permitted additional gold accumulation in the tumor.

The final group of small diameter NIR gold nanoparticles discussed here are gold nanocages. These particles are synthesized by first creating template silver nanoparticles and then replacing the silver with gold in a manner analogous to the HAuNS.[54] By adjusting the wall thickness of the nanocages, the absorption peak can be varied from 400 to 1200 nm, with an edge length range of 30 to 200 nm. Gold nanocages have been tested as contrast agents for optical coherence tomography [55] and as photothermal

therapeutic agents against breast cancer cells *in vitro*.[56-58] Gold nanocages have been successful in ablating tumors *in vivo* as well; Chen *et al.* performed a successful *in vivo* study using gold nanocages to ablate murine models with subcutaneous glioblastoma.[55] Tumors were treated 72 hours post injection with the NIR laser, and a 70% decrease in tumor metabolism in the nanocage treated group was observed using positron emission tomography (PET).

Gold-gold sulfide nanoparticles, hollow gold nanoshells, and gold nanocages each are NIR-tunable nanoparticles that have longer blood half lives *in vivo* due to their smaller size. Although no survival benefit was seen in a study comparing gold-gold sulfide nanoparticle-mediated photothermal therapy to gold-silica nanoshell-mediated photothermal therapy in mice, these nanoparticles may be advantageous for larger animal models, including humans, due to their longer blood half life and potential for higher gold nanoparticle accumulation in the tumor. We will next discuss gold colloidal nanospheres. These nanoparticles are not tunable to the NIR individually, but can be aggregated to red shift the plasmon to the desirable NIR window.

Gold Colloidal Nanospheres

The final group of gold nanoparticles discussed for hyperthermia applications are gold colloidal nanospheres. Previously, these solid gold spheres were solely investigated for their use as imaging probes.[12, 59, 60] However, the small size and relatively simple synthesis of these particles make them appealing for *in vivo* applications. El-Sayed and colleagues first reported on the use of gold colloidal nanospheres for the imaging and therapy of oral cancer cells *in vitro* using a continuous argon laser at 514 nm, which is closely coincident with the peak absorbance of the 40 nm particles.[61] Compared to

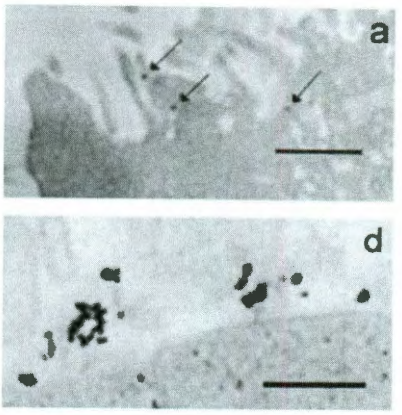

Figure 2-5. Transmission electron microscopy images of 40 nm gold colloidal nanospheres along breast cancer cell membrane. a) The cancer cell after a short incubation time with the nanoparticles (black arrows), while d) shows the breast cancer cells after a longer incubation with the nanoparticles. Nanoparticles can be seen grouping together on the cell surface. Scale bars = 500 nm. Adapted from [62].

normal, non-cancerous cells, it was demonstrated that cancerous cells targeted with nanoparticles were destroyed with 2-3 times less laser power. A key disadvantage to this study was the use of a visible wavelength laser. Although visible wavelengths can be used *in vitro*, *in vivo* applications of photothermal therapy prefer a NIR laser because of the decreased tissue attenuation of the light.

To shift the absorbance of gold colloidal nanospheres into the NIR, the nanoparticles can be aggregated or clustered together in close proximity (**Figure 2-5**). The close proximity of the nanoparticles to each other red-shifts the plasmon to the NIR region. El-Sayed *et al.* used a short-pulsed, NIR laser on small gold aggregates formed from 30 nm gold colloidal particles to selectively ablate oral cancer cells.[63] By operating in the NIR instead of the visible region, the laser power needed to kill the cancer cells was approximately 20 times less than that needed to destroy normal cells. Alternatively, a similar result has been achieved using gold nanoclusters and photothermal microbubbles (PTB). Here, non-aggregated gold colloid is incubated with cancer cells and subsequently internalized via endocytosis. The nanoparticles are at close

proximity to each other within the cell endosome, creating a resultant shift of the nanoparticle absorbance to the NIR.[62] Through the use of laser pulses in either the visible[64, 65] and NIR[62] regions, vapor bubbles ranging from 10^{-8} to 10^{-4} m[65] can be formed around the nanoclusters and irreversibly damage the cells. Moreover, these vapor bubbles are detectable throughout their lifespan with a photothermal microscope, presenting the ability to both image and treat the cancer simultaneously.[66] The potential of this unique photothermal bubble technique has been demonstrated for both leukemia[64, 65]and breast cancer cells.[62] It also illustrates that photothermal therapy can be achieved using nanoparticles that are not individually tunable to the NIR. This expands the number of possible gold nanoparticle solutions that can used for photothermal therapy. With the large number of possible solutions, one difficulty presented is how to select the best gold nanoparticle for a therapy application. The next section discusses important factors to consider when making this decision.

Gold Nanoparticle Selection Considerations

The first factors to consider are the innate properties of the selected gold nanoparticle variant. The efficiency with which a nanoparticle absorbs and scatters is an essential parameter to consider when choosing a particle for use in photothermal therapy, particularly if the particle needs to serve as both an imaging and treatment agent. From the perspective of photothermal therapy alone, the absorptive cross-section a key initial consideration. Calculating the absorption cross-section of gold-based nanoparticles can be achieved by using Mie-based theory or numerical methods such as discrete dipole approximation.[67-70] Particle design is optimized by maximizing the absorption

efficiency at a desired wavelength in a specific surrounding medium in order to achieve a maximum particle temperature and surface heat flux.[70, 71] Cole *et al.* compared the photothermal efficiencies of gold-silica nanoshells, gold-gold sulfide nanoshells, and gold nanorods.[44] They found that the photothermal transduction efficiencies, defined as the portion of the incident light being converted to photothermal power by the nanoparticle, varied less than a factor of three between the different particles studied.[44] This finding suggests that no particular nanoparticle has significant therapeutic advantage over the others in terms of heating efficiency.

With this in mind, considerations such as nanoparticle delivery become very important in selecting a gold nanoparticle variant. Maximal gold nanoparticle accumulation in the tumor with minimal accumulation of gold nanoparticles in non-target organs is highly desirable. When trying to optimize the tumor therapeutic response overall, however, another important consideration is the location of the tumor and the tissue penetration depth of the irradiating energy. Near-infrared laser light is limited to a depth of less than 1 centimeter in tissue, restricting photothermal therapy to superficial or easily accessible tumors. These two areas, NIR light penetration depth and nanoparticle delivery, are the current limiting factors for nanoparticle-mediated photothermal therapy. The remainder of the chapter will focus on discussing these issues and examining currently proposed solutions in the literature.

Focus #1: Penetration Depth of Near-Infrared Light

The penetration depth of NIR light in tissue is a key limiting factor in the expansion of gold nanoparticle hyperthermia. The selection of irradiation modality for

gold nanoparticle hyperthermia is a balance of three factors: sufficient depth penetration to reach the nanoparticle-laden cancerous tissue, extraneous heating of healthy tissue due to absorption of energy by tissue chromophores and off-target nanoparticles, and the properties of the chosen therapeutic nanoparticles. NIR light is generally favored in gold nanoparticle hyperthermia studies due to its low absorbance by tissue chromophores, which prevents it from damaging healthy tissue. To achieve a successful cancer ablation with any irradiation modality, the tissue must be heated to a minimum temperature for a minimum duration of time to induce tumor cell death. The necessary duration of heating is dictated by the temperature. Cytotoxic effects have been demonstrated in cells maintained at 42°C for 1 hour, but this duration can be shortened to 3-4 minutes by using a higher temperature of 70-80°C.[22, 23, 72, 73] In addition to temperature distribution concerns, the irradiating energy must reach the depth of the nanoparticles at an adequate intensity, or cancerous tissue may be heated insufficiently and survive. Here, we discuss three possible options for irradiation: NIR photothermal therapy (PTT), radiofrequency ablation (RFA), and magnetic fluid hyperthermia (MFH).

Near-Infrared (NIR) Photothermal Ablation

NIR laser light is a good choice for *in vivo* hyperthermia applications because of its low absorption by tissue chromophores, hemoglobin, and water. The absorption coefficient of these tissue chromophores is as much as 2 orders of magnitude greater in the visible range (400-600 nm) of light as compared to the NIR range (650-900 nm).[74, 75] Gold nanoparticle-mediated photothermal therapies are predominantly designed to operate in this window of wavelengths ("the NIR window") to minimize the attenuation of the energy resulting from undesired light-tissue interactions, and prevent undesirable

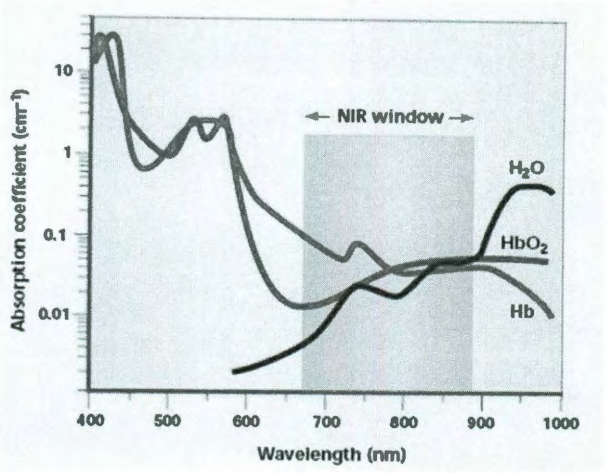

Figure 2-6. The NIR window. The wavelengths of light in the NIR window (pink box) are minimally absorbed by water, hemoglobin, and tissue pigments when compared to other wavelengths. Adapted from [74].

and damaging heating of healthy tissue (**Figure 2-6**). Upon tumor laser irradiation, NIR light is absorbed by the nanoparticles and heat dissipation is generated as a consequence of electron-phonon interactions. Hirsch *et al.* demonstrated a 4-6 mm depth of thermal damage in mice with subcutaneous tumors after intratumoral injection of gold-silica nanoshells and subsequent continuous wave NIR light exposure (λ = 820 nm, 4 W/cm^2, 6 min maximum time).[14]

The *in vivo* penetration depth of NIR light is dependent on a variety of factors, including the degree of light scattering and absorption within tissue.[14, 76] The heating of tissue is dependent on the NIR light intensity at a given point, on the absorptive cross-section of the gold nanoparticle, on the distribution and concentration of nanoparticles within the tissue, and on the degree of NIR light absorption by the tissue chromophores. Accurately modeling the heating profile of nanoparticle-laden tissue will be very important for optimizing thermal ablation in solid tumors, particularly because solid tumors are known to be highly inhomogeneous. The distribution of nanoparticles

within the tumor, placement and orientation of NIR light, and any variation in the optical and thermal properties of the tumor tissue will affect tumor heating. To understand and predict the effect of these variable, simulations of nanoparticle-laden tissues can be constructed using a variety of analytical and numerical approaches, such as light and heat diffusion theory, computational electromagnetic methods, and stochastic ray tracing.[76-79]

The simplest models assume homogeneous nanoparticle distribution and tissue properties. Elliott *et al.* modeled the laser fluence and temperature distribution of tissue phantoms embedded with gold-silica nanoshells of various optical densities. They demonstrated a maximum temperature change of 16°C for an 0.55 OD phantom and of 21°C for an 0.65 OD phantom using a 3-min 1.5W laser irradiation.[79] A disadvantage to this model was its inaccuracy in profiling regions of high nanoparticle concentration. Modeling of higher concentrations of nanoparticles is important due to the nature of gold nanoparticle distribution within the tumor. NIR narrow band imaging has revealed that gold nanoparticles tend to accumulate in highly concentrated pockets within the tumor, and that the gold nanoparticle distribution is very non-uniform.[80] The lack of uniformity and the high concentration of nanoparticles in certain regions impairs even tumor heating and provides challenges to modeling the temperature distribution of tissue during hyperthermia. In a later paper, they described an analytical model that was able to more accurately model higher concentrations of nanoshells. Using Green's function to solve the heat diffusion equation, they calculated the spatiotemporal thermal profile for phantoms with higher concentrations of nanoshells using the optical diffusion approximation.[77, 78]

The *in vitro* models described provide the theoretical basis for developing *in vivo* simulations. A recent study by von Maltzahn *et al.* demonstrated the potential of using computational simulations to model *in vivo* photothermal therapy and evaluate the effect of nanoparticle concentration on heating *in vivo*. An x-ray CT scan was used to characterize the distribution of intratumorally and intravenously administered PEGylated nanorods *in vivo*.[46] The high absorption efficiency of the gold nanorods in both the x-ray and NIR regions enabled real-time visualization and therapy, and demonstrates the utility of imaging and treating with the same nanoparticle.[46] This *in vivo* study was an initial step towards personalizing photothermal therapy to an individual tumor. By understanding how the nanoparticles are distributed, the temperature profile of the tumor can be simulated and evaluated to ensure adequate heating in all tumor regions. Although this model accounts for the inhomogeneity of nanoparticle distribution within the tumor, the models previously described do not account for variations in the tumor tissue optical properties.

Simulations based on nanoparticles distributed in actual tissue instead of synthetic tissue phantoms extend models to a more realistic medium. Vera *et al.* investigated the effects of gold-silica nanoshell concentration, laser power and laser arrangement on the thermal profile of gold nanoshell-laden human tissue from different organs *ex vivo*.[76] For this analysis, the optical and thermal properties of the tissue were extrapolated from previous studies at room temperature and assumed to remain constant during heating. Through this analysis, they found that when using a single, externally placed laser for therapy undesired overheating in one region could occur while leaving the rear region under-heated. They hypothesized that this uneven heating could be mitigated by the use

of an opposing dual-laser heating configuration. Practically, this would mean the minimally invasive placement of a fiber optic probe within the tumor to conduct NIR light, similar to what was done by Schwartz *et al.* in their study of nanoshell-mediated therapy for tumors in the brain.[35] To further optimize probe placement, simulations could be used to select the region of probe placement where maximal heating could be achieved by modeling and accounting for variations in the optical and thermal properties of tissue. A combination of all of the models discussed would allow simulations of *in vivo* photothermal therapy that selected the optimal laser and laser probe placement to account for variations in nanoparticle concentration and the inhomogeneity of tissue.

An additional modification that has been suggested for the enhancement of NIR therapy is the use of a pulse mode laser instead of a continuous wave laser. Pulsed lasers permit more efficient photothermal conversion because of lapses between the pulses, allowing additional time for electron-phonon relaxation. This translates to lower power usage with a pulsed laser than with a continuous mode laser. Tong et al demonstrated this using folate-conjugated gold nanorods. After nanorod binding to a folate-overexpressing cell line, exposure to a femtosecond-pulsed NIR laser at a power as low as 0.75 mW resulted in membrane blebbing, while a continuous wave laser required a power of 6 mW for the same effect.[21] Although this has potential for reducing laser power requirements and further minimizing damage to healthy tissue, this does not have an impact on the difficulties of deeper tissue penetration.

The limited penetration of NIR light in tissue confines gold-nanoparticle hyperthermia to solid tumors that are either directly accessible, such as skin cancer, or indirectly accessible via endoscopy or fiber optic placement. For cancers that cannot be

accessed via any of these methods, alternative irradiation methods may provide an avenue for gold nanoparticle hyperthermia treatment. We discuss two of these methods in the following subsection: radiofrequency ablation and magnetic fluid hyperthermia.

Alternatives to NIR Light

Radiofrequency ablation (RFA) was first established in the early 1900s as a method for cauterizing blood vessels during surgery. However, it was not explored for oncologic hyperthermia applications until the early 1990s. Conventional RFA treatments require an invasive procedure to place electrodes within the tumor, and tumor shrinkage is induced as a result of radiowave-induced vibrations of ions within tumor tissue, which give rise to friction and heat.[81] Radiowaves have significantly better penetration of tissue than NIR light, making RFA appealing for deeper solid tumors.[82] However, in exchange for the greater depth of penetration, there is greater attenuation of the energy by tissue. This attenuation can be mitigated by adding a mediating absorptive agent, such as gold nanoparticles, which increases the specificity of RFA treatments, protects normal tissue by lowering energy requirements, and decreases the need for invasive electrode placement.[19]

The addition of absorptive mediators such as gold nanoparticles[19, 83] or carbon nanotubes [84] to RFA enhances the creation of thermal lesions within liver tumors. In mice bearing subcutaneous tumors and treated with gold nanoparticle-mediated RFA, the temperature increase within the gold nanoparticle-treated tumors averaged 10°C compared to 4°C among control tumors injected with sterile water.[83] Gannon *et al.* also studied nanoparticle-assisted radiofrequency ablation of liver tumors using single-walled carbon nanotubes in New Zealand white rabbits with successful

results.[84] Although this method increases tissue penetration, it also increases the risk of damaging non-target tissues. Magnetic fluid hyperthermia (MFH) presents the possibility of increasing penetration while protecting non-target tissues.

MFH is another form of nanoparticle-assisted thermal therapy currently under investigation. This form of thermal therapy utilizes magnetically susceptible particles in suspension to emit heat in the presence of an alternating current (AC) magnetic field. The magnetic energy of the external alternating field is converted to internal energy within the nanoparticles and subsequently released as thermal energy through Brownian and Néel relaxations. Superparamagnetic particles are known to undergo this conversion at lower field strengths, and iron oxide nanoparticles are the most commonly used owing to their established biocompatibility and the availability of methods for chemical modification.[85] Since alternating magnetic fields do not tend to be susceptible to attenuation by tissue, the main advantage of MFH compared to other methods of heat delivery lies in its ability to treat deeply embedded tumors. In addition, nanoparticles used for MFH can also be used as contrast agents for magnetic resonance imaging, presenting a clear theranostic advantage.

Clinical trials using iron oxide nanoparticles for MFH of cancer are currently being performed by MagForce Nanotechnologies AG. Utilizing these particles with MFH has met with clinical success in a prostate cancer patient.[20] In this feasibility study, it was demonstrated that MFH could produce temperatures in the tumor sufficient to induce thermal insult following direct intratumoral delivery of iron oxide nanoparticles.[20] More recently, MFH has been applied to the treatment of glioblastoma.[86] The investigators delivered iron oxide nanoparticles directly to brain

tumors in 14 patients, who were then treated with a combination of radiation and MFH without any significant adverse responses to therapy.[86] These results are encouraging, and further development of MFH could yield an effective alternative to current treatment options for advanced cancers. One potential disadvantage for MFH could be the iron oxide nanoparticles typically used. One study incubating iron oxide nanoparticles with proliferating neurons found some cytotoxicity.[87] Because the toxicity of nanoparticles in general has not been thoroughly characterized, and these nanoparticles have not demonstrated acute toxicity *in vivo*, it is difficult to understand the ramifications of this finding. However, it does suggest that alternative magnetic nanoparticles of different materials should be pursued for biomedical applications pending a more complete understanding of nanoparticle toxicology.

Although MFH has not yet been applied using gold nanoparticles, a number of composite particles using gold and a magnetic material have been developed.[88-91] These composite particles present possibilities for either NIR photothermal ablation and optical imaging, or for MFH and MR imaging. Larson *et al.* synthesized γ-Fe_2O_3-Au core-shell nanoparticles and demonstrated their use as magnetic resonance imaging (MRI) contrast enhancing agents and as NIR absorbing agents for the targeted photothermal ablation of cancer *in vitro*.[88] Although the absorbance spectra for these particles did not show a pronounced peak within the NIR region, clustering of anti-EGFR-conjugated nanoparticles along cell surfaces allowed for sufficient heating to induce cancer cell death *in vitro* using a pulsed wave laser at 700 nm. Similarly, Kirui *et al.* demonstrated photothermal therapy and MR imaging potential with 25 nm dumbbell-shaped gold-iron oxide aggregates,[92] and Shah *et al.* used gold-iron oxide nanoparticles

for *ex vivo* photoacoustic imaging contrast to guide photothermal cancer therapy.[93] In the study by Shah and colleagues, they incorporated a simple model to relate the pressure change to the temperature rise caused by the energy absorption of the gold nanoparticles. With further development, composite gold-magnetic particles may represent a versatile, clinically relevant nanoparticle with sufficient flexibility to permit either photonic- or magnetically-controlled tumor ablation and imaging. This nanoparticle may represent the future of gold nanoparticle photothermal therapy due to the nanoparticle's flexibility for therapy and imaging.

The ability of gold nanoparticles to adapt to each of the three modalities discussed in this section (NIR PTT, RFA, and MFH) highlights their adaptability and potential for clinical cancer treatment. However, another key issue that impacts the efficacy of gold nanoparticle hyperthermia treatments *in vivo* is the delivery of sufficient gold nanoparticles to the tumor to attain a successful tumor ablation that eliminates all tumor cells. The next section addresses the issues of gold nanoparticle biodistribution and tumor delivery and discusses possible strategies for increasing the specificity of gold nanoparticle accumulation within the tumor.

Focus #2: Increasing *in vivo* Delivery of Gold Nanoparticles

The delivery of gold nanoparticles to the tumor site is an important consideration for photothermal therapy. Initial *in vivo* studies used direct intratumoral injection of the gold nanoparticles.[14] While this method was very successful in the subcutaneous tumors studied, most solid tumors are not easily accessible for direct injection. The lack of solid tumor accessibility led to a rapid transition to the use of intravenous injection for

delivery. Intravenously injected nanoparticles rapidly disperse throughout the entire body and accumulate within the tumor by the enhanced permeability and retention (EPR) effect. The EPR effect is a phenomenon that is causes by the malformed and angiogenic vasculature of tumors. Tumor blood vessels have larger fenestrations than normal blood vessels, allowing nanoparticles to passively accumulate in the tumor. However, the passage of nanoparticles through these fenestrations is dependent on both the size of the particles and the stage of tumor development; early-stage tumors have smaller fenestrations and thus lower nanoparticle accumulation.[94] In addition, passive accumulation of nanoparticles by the EPR effect is not very efficient for delivery.

In fact, gold nanoparticle tumor accumulation is typically a small percentage of the total injected dose, and non-target organs such as the liver and spleen receive the majority of the injected nanoparticles. Despite the inefficiency of gold nanoparticle delivery, it seems the gold nanoparticle concentration is adequate for ablation. However, it is possible that the delivery has an effect on the completeness of ablation. **Figure 2-7**

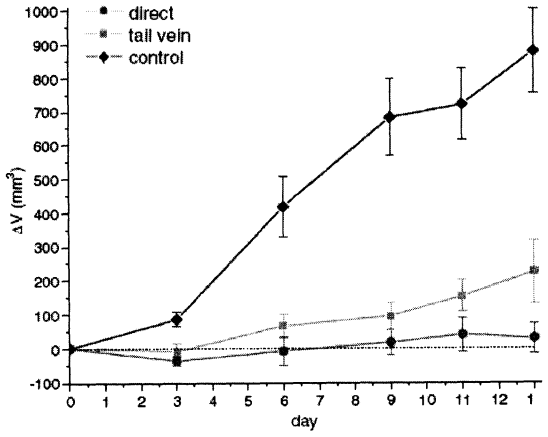

Figure 2-7. Tumor volume change over time following NIR light treatment for mice receiving PBS (control), intratumoral injection of PEGylated gold nanorods (direct), and systemically injected PEGylated gold nanorods (tail vein). Mice receiving treatment experienced less tumor growth than the control mice. However, mice receiving directly injected nanorods had improved survival beginning 11 days post-treatment, suggesting that mice injected by tail vein had a lower tumor concentration of gold nanorods.[38]

shows the change in tumor size following photothermal therapy using PEG-coated gold nanorods. Day 0 correlates with NIR laser treatment. The control group was treated with phosphate buffered saline (PBS), the tail vein group received an intravenous injection of gold nanorods prior to laser treatment, and the direct group received an intratumoral injection of gold nanorods prior to laser treatment. Mice treated using directly administered nanoparticles had smaller tumors at 11 days post-treatment than mice that received intravenously delivered nanoparticles, although this difference never achieved statistical significance at a 5% level.[38] When looking at the concentration of gold nanorods present in the tumors, NIR transmission images showed a measured extinction 4.35 times higher than the saline control in the directly injected tumors (2 min post-injection) and 2.00 times greater than the saline control than in the tail vein injected tumors (24 hours post-injection). This difference in nanoparticle concentration seems to have affected the totality of the ablation, and is suggestive that nanoparticle tumor accumulation is important for ensuring longer-term therapy success. With the goal of maximizing nanoparticle concentration in the tumor in mind, we will next discuss the biodistribution of gold nanoparticles within a mouse model and strategies to enhance gold nanoparticle tumor delivery.

Gold Nanoparticle Biodistribution in Mice

Nanoparticle biodistribution is influenced by the size and surface characteristics of the nanoparticle. Most nanoparticles developed for biomedical applications are coated with chains of polyethylene glycol (PEG) to prevent rapid clearance from the body by the reticuloendothelial system (RES). The addition of PEG to the nanoparticle surface increases the hydrodynamic diameter of the particle, which prevents filtration by

excretory organs, hinders nonspecific binding of proteins to the particle surface, and delays recognition of the particles by the reticuloendothelial system (RES).[95] The end result is increased nanoparticle blood half-life. However, the degree with which PEG coating increases the nanoparticle half-life is dependent on both the original nanoparticle size and the chain length of the PEG (**Figure 2-8**).

Zhang *et al.* found that after intravenous administration to mice, 20 nm PEG-coated (PEG molecular weight = 2000 g/mol) gold colloidal nanospheres had slower clearance, less uptake by RES cells, and higher accumulation in the tumor compared to 40 and 80 nm particles also coated with 2000 MW PEG.[95] Zhang et al attributed the higher clearance of the 40 and 80 nm nanoparticles to increased recognition by the RES due to larger nanoparticle size and a lower PEG layer density on the larger particles. Similarly, Terentyuk *et al.* compared 15 and 50 nm PEG-coated gold colloidal nanospheres with 160 nm PEG-coated gold silica nanoshells *in vivo* and concurred with Zhang and colleagues that the highest blood concentrations of gold at 24 hours were

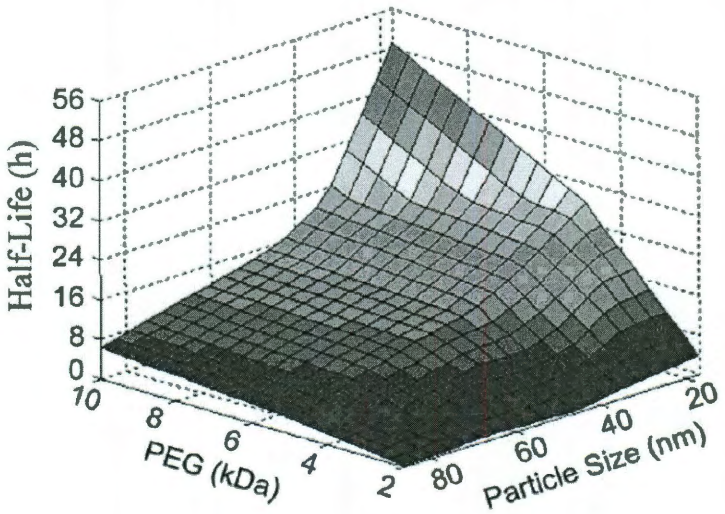

Figure 2-8. Effect of polyethylene glycol (PEG) chain length and particle size on the blood half-life of gold colloidal nanospheres. Smaller gold nanoparticles demonstrate increased PEG surface density, which correlates with increased half-life in the blood. Adapted from [96].

found for the smaller 15 nm particles.[97] Most recently, Perrault *et al.* conducted a systematic study that evaluated the effect of nanoparticle size and PEG coatings on blood circulation time. They showed that the increase in nanoparticle blood half-life due to the addition of PEG was more prominent in smaller versus larger total diameter nanoparticles (**Figure 2-8**).[96] A study by Gobin *et al.* comparing PEG-coated gold-gold sulfide nanoparticles (total diameter = 35-55 nm) to PEG-coated gold-silica nanoshells (total diameter = 120-160 nm) showed that gold-gold sulfide nanoparticles had a longer half life than the gold-silica nanoshells.[47] This would support the hypothesis that a smaller diameter NIR-tunable nanoparticle such as gold-gold sulfide nanoparticles would be advantageous for *in vivo* therapy.

In addition to nanoparticle size influencing clearance from the blood, it also influences the distribution of nanoparticles within the tumor. As discussed in the previous section, intratumoral distribution of the nanoparticles influences the heating of the tumor. Ideally, the nanoparticle distribution would be homogeneous throughout the tumor. In reality, Perrault *et al.* observed that nanoparticles in the 100 nm range stay in the perivascular regions of the tumor, while smaller particles (<60 nm) have more success dispersing throughout the tumor.[96] Tunnell *et al.* also observed non-uniformity of nanoparticle distribution, and observed that the gold-silica nanoshells (>100 nm diameter) remained in close proximity to the vasculature **(Figure 2-9)**.[80] Based on these studies, small nanoparticles are not only more difficult for the body to clear, but also have better tumor distribution than larger nanoparticles.

Small nanoparticles in the range also have an advantage in that they are in the optimal size range for cellular uptake.[98, 99] By endocytosing the nanoparticles into the

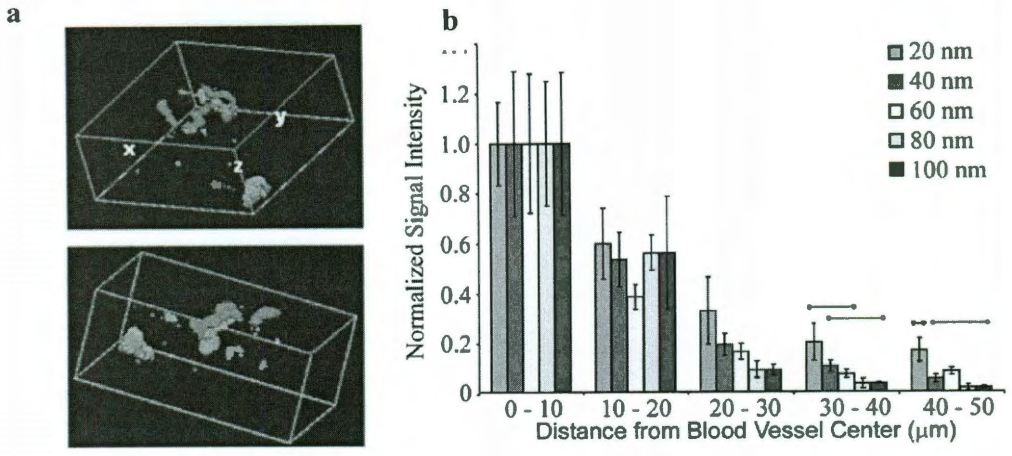

Figure 2-9. a) Gold-silica nanoshell distribution within a tumor *in vivo*. A two-photon confocal image was taken of an excised colon carcinoma tumor after accumulation of nanoshells. Tumor blood vessels labeled with fluorescein (red) and nanoshells (green) were imaged utilizing their two-photon characteristics. The perivascular relationship of silica-gold nanoshells (green) to the tumor vasculature (red) is clearly evident. Adapted from [26]. b) Gold colloidal nanosphere distribution with respect to distance from tumor blood vessels by densitometry analysis of tumor sections. Adapted from [96].

tumor cells, nanoparticle retention by the tumor could be increased, enhancing heating and therapy. Another influencing factor on nanoparticle endocytosis by the tumor is the nanoparticle surface charge. Kim *et al.* performed a study looking at positively and negatively charge gold nanoparticles in tumor cylindroid models *ex vivo*, and found that positively charged nanoparticles were more efficiently endocytosed by tumor cells, but negatively charged nanoparticles rapidly spread throughout the bulk of the tumor.[100] However, though this result is interesting, the study does not account for the influence of nanoparticle surface charge on the clearance of the nanoparticles *in vivo*. Studies looking at polymeric nanoparticles have found that a positively charged surface increases the clearance of nanoparticles by the liver and spleen.[101] Thus, the addition of charge to the nanoparticle surface to increase tumor retention of the nanoparticles must be balanced with the effect of nanoparticle surface charge on clearance. The end goal of nanoparticle

modifications should be to maximize the nanoparticle concentration within the tumor to ensure a complete tumor ablation.

Quantitative comparisons between nanoparticle variants reveal a very similar biodistribution, with the majority of the injected dose delivered to the spleen and liver. For example, James et al. studied gold-silica nanoshells (130 nm diameter) after intravenous administration to mice and noted a peak tumor accumulation of the nanoshells at 24 hours.[102] The concentration of gold reported in the liver and spleen at 24 hours was 20-25x the gold concentration observed in the tumor, indicating that < 5% of the total measured gold was in the tumor (**Figure 2-10**).[102] Gold nanoparticle liver accumulation is observed irrespective of particle size.[102-109] De Jong et al. found that 10, 50, 100 and 250 nm gold nanoparticles all accumulate in the liver, and suggested that this was caused by the high perfusion of blood through this organ.[105] However, both bare and PEG-coated gold nanoparticles can be found localized within Kupffer cells, phagocytic cells present in the liver, and this suggests that phagocytic uptake plays a significant role in the large gold accumulations seen in the liver.[104, 108, 110]

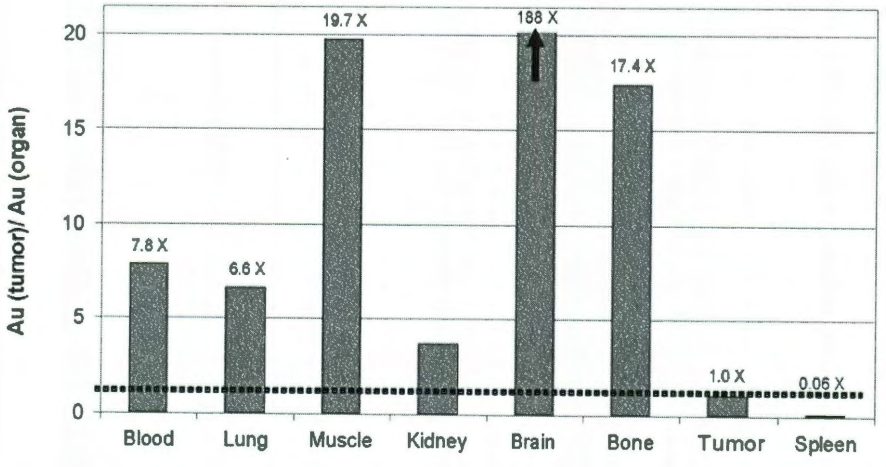

Figure 2-10. Biodistribution of silica-gold nanoshells in a mouse model following systemic administration via the tail vein. All organs show less accumulation than the tumor with the exception of the spleen, which has 16.7 times the gold of the tumor. [102]

The large amount of gold nanoparticles accumulating in non-target sites decreases the number of nanoparticles available for heating the tumor and presents difficulties when considering the use of gold nanoparticles for visualization and treatment of metastases. Redirecting nanoparticles from the liver and spleen to the tumor would improve the chance of therapeutic success, reduce the risk of undesired side effects, and permit improved differentiation between metastases and healthy tissue during imaging. The next subsection focuses on strategies designed to improve gold nanoparticle tumor accumulation, tumor retention, and biodistribution. The first group of these strategies focuses on the addition of molecules to the nanoparticle surface to increase nanoparticle retention by the tumor and decrease nanoparticle accumulation in non-target sites. The second group of strategies utilizes inorganic and cellular vehicles to transport nanoparticles to their destinations.

Strategies to Enhance Tumor Accumulation of Gold Nanoparticles

To optimize the delivery of gold nanoparticles and enhance ablative therapy, two types of strategy have been reported in the literature. The first strategy utilizes the addition of markers to the nanoparticle surface to increase the nanoparticle specificity for a particular cancer and to bind the nanoparticle directly to the cancer cell surface. The second strategy utilizes larger particles or cells to target the tumor with the rationale that these larger vehicles may not accumulate at such a high rate in non-target sites such as the liver. These vehicles carry the therapeutic nanoparticles to the tumor site where they then diffuse from the tumor vasculature into the tumor body. We begin the discussion with gold nanoparticle surface modifications.

Nanoparticle Surface Modifications

Conjugation to gold nanoparticle surfaces is simply accomplished using thiol or amine chemistry. By adding an antibody or other small molecule to the nanoparticle surface that targets the desired cancer, the specificity of tumor accumulation and tumor cell binding may be increased. *In vitro* studies using gold nanoparticles support this hypothesis. Loo *et al.* were the first to demonstrate the increased specificity of anti-HER2 modified nanoshells for HER2 overexpressing breast cancer in both *in vitro* darkfield imaging and *in vitro* photothermal therapy applications.[24, 28] The El-Sayed group subsequently demonstrated *in vitro* cancer ablation using anti-EGFR-conjugated gold nanorods,[36, 73] and other groups had similar findings antibodies for acute lymphoblastic leukemia, *Pseudomonas aeroginosa*, and medulloblastoma.[25, 65, 111] Similarly, small molecules specific for cancer cells have also been added to the surface of gold nanoparticles to increase specificity. It is hypothesized that these molecules will diffuse through tissue more efficiently than antibodies *in vivo* because of their smaller size. Black et al demonstrated using gold nanorods conjugated to modified deltorphin peptide that the nanorods specifically bound delta opium receptor expressing colon cancer cells.[112] This specificity was also demonstrated using a conjugation to bombesin, which was targeted breast and prostate cancer.[113]

An additional advantage of conjugating cancer-targeting moieties to gold nanoparticles is the ability to internalize nanoparticles into cancer cells. Jiang et al demonstrated that gold colloid conjugated to anti-HER2 were internalized into HER2-expressing breast cancer cells in a size dependent manner,[99] and Tong *et al.* used folate-conjugated nanorods to target folate-overexpressing KB cells for photothermal

therapy.[21] Other groups have used arginine-rich peptides to promote nanoparticle internalization.[114] However, Tong et al found that more laser power was required to kill cells with internalized nanorods versus cells with surface-bound nanorods.[21] This may prove a disadvantage for cancer therapy, particularly *in vivo* where it is desirable to minimize laser power. Moreover, the specificity of conjugated nanoparticles *in vitro* has not been duplicated *in vivo*.

In fact, *in vivo* studies using nanoparticles with surface targeting modifications have not shown widespread success in enhancing delivery. Eghtedari *et al.* compared PEG- and anti-HER2-PEG-coated nanorods administered to tumor-bearing mice.[115] While they presented qualitative histology data that seemed to show improved tumor accumulation using anti-HER2 nanorods, they did not present quantitative data indicating a delivery enhancement. Similarly, Li *et al.* used gold nanorods conjugated to antibodies for either the HER2 or EGFR receptor, and saw enhanced photoacoustic imaging contrast of squamous cell carcinoma tumors in mice with the targeted nanorods.[116] However, they presented quantitative data showing that 6.1% of the non-targeted nanorod injected dose and 8.88% of the anti-HER2 nanorod injected dose accumulated within the tumor. It is unclear if this was a statistically significant difference or not.

Similar studies have been performed with *in vivo* targeting of hollow gold nanoshells, which are ~30 nm in diameter before surface modification. Melancon *et al.* modified hollow gold nanoshells with anti-EGFR and presented qualitative evidence via histology showing that the antibody-coated surface increased the delivery of nanoparticles to the tumor when compared to nonspecifically targeted nanoparticles.[7] However, when quantitatively comparing *in vivo* anti-EGFR hollow gold nanoshell tumor

uptake to anti-IgG hollow gold nanoshell tumor uptake using radiolabeling, the uptake difference was not statistically significant. In addition, the radiolabeling showed increased accumulation of the anti-EGFR gold nanoparticles in the liver when compared to the anti-IgG gold nanoparticles.

In contrast, another study using melanocyte-stimulating hormone (MSH) analog-modified hollow gold nanoshells to target murine melanomas showed a statistically significant enhancement of tumor delivery by targeted hollow gold nanoshells (12.6± 3.1% of the injected dose per gram of lyophilized tissue for the MSH-modified versus 4.3 ± 1.2% of the injected dose per gram of lyophilized tissue) 4 hours post-injection.[6] These results are promising, but the choice of a 4 hour timepoint is surprising. The blood concentration of hollow gold nanoshells at 4 hours is between 11 and 13% of the injected dose per gram of blood for both the targeted and non-targeted nanoshells. Based on studies previously discussed that used gold-gold sulfide nanoparticles, which are of similar size to the hollow gold nanoshells, the timepoint of maximal tumor accumulation for hollow gold nanoshells should be much later. The perceived enhancement due to MSH targeting may in fact be due to selection of such an early timepoint, and only establishes that the MSH-conjugated nanoparticles more rapidly localize to the tumor than the non-targeted nanoparticles. The fundamental problem of using surface molecules to modulate nanoparticle tumor delivery is that nanoparticle delivery remains dependent on the EPR effect.

Vehicle-based strategies have an advantage over simple surface modifications in that they can be dependent or independent of the EPR effect. The next section discusses two of these methods for nanoparticle transport.

Vehicles for Nanoparticle Delivery

The first method proposed by Ferrari et al. uses a 3-4 μm porous silicon microparticle as a nanoparticle carrier. This method is dependent on the EPR effect, and has multiple steps (**Figure 2-11**).[93] First, nanoparticles would be loaded into the carrier particles. Next, the loaded carrier particles would be intravenously injected, would localize to the tumor vasculature, and would bind to the tumor blood vessel wall. Finally, the smaller therapeutic nanoparticles diffuse into the tumor. Targeting of the silicon particles would be achieved using a phage coating on the outside of the particle. Bacteriophage (phage) display libraries have been used to identify peptide ligands that specifically bind the integrins, proteoglycans, and other features unique to blood vessels undergoing angiogenesis.[117] Tumor blood vessels are by nature angiogenic, and by coating the primary particles with phages specific to angiogenic blood vessels, the

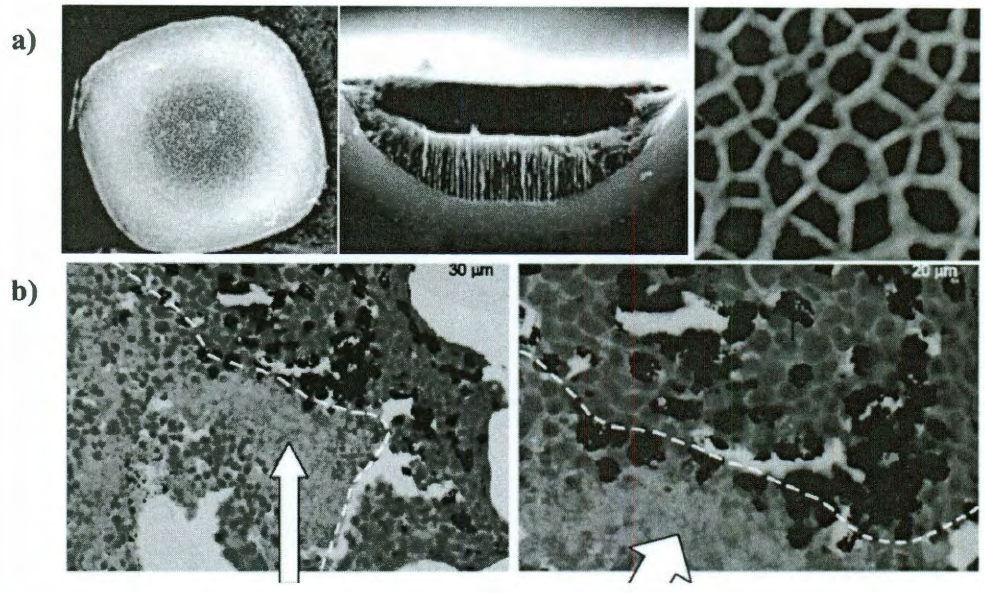

Figure 2-11. Vehicle delivery strategies for gold nanoparticles. a) Scanning electron microscope images of porous silicon microparticle carriers. Microparticles would be loaded with therapeutic nanoparticles and targeted to the tumor vasculature. Once in the tumor vicinity, the nanoparticles would locally diffuse out of the microparticle via the nanoscale pores. Adapted from [118]. b) Hematoxylin/eosin (H&E)-stained tumor tissue slices demonstrating the delivery of nanoparticle-laden macrophages (black cells) to the tumor. Adapted from [119].

primary particles could be targeted to the tumor vasculature for margination, adhesion, and, ultimately, delivery of therapeutic particles. Tasciotti *et al.* performed initial studies with the silicon microparticle carriers delivered quantum dots and single-walled carbon nanotubes (SWNTs) to a cell's cytosol *in vitro*.[118] This demonstration was encouraging for establishing the ability of this method to deliver particles *in vivo*. To date, no *in vivo* studies for tumor delivery with this technique have been published.

Another vehicular strategy that has been used in the literature is the aptly named "Trojan Horse" method, which is independent of the EPR effect (Figure 23).[119] Choi and colleagues hypothesized that macrophages could be used to actively deliver gold nanoparticles to a tumor. Gold-silica nanoshells were incubated with macrophages for 24 hours and internalized via phagocytosis. These nanoshell-loaded macrophages infiltrated tumor spheroids *in vitro* after 3 days of incubation and accumulated at the rim of the spheroid's core hypoxic region. Although this was not a significant enhancement of tumor core penetration, there was a marginal increase in gold nanoparticles reaching the hypoxic core. Their study demonstrates the possibility of using active carriers such as macrophages to delivery gold nanoparticles to the tumor site independent of the EPR effect.

Conclusions

NIR-absorbing gold nanoparticles, such as gold-silica nanoshells,[14, 34] gold nanorods,[36] and gold nanocages,[55, 58] have shown great promise as light absorbers for cancer therapy, demonstrating an ability to destroy cancerous lesions both *in vitro* and *in vivo*. As the design of gold nanoparticle-based thermal therapies continues to mature,

efforts towards clinical translation should focus on the need for: (1) improved methods for reaching deeper, hard to access tumors both through alternative irradiation modalities that possess low attenuation in tissue and improved fiber optic technologies for internal delivery of NIR light; (2) continuing progress towards modeling light-nanoparticle-tissue interactions during therapy and integration of these algorithms together with real-time imaging technologies to permit therapy optimization; and (3) improved delivery methods that will allow accumulation of a larger number of particles to the tumor site, which will enhance therapeutic efficacy. This thesis will seek to address the third of these three aims, improving gold nanoparticle delivery to the tumor, using T cells as a gold nanoparticle delivery vehicle that is independent of the EPR effect.

CHAPTER 3

T CELL-MEDIATED IMMUNE RESPONSE AGAINST TUMORS

Introduction

As highlighted in Chapter 2, gold nanoparticle photothermal therapy (PTT) has demonstrated efficacy against localized tumors in mice and would benefit from improvements in gold nanoparticle delivery. In this thesis, we demonstrate the use of T lymphocytes, a type of white blood cell that is important for immunity and tumor-tropic, as a delivery agent for gold nanoparticles in Chapters 5 and 6. We further expand the use of gold nanoparticles with T cells by using PTT as an adjuvant for adoptive T cell transfer immunotherapy of metastatic melanoma in Chapter 7. The combination of PTT and immunotherapy extends the scope of gold nanoparticle PTT to include distant and metastatic cancers that are not easily accessible or too extensive for ablation to be effective. Because immunotherapy is rooted in the physiology of the immune system and the immune system's response to malignancy, this chapter will explain the role of T cells in the immune system, the response of T cells to malignancy, and the effect of the tumor microenvironment on T cell immune response.

Mechanisms of the T Cell Immune Response

A fully functional immune system is critical for preventing and combating infection and malignancy. It is well known that patients with an impaired immune system are subject to a number of opportunistic infections and cancers that are not typically seen in the immunocompetent population. To protect its host from potentially lethal infections, the immune system uses a series of complex cell-cell and cell-receptor interactions that are designed to prevent and eliminate existing infections and to preserve healthy tissues and cells.

The immune system has two major mechanisms --- innate immunity and adaptive immunity (**Figure 3-1**). Innate immunity rapidly responds to microbe-specific molecular patterns not present on host cells, such as bacterial lipopolysaccharide (LPS), terminal mannose residues on glycoproteins, double-stranded RNA, and unmethylated CpG nucleotides.[120] This type of response is geared to rapidly respond to bacteria or other foreign invaders. Adaptive immunity permits a more specialized response to the invader (**Figure 3-2**). This type of immunity is slower, but targets specific molecules produced by the invading microbe. In addition, adaptive immunity has memory, or the ability to recognize a previously encountered antigen and generate a more rapid response upon repeat exposure. The specificity of the adaptive immunity arm also permits the generation of a large population of immune cells that narrowly target a particular molecule. This property is utilized in adoptive T cell transfer approaches, as discussed later in Chapter 6.

There are three groups of cells important for inducing an adaptive immune response: the naïve T and B lymphocytes, the antigen presenting cells (APCs), and the

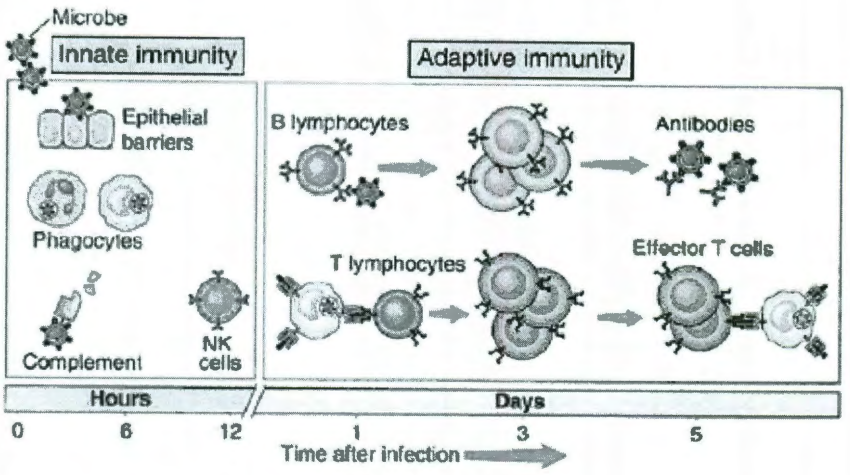

Figure 3-1. Cells of innate and adaptive immunity.[120]

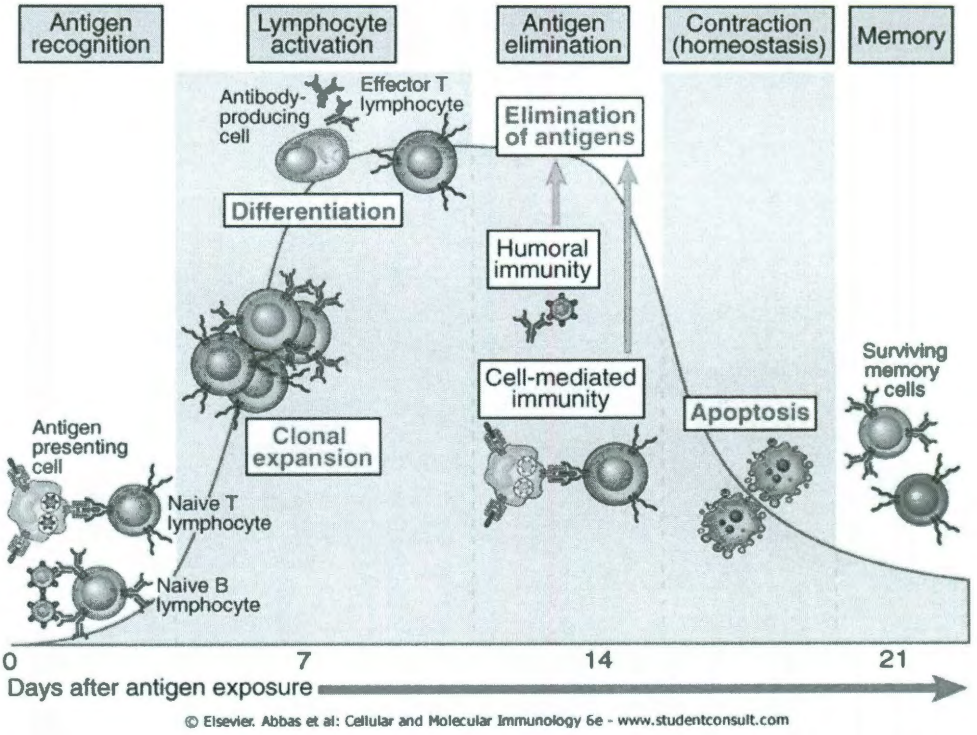

Figure 3-2. Immune response by the adaptive immune system.[120]

effector T and B cells. T cells are responsible for a cell-mediated response against pathogens; these cells recognize foreign antigens, then mature and differentiate into cells capable of directly killing the microbe or infected cell. B cells are responsbile for the humoral immune response; these cells recognize foreign antigens, then differentiate into cells that secrete antibodies for those antigens. In the remainder of the chapter, T lymphocytes will be the primary focus because of their importance in generating an immune response against tumor cells. First, however, we shall discuss the basic mechanism of the T cell immune response against pathogens.

T Cell Activation

The key receptor that allows T cells to recognize antigens is the T cell receptor (TCR). Individual T lymphocytes or T cells each possess their own unique TCR. This receptor is made up of two protein chains, typically an α and a β chain. Each chain of the heterodimer receptor has a unique variable region that facilitates T cell recognition of a wide variety of peptide antigens. This TCR diversity is achieved using random gene recombination during naive T lymphocyte development in the thymus. In the thymus, T cells are also selected for their ability to weakly bind to the host's major histocompatability (MHC)[b] molecules. T cells that do not bind the host's MHC molecules or bind too strongly are marked for apoptosis. In this way, T cells are developed that will be able to recognize antigens in the context of a professional APC but will not react to self-antigens that would lead to an immune response against healthy tissues. Mature naïve T cells leaving the thymus express a TCR and either CD8 or CD4

[b] In humans, these molecules are called human leukocyte antigens (HLA).[1]

on their cell surface. These naïve T cells will circulate in the blood and through lymph nodes until they are activated.

In order for T cell activation to occur, the T cell must not only recognize an antigen with its TCR, but the antigen must also be presented by a professional antigen presenting cell (APC) in the context of the appropriate MHC molecule and co-stimulatory molecules. This multi-step process reduces the possibility of a T cell responding against a self-antigen. In addition, there is a process for the processing of an antigen and the activation of an APC that further ensures that the immune system is responding to non-self antigens. Antigen processing by the APC is the first step in generating an immune response and ultimately inducing T cell activation. Although there are many different types of cells (e.g. dendritic cells, macrophages, and B cells) that can present antigens to T cells, dendritic cells are considered the most potent APCs for activating naïve T cells, and I shall focus my discussion on them.

Dendritic cells (DCs) are present in the epithelia of the skin, gut, and lungs. These DCs are immature and are not yet ready to stimulate T cell activation. Immature dendritic cells express surface receptors that recognize conserved microbial features called pathogen-associated molecular patterns (PAMPs), allowing the DC to internalize encountered microbes. Microbes further facilitate DC activation by binding specialized toll-like receptors (TLR) on the DCs, macrophages, and parenchymal cells present in the tissue. TLRs are able to stimulate an innate immune response in the form of inflammatory cytokines such as interleukin-1 (IL-1) and tumor necrosis factor (TNF). The combination of microbe endocytosis, TLR activation, and cytokine secretion

results in DC activation. The activated dendritic cell detaches from the epithelium and migrates to the tissue-draining lymph nodes. As the DC migrates, the DC matures by increasing its expression of MHC and other costimulatory molecules such as CD80 (B7-1) and CD86 (B7-2).[121] The mature DC arrives at the lymph node prepared to activate naïve T cells against the encountered microbial antigen.

In order for T cells to recognize and respond to an antigen, it must be presented in the context of an MHC molecule on the surface of the DC. MHC molecules consist of two peptide chains that are non-covalently associated on the cell surface, and are only stably expressed on the APC surface when they are displaying a peptide antigen. There are two classes of MHC associated with antigen presentation. The two classes have slightly different protein crystal structures: class I MHC molecules have one α chain and a smaller β_2 microglobulin peptide, while class II MHC molecules have an α and a β chain. The tissue distribution of these molecules is also different by class. Class I MHC molecules are found on all nucleated cells and platelets in the host organism, while class II MHC molecules are only found on APCs, although their expression can be induced on endothelial cells and fibroblasts by interaction with interferon-γ (IFN-γ).[121]

This difference in the tissue distribution of MHC molecules also correlates with the type of antigens presented by each class (Table 3-1). Class I MHC molecules display protein antigens from intracellular microbes (e.g. viruses that live inside host cells). Because every nucleated cell in the host expresses MHC class I molecules, infected parenchymal cells or APCs are able to display intracellular antigens on MHC class I molecules for recognition by CD8+ T cells. Class I MHC molecules can only be recognized by CD8+ T cells, which is important because only CD8+ T cells are able to

Table 3-1. Major histocompatibility complex properties. Adapted from [120].

MHC Class	Distribution of MHC	Type of Antigen Displayed	Responding T Cell
I	All nucleated cells and platelets	Intracellular microbe proteins; viral proteins; self proteins	CD8+ cytotoxic T cells
II	Antigen presenting cells	Extracellular microbial proteins	CD4+ helper T cells

mount an effective cytotoxic response against infected host cells. Class II MHC molecules display extracellular protein antigens on APCs. Class II MHC molecules can only be recognized by CD4+ or helper T cells, which secrete cytokines to induce the proper effector response to the extracellular microbes. This class restriction ensures that the proper effector response is induced for the antigen-producing microbe.

Because the two different MHC molecule classes display microbes from different origins, i.e. class I displays intracellular microbial antigens while class II displays extracellular microbial antigens, the process of preparing an antigen for MHC presentation is different for the two classes. For class I MHC display, the antigen proteins are first unfolded, ubiquinated, and then digested in the proteasome of the cell. This process is performed on any cytoplasmic protein in the cell, including abnormal proteins produced by tumors and normal, aged proteins of the cell. After digestion in the proteasome, the peptide fragments are transported into the endoplasmic reticulum by the transporter associated with antigen processing (TAP).[120] The peptides bind with newly translated MHC I molecules, and are then transported from endoplasmic reticulum to golgi apparatus to the cell surface.

For MHC II antigen loading, the antigen must first be endocytosed or pinocytosed into the APC. The endosome or phagosome containing the internalized antigen then merges with a lysosome, where the proteins are enzymatically digested into fragments. Meanwhile, class II MHC molecules are being synthesized in the endoplasmic reticulum. However, these synthesized molecules have a peptide known as class II invariant chain peptide (CLIP) that blocks the antigen-binding site of the class II MHC. This prevents the class II MHC molecules from binding peptides destined for the MHC class I molecules in the ER. Once the MHC class II molecule leaves the ER in an exocytic vesicle, it merges with the endosome bearing lysosome-digested extracellular peptides. The endosome bearing the digested peptides also contains a protein that removes CLIP from the MHC II molecule, permitting binding of the peptides. This CLIP-removing protein is called HLA-DM in humans, H-2M in mice.[120] If the MHC molecule is able to bind, it becomes stable and is transported to the APC surface for presentation. If the MHC molecule does not bind a peptide, it is ultimately degraded. Once the APC or parenchymal is displaying an antigen on a MHC, it is possible for a T cell to recognize the antigen and become activated.

The T cell requires a minimum of two signals for activation and effector response (**Figure 3-3**). First, the T cell must recognize the cognate antigen via its TCR in the context of MHC presentation (Signal 1). However, recognition of the antigen alone is not sufficient for activation. The antigen must also be presented in the context of

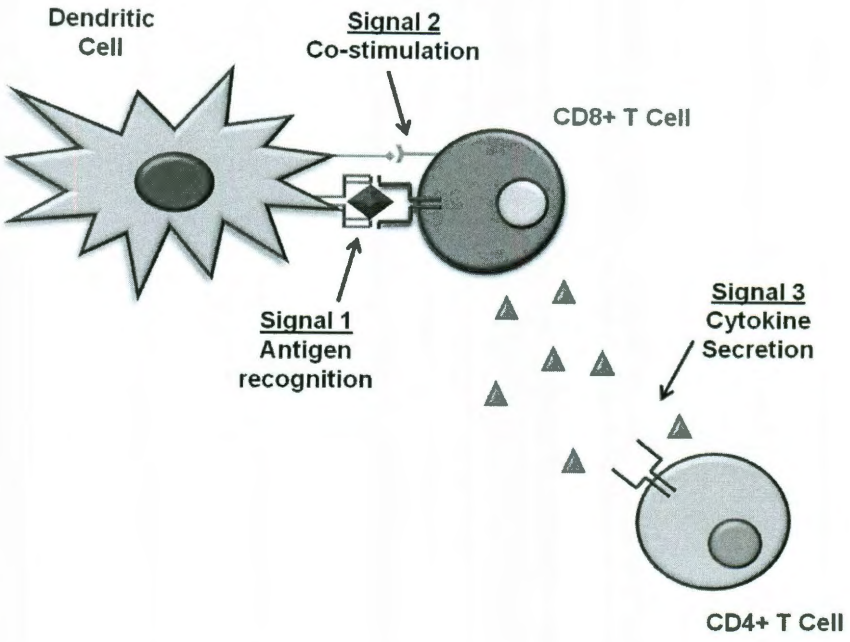

Figure 3-3. Activation of T lymphocyte by a mature dendritic cell. Antigen is processed by the dendritic cell and presented in the context of MHC molecules (Signal 1). The T cell receptor recognizes the antigen on the MHC, as well as the co-stimulatory signals (Signal 2), such as B7-CD28 interaction. These interactions can result in T cell activation, leading to clonal proliferation and differentiation. However, a third signal in the form of helper T cell cytokine secretion can be required for an effector response (Signal 3) in the case of tumor cells and some viral infections.

co-stimulatory signals such as CD80 (B7-1) or CD86 (B7-2) costimulatory molecule expression on the APC (Signal 2), which bind CD28 on T cells. Other co-stimulatory signals include high affinity binding of leukocyte function-associated antigen-1 (LFA-1) on the T cell to intercellular adhesion molecule-1 (ICAM-1) on the APC and the binding of CD40L on the T cell to CD40 on APCs. The binding of LFA-1 to ICAM-1 allows the T cell to bind to the APC long enough to accomplish activation via an intracellular signaling cascade. The binding of CD40L to CD40 results in the APCs producing the chemokines and cytokines necessary to convert LFA-1 on the T cell from the low affinity to high affinity binding state and to induce increased expression of B7 proteins and other co-stimulatory molecules, both of which are essential for T cell activation.

The two-signal requirement for activation prevents the lymphocyte from responding to harmless stimuli or the organism's own normal proteins or cells. T cells that encounter a cognate antigen for their TCR but insufficient additional co-stimulation will become anergic or unresponsive to the antigen. This requirement for co-stimulation explains why adminstering a protein antigen alone fails to generate a vaccine response. Without co-administration with molecules or compounds that are able to induce an innate immune response, there is insufficient cytokine secretion to induce co-stimulation. However, when peptide antigens are injected with adjuvant compounds that can induce an innate immune response, T cells will be activated and will produce a clonal population that recognizes the peptide antigen.

In the case of some viral infections or malignancy that infect parenchymal cells, not APCs, three, not two, events are required for CD8+ T cell response. First, the presentation of the antigen on class I MHC molecules by an APC (signal 1). Second, co-stimulation of the T cell by the APC (signal 2). Finally, additional cytokine stimulation from CD4+ T cells (signal 3). Without these 3 signals, CD8+ T cells will not be sufficiently activated to generate an effective response against these intracellular antigens. In order for these three signals to occur, the intracellular antigens must be presented on both class I and class II MHC molecules. Parenchymal cells do not express class II MHC molecules --- these are only present on APCs. It is hypothesized that APCs phagocytose infected or malignant host cells to allow the antigens of these cells to be presented by the APC[120], or that the APC internalizes intracellular microbes that are transiently in the extracellular space and transfers them to class I MHC molecules[122]. The process of the APC presenting the infected or malignant cells' antigens on both its

MHC I and II receptors as well as the appropriate co-stimulatory molecules is known as cross-presentation or cross-priming. The cross-presentation process is thought to involve autophagy, reverse trafficking of proteins from the ER into the cytosol, phagolysosomal rupture, and/or the loading of class I MHC molecules in the cytosol.[122] Cross-presentation activates both CD4+ and CD8+ T cells, allowing the production of the cytokines necessary for a CD8+ T cell-derived CTL response to intracellular pathogens that do not directly affect APCs. The occurence of cross-presentation is also key to inducing an effective anti-tumor response from T cells.

After the T cells are sufficiently activated through recognition of the cognate antigen and adequate co-stimulation, the T cell begins secreting IL-2 to promote T cell clone proliferation. Naïve T cells only weakly bind IL-2, but activated T cells strongly bind IL-2 due to the production of a third chain for the IL-2 receptor that increases IL-2 binding affinity. Autocrine stimulation by IL-2 results in the proliferation of the antigen-specific T cell clones. These clones begin to differentiate into effector cells that produce the countering immune response to the antigen-generating microbe or cell. After differentiation, a fraction of these effector cells remain in the lymph nodes and another small fraction of the activated T cells become memory cells, and do not differentiate into effector cells. The memory cells remain in the body, dormant, prepared to stimulate a rapid response in the event the antigen is re-experienced by the host. The majority of the activated T cells migrate from the lymph nodes into the blood to the infection site and address the infection through their effector response.

T Cell Effector Response

After leaving the lymph nodes and entering the bloodstream, the T cells must first localize or home to the location of the infection or malignancy. Within the infected tissue, the innate immune cells produce inflammatory cytokines and chemokines that signal the local endothelial cells to upregulate the expression of E-selectin, P-selectin, and integrin ligand on the blood vessel surface (**Figure 3-4**). Passing T cells in the blood will weakly bind to the selectins on the endothelial cell surface by surface carbohydrates, and begin to "roll" along the blood vessel surface. Activated T cells express a high affinity integrin on their cell surface, allowing them to halt the rolling by binding to integrin ligand on the endothelial cell surface. In contrast, naive T cells express a low affinity integrin on their cell surface. After binding to the endothelial cell's integrin ligand, the T cell reorganizes its cytoskeleton and uses PECAM-1 (also known as CD31) to extravasate into the infected tissue. This homing process from the lymph node to the site of infection takes approximately 24 to 48 hours. Once the effector T cell encounters its cognate antigen in the tissues, the T cell increases expression of very late activation

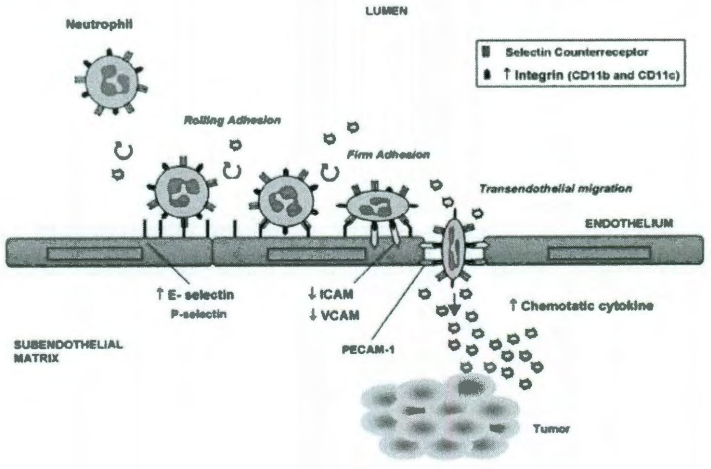

Figure 3-4. Migration of neutrophils into tumor site. This is the same mechanism that is used by T lymphocytes to extravasate to the tumor site. Adapted from [123].

(VLA) integrins that binds to extracellular matrix components such as hyaluronic acid and fibronectin.[120] In this way, effector T cells that recognize their cognate antigen remain in infected tissue longer to perform their effector response.

The effector response of the T cell is dictated by the type of T cell (CD8+ or CD4+). While cytoplasmic antigens induce a CD8+ T cell response, extracellular antigens induce a CD4+ T cell response. CD8+ T cells differentiate into cytolytic T cells (CTLs), and are able to kill infected or malignant host cells. When a CTL encounters an infected cell presenting its cognate antigen on a class I MHC molecule, the CTL firmly binds to that cell. The CTL then releases granzymes and perforins into the targeted cell, and the cell subsequently undergoes apoptosis. CD8+ CTLs also secrete IFN-γ, a powerful activator of macrophages. IFN-γ signals the macrophages to phagocytose and destroy microbes, while also signaling the macrophages, which can function as APCs, to increase the expression of class II MHC molecules and B7 co-stimulatory molecules. In this way, the CTLs destroy cytoplasmic microbes and lead to the activation of CD4+ helper T cells against the microbes as well. Whereas CD8+ CTLs are able to directly destroy microbes, CD4+ helper T cells serve primarily as signaling intermediaries.

There are two primary types of CD4+ T cell responses: the T_H1 response or the T_H2 response. The cytokine and chemokine environment of the infected tissue controls which response is given by the helper T cells. If IL-12 is present and being produced by the local APCs, the production of a T_H1 cell response is favored. If IL-12 is not present, then the autosecretion of IL-4 by the helper T cells favors a T_H2 response. T_H1 CD4+ T cells are strong secretors of IFN-γ, which, as discussed in the previous paragraph, activates macrophages. T_H1 cells also activate macrophages by stimulating them through

the CD40L-CD40 interaction. The signals given by T_H1 cells induce the macrophages to produce increased amounts of reactive oxygen species and nitric oxide that are used to kill phagocytosed microbes. T_H2 cells secrete IL-4 and IL-5, and are important mediators of the humoral or antibody-mediated immune response against certain types of parasites via eosinophils. The T_H2 cells also produce Il-10 and IL-13, which inhibit macrophage activation. Although CD8+ CTLs are able to directly attack malignant cells, the profile of the effector CD4+ helper T cells is thought to influence the efficacy of the CTL response. Melanoma patients that respond well to immunotherapies tend to have a predominantly T_H1 helper T cell profile, while patients that do not respond seem to have a predominantly T_H2 helper T cell profile.[124] This supports the importance of both CD8+ and CD4+ T cells in the immune response to cancer.

Now that the basic mechanism of T cell immunity has been established, I shall turn my attention to the role of the immune system in responding to malignancy. Based on the discussion thus far, the immune system has the ability to identify malignant cells and destroy them, yet sometimes fails to accomplish this end goal. The next section will discuss the role of the immune system in tumor development and the mechanisms used by the tumor to evade immune detection and response.

The Role of the Immune System in Tumor Progression

The response of the immune system to tumor development has three theoretical phases: elimination, equilibrium, and escape (**Figure 3-5**). In the first phase, elimination, a combination of CD8+ T lymphocytes, intraepithelial lymphocytes ($\gamma\delta$ T cells), macrophages, and natural killer (NK) cells are able to attack and destroy the malignant cells. If the immune system fails to eliminate the tumor cells, the tumor

continues to evolve genetically, altering its antigen expression and developing other resistance mechanisms that permit the malignant cells to survive (**Table 3-2**). The immune system assists in the selection of these genetic changes by destroying vulnerable tumor cells, leaving behind the resistant tumor cells. When the proliferation of the tumor cells overtakes the rate at which the immune cells can destroy tumor cells, the tumor has reached the escape phase. At this stage, the tumor is producing immunosuppressive cytokines and molecules, preventing an effective immune response by the host.

Tumor suppression of the immune response is not well understood and is an area currently under study. One difficulty seems to be that CTLs have impaired killing of

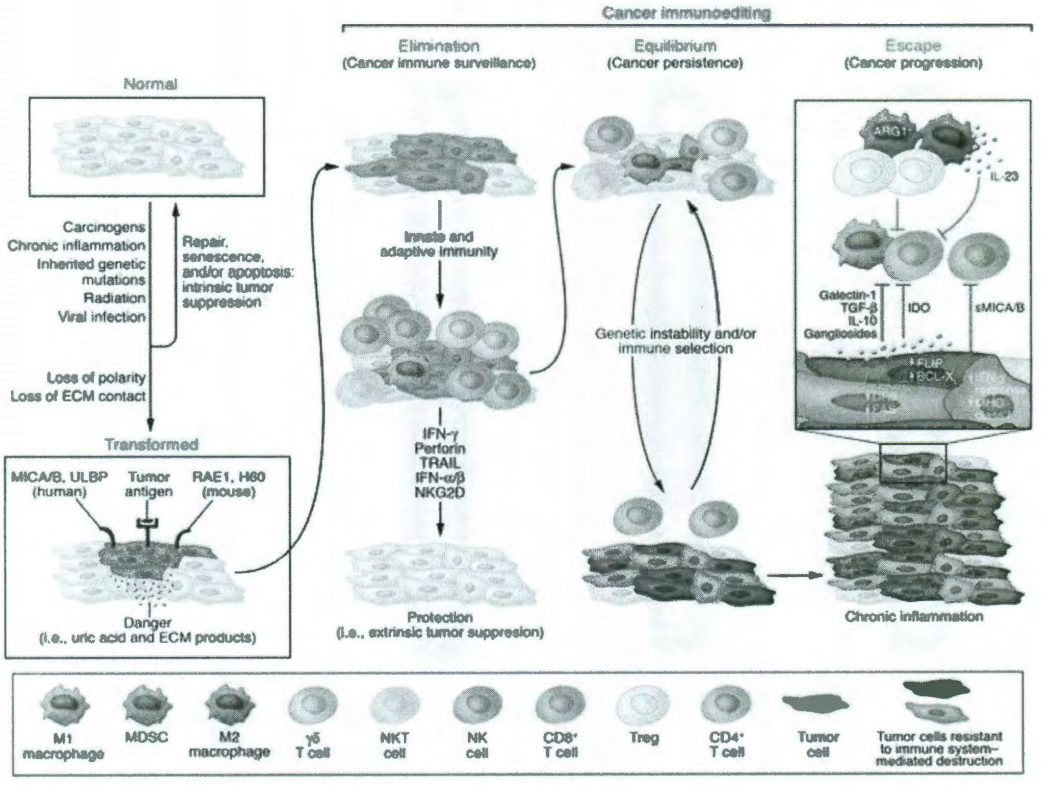

Figure 3-5. Host immune response to cancer. DR5 = death receptor 5, IDO = indoleamine 2,3-dioxygenase, MICA/B = MHC class I chain-related antigens A and B, RAE1 = retinoic acid early transcript 1, sMICA/B = soluble MICA/B, ULBP = UL 16-binding protein.[125]

Table 3-2. Mechanisms orchestrated by the tumor that contribute to its escape from the host immune system (adapted from [126])

A. Interference with the induction of anti-tumor immune responses	1. Decreased expression of costimulatory molecules on the tumor or APC 2. Alterations in TCR signaling in TIL 3. Death receptor/ligand signaling and 'tumor counterattack' 4. Dysfunction of DC and inadequate cross-presentation of TAA to T cells 5. DC apoptosis in the tumor microenvironment
B. Inadequate effector cell function in the tumor microenvironment	1. Suppression of T-cell responses by T_{reg} 2. Suppression of immune cells by myeloid suppressor cells (MSC) 3. Apoptosis of effector T cells in the tumor and in the periphery 4. Microvesicles (MV, exosomes) secreted by human tumors and inducing apoptosis of $CD8^+$ effector T cells
C. Insufficient recognition signals	1. Downregulation of surface expression of HLA molecules on tumor cells 2. Downregulation of surface TAA displayed by tumor cells: antigen loss variants 3. Alterations in APM component expression in tumor cells or APC 4. Suppression of NK activity in the tumor microenvironment
D. Development of immunoresistance by the tumor	1. Lack of susceptibility to immune effector cells 2. Immunoselection of resistant variants 3. Tumor stem cells

tumor cells in the tumor microenvironment. An *in vivo* study performed using tumor-antigen specific T cells demonstrated that the CTLs took an average time of 6 hours to kill a tumor cell, while a normal T cell can kill a cell in about 25 minutes.[127] Part of the mechanism behind this CTL impairment may be the tumor antigen itself. Tumor antigens are a mutant form of a self-protein, a normal protein that is overexpressed in tumor cells, or a normal protein that is being expressed at the wrong stage of development.[120] The fact that these antigens were previously self-molecules ignored by the immune system may prevent CTLs from generating an effective response against them after malignant transformation; in fact, this similarity to self-antigens is likely to induce T cell anergy (failure of the T cell to react to the antigen).[128] The lack of co-stimulatory molecules on tumor cells also prevents T cell activation, even when the tumor cell is presenting tumor antigens on its MHC class I molecules.[120] Moreover, to induce a truly effective response, the tumor antigen must be cross-presented on both MHC class I and MHC class II molecules by an APC. A lack of cross-presentation impairs the T cell immune response to the tumor.[126]

However, the lack of a T cell response to the tumor is not simply due to a lack of effective T cell activation. Zippelius et al collected T cells from the blood of Stage III/IV melanoma patients and found that the CD8+ T cells targeting MART-1, a marker of melanocytes, could destroy melanoma cells *in vitro*, but *in vivo* the same MART-1 T cells were anergic.[129] This suggests that the tumor microenvironment possesses additional factors that suppress T cell effector response and induce T cell anergy. Research into this area thus far has revealed that tumor-produced cytokines, immunosuppressive cells, and other factors are part of the myriad of tumor-induced defense mechanisms that prevent an

effective immune system offense. These mechanisms are summarized in **Table 3-2**. We will next briefly discuss the key immunosuppressive players in the tumor microenvironment as we may influence the prevalence and effectiveness of these players using our combination of nanoparticle photothermal therapy and immunotherapy.

There are several cell types that serve an inhibitory role in the tumor microenvironment. Important examples include T regulatory cells, tumor-associated macrophages (TAMs), and myeloid-derived suppressor cells (MDSCs).[130] The first cell type mentioned, T regulatory cells ($CD4^+$ $CD25^{high}$ $Foxp3^+$), are designed to prevent the response of CTLs and helper T cells against normal self-antigens. Regulatory T cells induce anergy in autoimmune-responding T cells by a combination of TGF-β and IL-10 secretion as well as contact-dependent mechanisms.[120] In the tumor microenvironment, T regulatory cells are found to be enriched (5-15% of tumor infiltrating lymphocytes) compared to their presence in the peripheral blood, and are able to suppress the ability of CTLs to release cytotoxic granules and kill malignant cells.[126]

Within the tumor, dendritic cells contribute to regulatory T cell activation through the binding of CTLA-4. The coupling of CTLA-4 on the regulatory T cell with CD80 and CD86 on the dendritic cells results in a high level of indoleamine 2,3-dioxygenase (IDO) expression, which impairs T cell proliferation, induces T cell anergy, and enhances a T cell's vulnerability to apoptosis.[128] The enriched regulatory T cell population in the tumor prevents tumor-antigen recognizing T cells from generating a cytotoxic response against the tumor cells. The role of T regulatory cells is not limited to influencing other

T cells, however. T regulatory cells also drive the macrophages present in the tumor (tumor associated macrophages or TAMs) to favor immunosuppressive functions.[131]

As discussed earlier in the chapter, macrophages can serve as innate immune defenders and antigen presenting cells. However, like helper T cells, macrophages can be polarized to favor one type of immune response over the other. In tumors, M1 macrophages are produced in the presence of IFN-γ and are able to eradicate tumor cells, while M2 macrophages are produced in response to IL-10 and are thought to be immunosuppressive.[132] These M2 macrophages promote immunosuppression by releasing reactive oxygen species (ROS) and peroxynitrite, decreasing TCR binding affinity for professionally presented antigens by adding nitrates to tyrosine residues on the T cell receptor complex of CTLs.[130] M2 macrophages also secrete IL-10 and prostaglandins, which also can inhibit T cell function.[126] Moreover, M2 macrophages are thought to have a role in promoting tumor growth and expansion through the secretion of proangiogenic factors such as VEGF, TNF-α, IL-8, and extracellular matrix proteases,[133] and it has been observed that tumor cells are more motile when within close proximity of M2 macrophages.[130] Like regulatory T cells, M2 TAMs protect the tumor from immune surveillance, but in addition they also promote tumor expansion.

Myeloid-derived suppressor cells (MDSCs) also create a tumor environment that favors immunosuppression and metastasis. MDSCs ($CD11b^+$ $Gr1^+$ in mice) are immature cells of bone marrow origin that occur in cancer patients and accumulate at the tumor site due to tumor secretion of IL-10, VEGF, and GM-CSF.[126] They enhance immunosuppression within the tumor through the increased secretion and production of inhibitory cytokines, nitric oxide, ROS, and arginase.[133] MDSCs also migrate to

tumor-draining lymph nodes and interfere with DC priming of T cells. MDSCs are believed to promote tumor angiogenesis independent of VEGF, thus contributing to tumor progression and proliferation.[133]

The combination of these three immunosuppressive cell types as well as the tumor cells producing their own immunosuppressive cytokines prevents the endogenous immune system from successfully combating tumor growth. Despite these challenges, recent immunotherapy clinical trials have demonstrated that collecting, expanding, and reinjecting tumor antigen-specific T cells into patients has clinical benefits for cancer treatment. The final section of this chapter will discuss adoptive T cell immunotherapy, its preliminary successes in clinical trials, and areas where combining gold nanoparticle photothermal therapy with adoptive T cell transfer may present some treatment benefits.

Adoptive T Cell Immunotherapy

Immunotherapy is a very broad term that can refer to many different types of immune system derived treatments. Commonly used immunotherapy-based cancer therapies include trastuzumab (Herceptin®), an antibody used for the treatment of advanced HER2+ breast cancer (see Chapter 4), Bacille Calmette-Guérin (BCG), a mycobacteria used to treat early bladder cancer, and the human papillomavirus (HPV) vaccine, a non-infectious virus-like particle mixture used to prevent cervical cancer. More active immunotherapy treatments, such as dendritic cell and T cell vaccines, are currently under development. Because CD8+ T cells can directly target and destroy cancer cells, they are considered the gold standard cell for cancer immunotherapies.

Adoptive T cell immunotherapy uses T cells derived from either a tumor biopsy sample or the peripheral blood of the patient and expands them *in vitro* for reinjection.[8] Patients receiving transferred T cells may also receive a lymphodepleting regimen using radiation and/or chemotherapy in addition to high doses of interleukin-2 (IL-2). These adjuvant treatments have been demonstrated to enhance the clinical response of the tumor to T cell therapy.[134, 135] A disadvantage to both the lymphodepletion regimen and the high dose IL-2, however, is that both of these regimens are known to have potentially serious side effects, including infection, capillary leak syndrome, hypotension, fever, cardiac arrhythmias, and allergic reactions.[136] Adding an adjuvant regimen, such as gold nanoparticle photothermal therapy, that obviates the need for these drugs would reduce the morbidity of T cell immunotherapy treatment.

To date, T cell-based immunotherapy has been most successful against metastatic melanoma, but have been used against other metastatic cancers with some degree of success.[8-10] Most recently, a clinical trial with melanoma patients receiving adoptive T cell transfer with lymphodepleting chemotherapy +/- whole body radiation demonstrated success against brain metastases, with 15 of 26 patients attaining a complete or partial response of the brain metastases to therapy.[137] One difficulty with using the patient's own unmodified T cells from a tumor biopsy sample or peripheral blood is the difficulty in isolating T cells that are specific for tumor antigens. One solution that has been proposed is using T cells that are genetically modified to target specific tumor antigens. This was first demonstrated using T cells targeted against MART-1, a melanoma tumor antigen.[138] Using retrovirus, the antigen-specific portions of the MART-1-specific T cell receptor were inserted into autologous T cells

isolated from the peripheral blood. Two patients from this trial demonstrated a shrinking of their cancerous lesions and persistence of the engineered T cells for 1 year in the peripheral circulation, demonstrating the viability of this approach for generating large numbers of tumor antigen-specific T cells.

Genetic modification of the T cell receptor to produce large numbers of antigen-specific T cells has also seen some success. In two different clinical trials, T cells were retrovirally modified with T cell receptors (TCRs) specific for tumor antigens. In the first trial, autologous T cells were modified with a TCR specific for NY-ESO-1, an antigen commonly expressed in 10-50% of metastatic melanomas and 80% of synovial cell sarcomas.[139] This trial demonstrated an overall response rate of 45% for metastatic melanoma and 67% for synovial cell sarcoma. Another trial retrovirally modified T cells to target carcinoembryonic antigen (CEA), which is commonly expressed in metastatic colon cancer. In this trial using 3 patients with metastatic colon cancer, a sharp drop in CEA blood levels was seen in all three patients.[140] One out of three patients had a clinical partial response to treatment, but all patients experienced moderate to severe colitis beginning 1 week after treatment and resolving over 4-6 weeks as well as progressing cancer after 6 months. Despite the lack of long term success with the TCR-modified T cells, the increase in T cell function seen was encouraging.

One potential risk with this genetic engineering strategy is the development of hybrid T cell receptors. Native T cell receptors in the recipient T cell can trade portions of the donor T cell receptor with portions of the native T cell receptor, resulting in possible loss of T cell specificity for the tumor or in possible self-recognition and life-

threatening graft vs. host disease.[141] Because of this risk, an alternative strategy has been proposed using chimeric antigen receptors (CARs).

To create a CAR, the antigen-specific chain of a monoclonal antibody is engineered into a T cell and linked to the intracellular signaling within the T cell needed for immune response. Antibodies have an advantage over native TCRs because of their ability to respond to carbohydrates and lipid antigens in addition to peptide antigens. The engineering of the CAR into the T cell permits T cell response to non-protein tumor antigens, as well as eliminating the requirement for the MHC complex recognition.[10] It does not, however, remove the requirement for co-stimulation, which is required to permit full T cell activation. Because co-stimulation within the tumor tends to reduced, it may be necessary to provide co-stimulation through additional cloning of co-stimulatory molecules, such as CD28, into the CAR.[10] Di Stasi and colleagues recently demonstrated that the genetic modification of T cells with a CAR targeted to CD30 and constitutive expression of chemokine receptor 4 (CCR4) increased T cell migration and anti-tumor response to Hodgkin lymphoma in mice and reduced the development of regulatory T cells from these CAR+ CCR4+ T cells (**Figure 3-6**).[142] Alternatively, the T cells genetically modified with CARs could be stimulated through their native TCR by vaccinating the T cells against a virus that is present in the host.[10] This would ensure consistent T cell activation and co-stimulation.

Although T cell adoptive transfer has demonstrated some successes in clinical trials, the challenges of the immunosuppressive tumor microenvironment have prevented a high percentage of complete and durable clinical responses. The addition of an adjuvant treatment such as gold nanoparticle photothermal therapy may benefit T cell

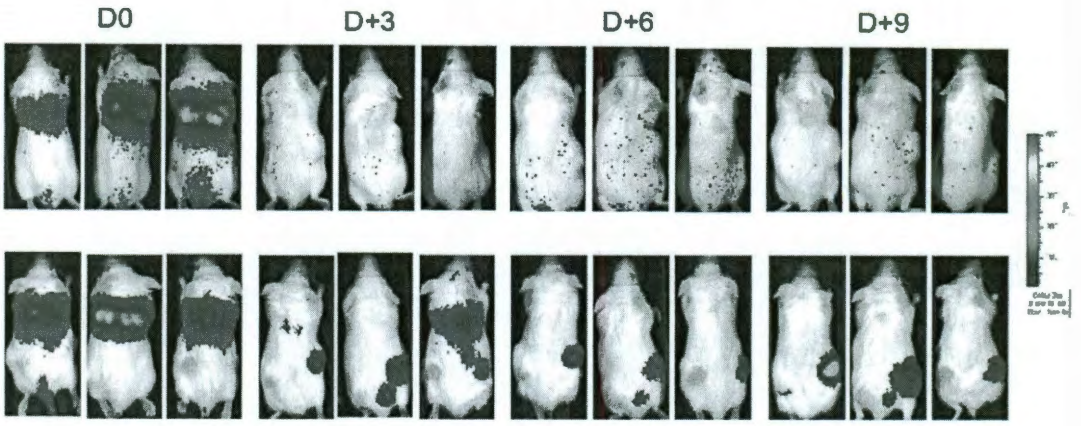

Figure 3-6. Bioluminescent imaging performed using firefly-luciferase modified T cells and SCID mice with subcutaneously xenografted Hodgkin's Lymphoma (right flank). Top row shows unmodified T cells while bottom row shows T cells genetically modified with a CAR targeting CD30 and the CCR4 receptor. D0 correlates with the day of injection, D+3 with 3 days post-injection, D+6 with 6 days post-injection, and D+9 with 9 days post-injection. At day 9 post-injection, the genetically modified T cells are seen to persist in the tumor while non-modified T cells do not persist. Adapted from [142].

immunotherapy by providing increased tumor antigen presentation and co-stimulation, ultimately leading to an improved CTL anti-tumor response. In addition to this benefit, the use of PTT as an adjuvant may reduce the need for the high-dose IL-2 regimen that is commonly used in patients receiving T cell transfer. In the remaining chapters of this thesis, I will demonstrate the combination of immunotherapy with gold nanoparticle PTT to enhance gold nanoparticle delivery to the tumor for PTT, as well as demonstrate the additive effects of PTT on immunotherapy.

CHAPTER 4[c]

NANOSHELL THERAPY OF TRASTUZUMAB-RESISTANT BREAST CANCER CELL LINES

Introduction

In Chapter 2 of this thesis, the advantages of gold nanoparticle photothermal therapy (PTT) for cancer treatment were outlined. One application of PTT has that has been very lightly explored is the use of PTT against chemotherapy resistant cancers. To date, gold nanoparticle-mediated treatment has only been applied to chemotherapy-sensitive cell lines. Many cancers rapidly adapt to chemotherapeutics and develop resistance mechanisms that ultimately evade treatment. Because PTT ablates tumors with heat, we hypothesize that treating a chemotherapy-resistant cancer with PTT will evade any innate resistance and result in cancer cell death.

For our initial testing of this hypothesis, we chose to focus on trastuzumab-resistant breast cancer *in vitro*. In 2006, a therapeutic antibody against HER2 receptor, known as trastuzumab (Herceptin®), was brought to market as the first of the molecular therapeutic drugs for breast cancer. It is a commonly used adjuvant treatment for metastatic HER2+ breast cancers, which are known to be aggressive and to have a tendency to recur.[143, 144] Trastuzumab binds to the HER2 receptor and halts tumor cell growth through suppressing HER2 signaling and elevating the levels of $p27^{KIP1}$

---

[c] Adapted from: Carpin LB, Bickford LR, Agollah G, Yu TK, Schiff R, Li Y, Drezek RA, "Immunoconjugated Gold Nanoshell-Mediated Photothermal Ablation of Trastuzumab-Resistant Breast Cancer Cells";*Breast Cancer Research and Treatment*, 125(1):27-34 (2011).

protein.[143] Initial clinical trial results against metastatic breast cancer were positive, and trastuzumab was subsequently approved for use.[145, 146]

Despite the initial successes of trastuzumab, the trastuzumab resistance has presented a major barrier. The majority of patients are intrinsically resistant to trastuzumab prior to starting therapy,[147] and most initially responsive patients develop resistance to treatment within a year.[143] The development of trastuzumab resistance has been attributed to a variety of mechanisms, including overexpression of glycoprotein MUC4,[148] overexpression of insulin-like growth factor 1 (IGF-1),[149] and constitutive P13K/Akt activity.[150] In addition, although a mutation of the extracellular component of the HER2 receptor that results in trastuzumab resistance is theoretically possible, in most cases of resistance this does not occur.[143] This presents the possibility of using an antibody generated against the HER2 receptor as a targeting modality for nanoshell-mediated therapy. Gold nanoshell photothermal therapy could potentially be used to ablate these treatment-resistant breast cancers, presenting a new possibility for treating difficult cancers.

By adding surface-conjugated ligands to gold nanoparticles, such as antibodies, polymers, or DNA, the nanoshells demonstrate increased target specificity *in vitro*.[14, 151, 152] In the case of HER2+ breast cancer, Loo et al demonstrated that gold-silica nanoshells conjugated to anti-HER2 can be successfully used to target and ablate chemotherapy-sensitive breast cancer cells in culture.[24] Here, we will demonstrate that antiHER2-conjugated silica-gold nanoshells can mediate effective targeting and photothermal ablation of cultured two antiHER2-resistant breast cancer cell lines – JIMT-1 has a lower level of anti-HER2 binding due to overexpression of MUC4,[148] and

BT474 AZ LR is resistant to both trastuzumab and lapatinib, an second generation agent developed for use against trastuzumab-resistant breast cancers.

Materials and Methods

Breast Cancer Cell Lines

Three HER2-overexpressing breast cancer cell lines were chosen for this study: SK-BR-3, JIMT-1, and BT474 AZ LR. The SK-BR-3 cell line is trastuzumab sensitive, while the JIMT-1 cell line and BT474 AZ LR cell line are both trastuzumab resistant. The BT474 AZ LR cell line is also resistant to lapatinib, a second line agent developed for trastuzumab-resistant breast cancers. The MCF10A cell line, which is an immortalized, HER2 negative breast epithelial cell line, was used as a control. The SK-BR-3 and JIMT-1 cell lines were both cultured in McCoy's 5A and Dulbecco's Modified Essential Medium, respectively, supplemented with 10% fetal bovine serum (FBS) and 1% penicillin-streptomycin. The BT474 AZ LR cell line was cultured in Dulbecco's Modified Essential Medium High Glucose supplemented with 10% FBS and 1% penicillin-streptomycin-glutamine and with 0.1 μg/mL of lapatinib to maintain HER2 therapy resistance. The MCF10A cells were cultured in Mammary Epithelial Basal Medium (MEBM) supplemented with a BulletKit (Clonetics). All cells were maintained at 37°C in a 5% CO_2 atmosphere.

Quantification of HER2 Receptor Antigens on Cell Surface

Quantification of HER2 surface receptors was performed as described by Bickford et al.[27] Cells were grown to confluence, trypsinized, counted, and incubated

with either media alone, PE anti-human CD340 (erbB2/HER-2) antibody, or PE mouse IgG1 isotype control antibody for 30 minutes on ice in the dark. The IgG1 isotype serves a background signal correction. The cells were then washed in 1x PBS, resuspended in 500 µl of cell staining buffer, and stored on ice until analysis. Immunofluorescence intensity was determined by flow cytometry at The University of Texas M.D. Anderson Cancer Center (MDACC) flow cytometry core. To correlate the immunofluorescence intensity with the quantity of HER2 antigens available for binding on each cell, a Quantum Simply Cellular anti-Mouse IgG kit was used. This kit has 4 different sets of microbeads possessing a known number of antigen binding sites, which permits the development of a calibration curve correlating immunofluorescence intensity with the quantity of antigen binding sites. The curve is then used to calculate the number of antigen binding sites per cell.

Silica-Gold Nanoshells and Antibody Conjugation

The silica-gold nanoshells were synthesized using previously described methods.[24, 28, 32] In brief, silica cores were created using the Stöber method,[153] and the silica core surface was functionalized with amine groups. These amine groups were then used to seed 4-7 nm gold colloid onto the silica surface. The size of the silica cores was determined to be 120 nm by scanning electron microscopy (SEM) prior to gold seeding. The gold shell was then completed by adding additional gold solution, potassium carbonate, and formaldehyde. After synthesis, the UV-Vis spectrum of the

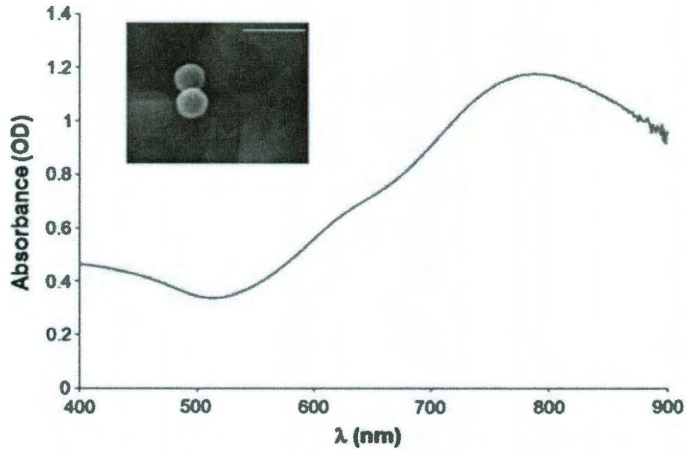

Figure 4-1. Absorbance spectrum of the silica-gold nanoshells (silica core radius = 60 nm, total radius = 75 nm). Inset shows SEM image of the nanoshells; scale bar is 300 nm.

nanoshells was correlated with Mie Theory to determine the absorption, extinction, and scattering coefficients of the nanoshells, and subsequently the approximate concentration. The average nanoshell diameter was confirmed to be 150 ± 10 nm by SEM. The nanoshell extinction peak was determined to be 780 nm with a concentration of 3.85 x 10^9 nanoparticles/mL (**Figure 4-1**).

To modify the surfaces of the nanoshells with anti-HER2 antibody, the methods of Loo et al were employed.[24] The anti-HER2 antibody (C-erbB-2/HER-2/*neu* Ab-4, Lab Vision Corporation) was incubated with a custom orthopyridyl-disulfide-polyethylene glycol-N-hydroxysuccinimide ester (OPSS-PEG-NHS, MW = 2kD, CreativeBiochem Laboratories) linker at a molar ratio of 3:1 in sodium bicarbonate (100 mM, pH 8.5) overnight on ice at 4°C. Aliquots were then stored at -80°C until use, when they were thawed on ice. The antibody binds to the OPSS-PEG-NHS linker via the amide group, and adsorbs to the gold surface of the nanoshell via the thiols of the OPSS group. To attach the antibody-linker to the gold nanoshells, nanoshells were incubated with the antibody-linker at 4°C for 2 hours, then 1 mM polyethylene glycol-thiol (PEG-SH, MW = 5kD, Nektar) was added and the nanoshells were incubated overnight at 4°C

for further stabilization. After nanoshell conjugation, the unreacted PEG-linker and PEG-SH were removed by centrifugation of the nanoshell solution and removal of the supernatant. The anti-HER2 nanoshells were then resuspended in cell-line appropriate media prior to use in cell studies.

Two-Photon Laser Scanning Microscopy to Confirm Binding Efficiency

For *in vitro* two photon nanoshell binding studies, ~5 x 10^5 cells in suspension from each cell line (MCF10A, SK-BR-3, JIMT-1, and BT474 AZ LR) were incubated with 1.73 x 10^9 nanoshells in 1 mL of media for 1 hour at 37°C with rotation in a hybridization oven. Cell incubated with media alone were used as a control. After the incubation, the cell lines were washed three times with 1 mL of 1x phosphate-buffered saline (PBS) to remove unbound nanoshells, and resuspended in 0.5 mL of cell line appropriate media. Each treatment and control group was then seeded onto an inverted coverslip and allowed to attach overnight. A Zeiss Laser Scanning Microscope 510 META multiphoton system was used in combination with a Coherent Chameleon femtosecond mode locked Ti:sapphire laser for imaging.

Nanoshell-Mediated Photothermal Therapy

For *in vitro* photothermal ablation studies, ~5 x 10^5 cells in suspension from each cell line (MCF10A, SK-BR-3, JIMT-1, and BT474 AZ LR) were incubated with 1.71 x 10^{10} nanoshells as described above. Media alone was again used as a control. Cells were washed with PBS and seeded in coverslips as described above.

Laser irradiation of the cells was performed in a similar manner to previous photothermal therapy studies.[24, 30, 32] After the cells were attached, each well was uncovered, placed on top of a glass microscope slide, and exposed to an 808 nm NIR

diode laser at 80 W/cm^2 with a 1.5 mm spot size for 5 minutes. Following laser irradiation, the cells were returned to the 37°C incubator with 5% CO_2 for several hours. Live/dead viability staining was then performed using an Invitrogen Live/Dead viability/cytotoxicity kit and cells were imaged using a Zeiss Axiovert 135 Fluorescence microscope. To confirm nanoshell binding, silver staining was performed using Sigma Aldrich Silver Enhancement solutions, followed by brightfield imaging.

Results

Quantification of Antigen Binding

Using flow cytometry, the number of antigen binding sites for each cell line was determined, as displayed in **Figure 4-2**. Data for the MCF10A, SK-BR3, and JIMT-1 cell lines are being reused with permission from [27]. A one-factor ANOVA test indicated significant differences between cell lines in the number of binding sites ($p <$

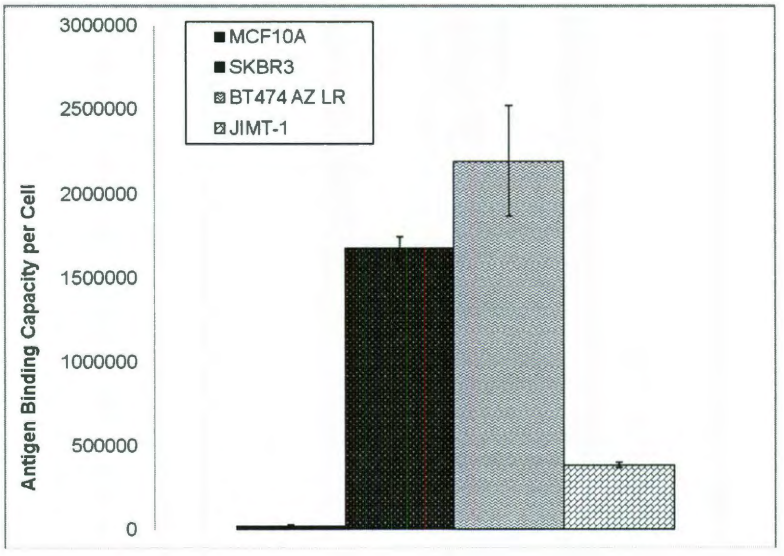

Figure 4-2. Anti-HER2 binding capacity of each breast cancer cell line, determined by flow cytometry. The HER2+ cell lines (SK-BR-3, JIMT-1, BT474 AZ LR) show a significantly higher binding capacity than the HER2- cell line (MCF10A). MCF10A, SKBR3, and JIMT-1 data adapted from [27, 154].

0.01). Each of the HER2+ breast cancer lines used in this study had a larger number of anti-HER2 binding sites than the normal epithelial cell line, MCF10A ($2.43 \times 10^4 \pm 3.77 \times 10^3$ receptors), by the Tukey comparison test ($p<0.01$). The BT474 AZ LR cell line had the greatest anti-HER2 binding capacity ($2.19 \times 10^6 \pm 3.25 \times 10^5$ receptors), followed by the SK-BR-3 ($1.68 \times 10^6 \pm 6.78 \times 10^4$ receptors) and then the JIMT-1 ($3.82 \times 10^5 \pm 1.47 \times 10^4$ receptors) cell lines. Notably, the JIMT-1 cell line has a significantly lower HER2 binding site expression when compared to the SK-BR-3 and BT474 AZ LR cell lines ($p < 0.01$).

Two Photon Microscopy of Nanoshell-Cell Binding

Nanoshell binding is evaluated through two-photon laser scanning microscopy in **Figure 4-3**. The figure shows phase contrast images overlaid with the two photon images. The cells incubated with media only demonstrate no nanoshell signal. The

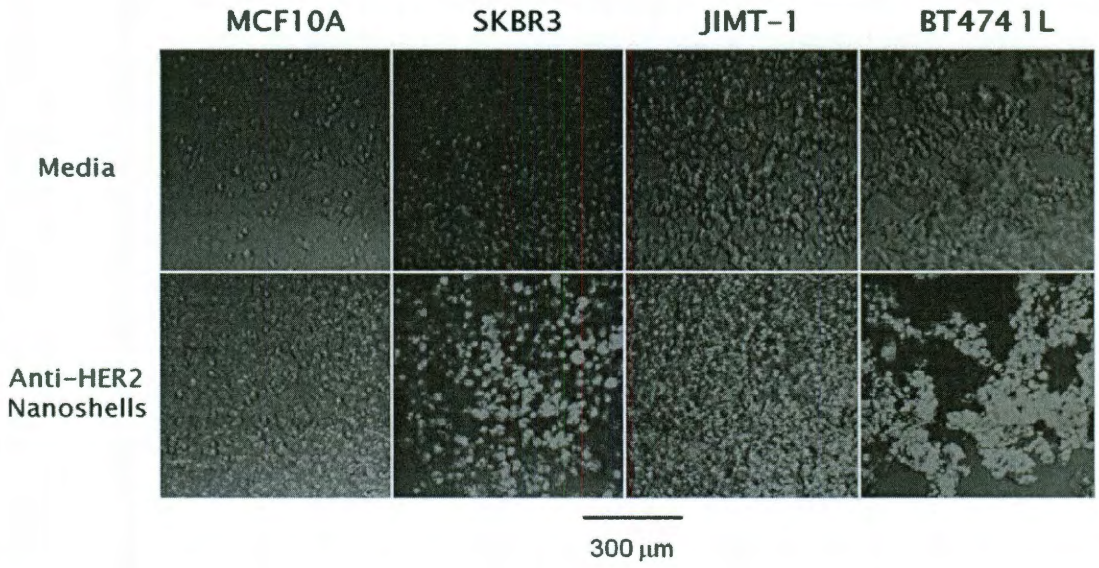

Figure 4-3. Verification of nanoshell binding using two-photon laser scanning microscopy. Images depicted are phase contrast images overlaid with two photon images, where red is nanoshell signal. SK-BR-3, JIMT-1, and BT474 AZ LR cell lines, all HER2+, show greater binding of the anti-HER2 nanoshells than the MCF10A normal epithelial cell line.

HER2+ cell lines incubated with nanoshells each show nanoshell signal, while the HER2- cell line shows significantly less. The SK-BR-3 and BT474 AZ LR cell lines show the most nanoshell binding. The JIMT-1 cell line demonstrates less nanoshell binding than the SK-BR-3 and BT474 AZ LR cell lines, but greater nanoshell binding than the MCF10A cell line. There is some degree of binding seen with the MCF10A cell line, but this binding is still significantly less than the HER2+ breast cancer cells.

Nanoshell-Mediated Cell Destruction of Trastuzumab-Resistant Cell Lines

Figure 4-4 shows the live/dead imaging and silver staining for the treatment and

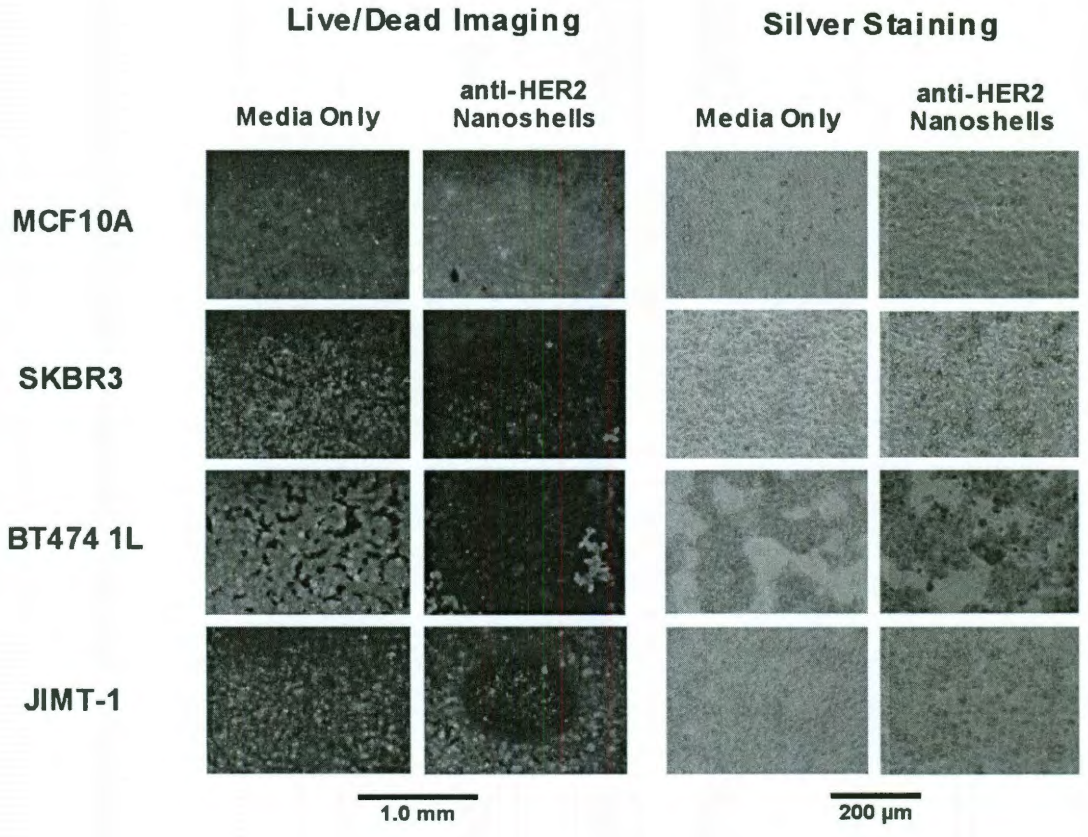

Figure 4-4. Photothermal therapy results. Live/dead imaging demonstrates cell ablation in HER2+ cell lines (SK-BR-3, JIMT-1, BT474 AZ LR) treated with anti-HER2 nanoshells and NIR laser irradiation (red ethidium homodimer stain = dead cells, green calcein stain = live cells). Silver staining shows nanoshell binding for each of the HER2+ cell lines.

media control group of each cell line. None of the media alone groups show evidence of cell death on the live/dead images or evidence of nanoshell binding on the silver stain. The silver staining confirms that nanoshells are bound to each of the HER2+ cell lines (SK-BR-3, BT474 AZ LR, JIMT-1), with minimal nanoshell binding to the HER2- MCF10A cell line. The MCF10A-nanoshell group does not demonstrate localized area of cell death, while each of the HER2+ breast cancer-nanoshell groups show a clearly defined region of dead cells (red) corresponding to the laser spot surrounded by non-irradiated, nanoshell-bound live cells (green).

Discussion

Anti-HER2 resistance continues to be a challenge for clinicians treating advanced cancers. Gold nanoparticle-mediated photothermal therapy could present new possibilities for cancers that are currently resistant to conventional chemotherapy and radiation treatments. The objective of this study was to demonstrate that immunoconjugated silica-gold nanoshells can effectively destroy both chemotherapy-sensitive and chemotherapy-resistant breast cancer cell lines. Two trastuzumab-resistant breast cancer cell lines were selected for testing, JIMT-1 and BT474 AZ LR. A trastuzumab-sensitive breast cancer cell line, SK-BR-3, and a HER2 negative normal epithelial cell line, MCF10A, were also chosen as positive and negative binding controls. Each of the HER2+ breast cancer cell lines selected were effectively ablated using nanoshell-mediated photothermal therapy. These results suggest gold nanoparticle-mediated photothermal therapy may have potential to be employed against chemotherapy resistant breast cancers *in vivo*.

As the first step of this study, we evaluated nanoshell binding efficiency using two-photon laser scanning microscopy. Silica-gold nanoshells have demonstrated two-photon properties, and can be used to label HER2+ breast cancer cells *in vitro*.[25, 26] Nanoshell binding has also been demonstrated using darkfield microscopy [28] and optical coherence tomography,[15] which depend on the enhanced scattering of the nanoshells for contrast. However, for future *in vivo* studies, two-photon luminescence may prove superior in bulk tissue to these scatter-based techniques. This is due to the improved signal to noise ratio of two photon microscopy, as well as its demonstrated ability to more effectively investigate the nanoshell distribution within the tumor with the assistance of software.[26] In **Figure 4-3**, we observe that the antiHER2 conjugated silica-gold nanoshells bind specifically to trastuzumab-resistant HER2+ breast cancer cell lines, with very little binding to the normal breast epithelial cell line, MCF10A (**Figure 4-3** and **Figure 4-4**). The degree of nanoshell binding shown by both the two-photon and silver stain images seems to correlate with the HER2 antigen binding capacity of the breast cancer cell lines. The JIMT-1 cell line has the lowest anti-HER2 binding capacity of the three breast cancer lines studied. Nagy et al found that only 20% of HER2 receptors are available for trastuzumab binding due to obstruction of the extracellular component of the HER2 receptor by MUC4.[148] Despite this, anti-HER2 nanoshell binding is still clearly seen in both the two-photon and silver stain images, though to a lesser degree than the other two HER2+ lines. Importantly, this lesser degree of binding is still sufficient for the photothermal destruction of the JIMT-1 cells, while the action of trastuzumab is impaired against these cells.[148] In the case of the BT474 AZ LR cell line, the nanoshell binding is more than adequate to ensure cell death upon NIR laser

irradiation. Photothermal therapy is also effective against the BT474 AZ LR cell line, while the action of both trastuzumab and lapatinib, a second generation agent, are impaired against these cells.

Using silica-gold nanoshells as a mediating absorptive agent for photothermal therapy has advantages over conventional hyperthermia treatments. In **Figure 4-4**, the ablated areas (red) are surrounded by living, healthy cells (green), and cell lines with minimal or no nanoshell binding show no regions of cell death. Only HER2+ cells with bound nanoshells in the region of the laser spot are ablated. Targeting the gold nanoparticles with an antibody or peptide permits single cell specificity *in vitro*.[21, 112] This specificity is important during *in vivo* studies, when healthy tissues such as skin will be in between the laser and the cancerous tissue. Because nanoshells efficiently absorb the irradiating laser energy and convert it to heat, the laser power requirements to induce cell death are lowered. In conventional hyperthermia treatments, this specificity is lacking, as the power of the irradiating energy source must be high enough to kill cells without the assistance of a mediating agent. Thus, using nanoshells as part of photothermal therapy *in vitro* lowers the power requirements of the irradiating energy, as well as increasing the specificity of therapy for malignant cells.

Figure 4-4 does demonstrate some variation in the size of the ablated regions. This variation was seen consistently among several replicate experiments. These differences are likely due to variations in the laser intensity distribution, the degree of cell confluence, and density of HER2 receptors on the cell surfaces. In order for cell death to occur, a temperature of 70-80° C must be achieved for approximately 4 minutes.[36] The net temperature increase of the cells within the laser spot is dependent on a combination

of variables, including: the absorptive cross-section of the silica-gold nanoshells, the physical distribution of the nanoshells among the cells, the intensity and duration of the laser illumination, and the heat transfer and dissipation properties of the cells and media.[155] Non-uniform laser intensity could lead to cells at the periphery of the spot receiving less laser power,[156] resulting in the minimum temperature and duration needed for cell death not being achieved. However, the laser spot size, power, and duration were held consistent throughout each of the treatment groups and experiments, so it is unlikely that in this case it is a large contributor to the variation seen in ablation. The nanoshell binding density could also be playing a significant role, and, based on the information in **Figure 4-2** and **Figure 4-3**, is a likely contributor to the variation in ablated area size.

The low anti-HER2 binding capacity of the JIMT-1 cell line versus the higher binding capacities of the SK-BR-3 and BT474 AZ LR cell lines correlates with the small ablated area for the JIMT-1 cells and the larger ablated areas for the SK-BR-3 and BT474 AZ LR cells. This supports the nanoshell binding density being a major contributor to the variation in ablation size. However, although the SK-BR-3 cell line has a lower anti-HER2 binding capacity than the BT474 AZ LR cell line, the size of the ablated area for this cell line is larger. This could be due to several factors. Some of this variation may be due to the differences in how the SK-BR-3 and BT474 AZ LR cell lines tend to grow. The SK-BR-3 cells grow in a monolayer, while the BT474 AZ LR cell line tends to grow in conglomerates. These growth differences may have resulted in different heating profiles between the two cell lines, affecting the sizes of the ablated regions. Another possible contributing factor is differences in thermal sensitivity between the SK-BR-3

and BT474 AZ LR cell lines, which has been seen in response to conventional hyperthermia treatments in tumors resected from breast cancer patients.[157] Regardless of variation in the size of the ablated regions, each of the HER2+ breast cancer cell lines was successfully ablated using nanoshell-mediated photothermal therapy. Each of these variables (laser intensity profile, nanoshell binding density, the tumor cell density/ tumor shape, the thermal sensitivity of the tumor) will need to be considered in applying and optimizing nanoshell-mediated therapy to trastuzumab-resistant cancers *in vivo*.

Conclusions

The successful application of gold nanoshell-mediated photothermal therapy to trastuzumab-resistant breast cancer cells *in vitro* suggests a promising new approach for the treatment of advanced HER2+ breast cancers. By virtue of its physical means of destroying cancer, nanoshell-mediated thermal ablation of these types of cancer has an innate advantage over trastuzumab, lapatinib and other antibody or small molecule-based therapies. Gold nanoparticle-mediated photothermal therapies also have demonstrated synergistic cell killing in combination with chemotherapy *in vitro* and radiation *in vivo*,[152, 158] suggesting that the combination of conventional treatments and this technology could also be beneficial for cancer therapy.

CHAPTER 5[d]

T CELLS AS IN VIVO GOLD NANOPARTICLE DELIVERY VEHICLES

Introduction

As discussed in detail in Chapter 2, attempts at augmenting gold nanoparticle tumor delivery have included a variety of nanoparticle surface modifications, including conjugation with antibodies[7] and other tumor targeting molecules [6]; however, inclusion of targeting ligands has only modestly improved tumor accumulation and specificity. This is likely due to the reliance of these nanoparticles on passive accumulation through EPR, which is highly dependent on adequate blood flow to the tumor. Therefore, tumors or tumor regions that exhibit poor vasculature and hypoxia are less likely to be effectively targeted using nanoparticles, ultimately limiting their therapeutic use.

Choi et al. recently demonstrated that macrophages could be used as a cellular delivery vehicle to deposit AuNPs in tumors and hypoxic tumor tissues, facilitating delivery through active cellular migration and extravasation in response to chemotactic factors produced by malignant cells.[119] These encouraging results suggested that other immune cells might be used as cellular delivery vehicles. In this study, we assessed the capacity of activated T cells to function as chaperones for AuNPs. Unlike macrophage, T cells are readily isolated and expanded *in vitro*, and upon infusion, circulate throughout the body and migrate into tumors in response to tumor-associated chemokines. This

[d] Adapted from: Kennedy LC*, Bear AS*, Young JK, Lewinski NA, Kim J, Foster AE, Drezek RA, "T Cells Enhance Gold Nanoparticle Delivery to Tumors *in vivo*"; Nanoscale Research Letters, 6:283 (2011).

tumor-tropic property permits their use as cellular vehicles for the delivery of molecular therapeutics.[159-162]

Combining the advantages of T cells with nanotechnology has the potential to generate innovative new approaches to cancer therapy. Several studies have demonstrated that T cells may serve as efficient drug delivery vehicles for the treatment of cancer, including transport of magnetic particles bearing doxorubicin and for use in boron neutron capture therapy.[163, 164] Here we have explored whether T cells can be used as AuNP carriers to increase delivery to tumor sites *in vivo* using gold colloidal nanospheres (40-45 nm), comparable in size to hollow gold nanoshells and gold-gold sulfide nanoparticles used for PTT. Although gold colloid in this size range has maximal absorbance in the visible wavelengths, there are several variants of AuNPs that are of similar size (25-60 nm) and absorb optimally in the NIR region, permitting translation of this delivery method for PTT. These gold nanoparticle variants include gold–gold sulfide nanoparticles, hollow gold nanoshells, and gold nanocubes, all of which have demonstrated efficacy as PTT-mediating agents in mouse studies.[165] Additionally, there have been studies demonstrating photothermal therapy using gold colloid that has been strategically aggregated to red-shift the peak absorbance into the NIR.[62, 63]

The possible applications of a AuNP-T cell delivery system could further be extended to imaging and drug delivery applications, as gold nanoparticles also have demonstrated potential as scatter- and absorption-based imaging contrast agents[15, 26, 36, 60] and drug delivery agents[166]. In this study, we demonstrate that gold colloid is readily taken up by activated human T cells without impairing their viability or cellular

functions, and that following intravenous infusion into tumor bearing micecan more efficiently deliver AuNPs to distant tumor sites.

Methods

In vitro Characterization Studies

AuNP Synthesis and PEGylation

Gold(III) chloride trihydrate ($HAuCl_4 \cdot 3H_2O$ 99%) and potassium carbonate anhydrous (K_2CO_3 99%) were purchased from Sigma-Aldrich (St. Louis, MO). Deionized water was provided by a Milli-Q system. In this synthesis method, Au^{3+} is reduced to Au^0 using CO as a reducing agent. A 0.38 mM $HAuCl_4$ solution was prepared and aged in an amber bottle at 4°C for a minimum of 72 h prior to use. After aging the chloroauric acid solution, the temperature was allowed to gradually rise to 16°C. A 1.8 mM K_2CO_3 solution was then prepared by adding 75 mg of K_2CO_3 to the aged 200 mL $HAuCl_4$ solution. This solution was aged for 30 min prior to aeration with CO gas. A 40 mL volume of the aged solution was added to the beaker and stirred continuously prior to aeration. CO gas (Matheson-Trigas) was injected into the continuously stirring solution at a flow rate of 30.5 mL/min. The CO flow was controlled via a flow rate control valve. A visible color change from clear to dark purple to red is observed during synthesis, indicating formation of AuNPs. TEM images were taken to confirm size and monodispersity. Particles were sterilized by filtration through a 0.22 μm polyethersulfone filter. To stabilize the particles in preparation for mouse injection, 0.5 mM polyethylene glycol-thiol (PEG-SH, MW = 5 kD, Nektar) was added to the

particles. After a 24-h incubation, excess PEG-SH was removed by centrifugation and PEGylated particle stability was confirmed by increasing solution tonicity with 1 M NaCl. Dynamic light scattering measurements were taken to assess the hydrodynamic diameter of the PEGylated gold colloid.

T Cell Isolation and Preparation

Peripheral blood was obtained with informed consent from willing healthy donors using a Baylor College of Medicine Institutional Review Board approved protocol. Peripheral blood mononuclear cells (PBMC) were isolated by Ficoll gradient centrifugation (Lymphoprep, Nycomed, Oslow, Norway). PBMC were used to generate EBV-transformed B cells lines (LCL) and T cell lines. LCL and T cells were maintained in RPMI 1640 supplemented with 10% fetal calf serum (FCS; Hyclone, Logan, UT) and 2 mM GlutaMAX (Invitrogen, Carlsbad, CA). For T cell expansion, non-tissue culture treated 24-well plates were coated with OKT3 (1 μg/mL; Ortho Pharmaceuticals, Raritan, NJ) and anti-CD28 antibody (1 μg/mL; BD Biosciences, San Diego, CA) overnight at 4°C. Plates were washed and 2×10^6 PBMC were plated per well in complete RPMI supplemented with 100 U/mL recombinant human interleukin-2 (IL-2). On day 3, T cell blasts were harvested and further expanded or transduced in IL-2 supplemented media.

T Cell Internalization of AuNPs

Day 7 OKT3 blasts were harvested and suspended in complete RPMI supplemented with IL-2 and 0, 0.05, 0.1, 0.25, 0.5, or 1 nM of AuNPs for 24 h (1 mole = 6.022×10^{23} nanoparticles). Cells were harvested and washed a minimum of three times using 1× phosphate-buffered saline (PBS) prior to subsequent experiments. To confirm loading, T cells were imaged using darkfield microscopy. To quantitatively

characterize loading, 2×10^6 T cells per sample were prepared for ICP-OES analysis by digesting the cells in three parts trace metal grade hydrochloric acid (Fisher Scientific, Pittsburgh, PA) and one part trace metal grade nitric acid (EMD Chemicals, Gibbstown, NJ) overnight. Samples were then diluted to 10 mL in distilled water and filtered. T cells incubated with media alone were used as a control.

T Cell Viability and Functionality after AuNP Loading

To determine the effect of AuNP loading on T cell phenotype, we used the following monoclonal antibodies conjugated to FITC, PE, PerCP, or APC (BD Biosciences): CD3, CD4, CD8, CD45RA, CD45RO, CD56, CD62L, CCR5, and CCR7. An Annexin V apoptosis detection kit (BD Biosciences) was used to determine T cell viability post-AuNP loading. Cells were analyzed using a FACSCalibur flow cytometer (BD Biosciences) and FCSExpress software (De Novo Software, Los Angeles, CA). A [^{3}H] thymidine incorporation assay was used to assess the effects of AuNP loading on T cell proliferation. Following AuNP loading, T cells were seeded in triplicate into 96-well round bottom plates at 1×10^5 cells per well in complete RPMI containing 100 U/mL IL-2 for 24 h. T cells were then pulsed with 5 μCi [^{3}H] thymidine (Amersham Pharmacia Biotech, Piscataway, NJ) overnight. Cells were then harvested onto glass filter strips and analyzed using a TriCarb 2500 RT β-counter (Packard Biosciences, Downers Grove, IL).

To determine if AuNP-loaded T cells retain the ability to migrate *in vitro*, we used a transwell migration assay. T cells were labeled with 50 μCi Chromium^{51} (Cr^{51}; MP Biomedicals, Solon, OH) and 1.5×10^5 cells were placed in the upper chamber of 24-well 6.5 mm diameter, 5 μm pore size transwell chambers (Costar Transwell, Corning, NY). Media alone or LCL tumor supernatant was placed in the bottom chamber. Plates were

then incubated for 3 h at 37°C. Cells in the bottom chamber were then harvested and analyzed using a γ-counter (Cobra Quantum, Perkin Elmer, Shelton, CT). Specific migration was calculated using the following equation: Specific Migration (%) = (Experimental [LCL supernatant] – Spontaneous [media alone])/(Maximum [1.5×10^5 cells] – Spontaneous [media alone]) × 100. To measure the ability of AuNP-loaded T cells to secrete IFN-γ following mitogenic stimulation, 2×10^5 T cells were seeded into 96-well round bottom plates for 24 h. T cells were then stimulated with 25 ng/mL phorbol myristate acetate (PMA; Sigma-Aldrich, St. Louis, MO) and 1 μg/mL Ionomycin (I; Sigma-Aldrich). Following 2 h of PMA-I stimulation, Brefeldin A (Sigma) was added to allow for intracellular cytokine retention. Four hours later, cells were permeabilized using 1% Saponin (Sigma) and IFN-γ expression was detected by intracellular cytokine staining using PE-conjugated anti-IFN-γ monoclonal antibody (BD Biosciences).

In vivo Delivery Studies

SCID Xenograft Model

In vivo migration, AuNP delivery, and biodistribution studies were performed using severe combined immune deficient mice (SCID [strain ICR-Prkdc(scid)]; Taconic, Hudson, NY). All mouse experiments were performed under a Baylor College of Medicine Institutional Animal Care and Use Committee (IACUC) approved protocol. 1×10^7 LCL tumor cells were resuspended in Matrigel (BD Biosciences) and injected subcutaneously (s.c.) into the shaved right flanks of mice. Tumors were allowed to establish and grow to at least 0.5 mm × 0.5 mm in size (2-3 weeks) before use.

Mouse Injections and Sample Collection

To prepare AuNP-T cell injections, T cells were prepared as above and incubated with 0.5 nM AuNPs for 24 hours. Cells were harvested and washed extensively using 1× PBS prior to injection. For delivery studies, mice received either PBS, 1×10^7 AuNP-T cells, or 1×10^{11} PEGylated AuNPs via the tail vein in a 200 µL bolus. These dosages were selected based on previous *in vivo* studies using AuNPs and adoptively transferred T cells. To determine optimal time points for delivery analysis, tumors were resected at either 4, 8, 24, or 48 hours for the PEGylated AuNP group and 24 or 48 hours for the AuNP-T cell group. In addition, plasma as well as portions of the liver, spleen, kidneys, small intestine, muscle, heart, lung, bone, and brain were also collected for analysis at 4, 8, or 24 hours for the PEGylated AuNP group and 24 or 48 hours for the AuNP-T cell group. All tissues, including tumors, were flash frozen with liquid nitrogen after collection and stored at -80°C until analysis.

Bioluminescent Imaging

To determine if AuNP-loaded T cells can migrate to tumors *in vivo* and thereby deliver AuNP to the tumor site, T cells were transduced with retrovirus encoding GFP*luc* as previously described by our group [167]. Transduced cells were then loaded with AuNPs for 24 h then injected intravenously (i.v.) via the tail vein (1×10^7 T cells per mouse). Forty-eight hours post-T cell infusion, the biodistribution of T cells was visualized using the *In Vivo* Imaging System (IVIS; Xenogen) following intraperitoneal (i.p.) injection of 150 mg/kg D-luciferin (Xenogen, Alameda, CA).

Ex vivo Tissue Analysis and Imaging

To image AuNP-T cells within the tumor, tumors were thawed in a 37°C water bath and embedded in optimal cutting temperature (O.C.T.) compound (Sakura Finetek USA, Inc., Torrence, CA) using dry ice. The embedded tissue was then sectioned into 8 μm slices using a cryostat, dried overnight at room temperature, and stored at -80°C. Tissue sections were then fixed with acetone and stained for CD3 using anti-CD3 (Abcam ab5690, Cambridge, MA) as the primary antibody and the Invitrogen Histostain® Plus Broad Spectrum (AEC) kit. Slides were coverslipped with immunomount (Thermo Scientific, Pittsburgh, PA) and imaged by bright field and dark field microscopy. Resected mouse tissues were prepared and analyzed for gold content using ICP-MS and ICP-OES. Samples were lyophilized and weighed, then digested and prepared as previously described. Samples of the AuNP-T cell and AuNP boluses were also analyzed to confirm the amount of gold systemically administered.

Statistical Methods

For the biodistribution analysis, we performed a one-way ANOVA followed by Tukey's method. Each organ was examined individually at various time points for each treatment group ($n = 3$ for all time points and treatment groups). Significance was set at $P < 0.05$. An asterisk indicates significant differences between every possible AuNP:AuNP-T cell comparison pair at all time points for each organ. For the tumor delivery analysis, we used a Student's *t*-test to compare AuNP systemic administration to AuNP-T cell delivery. For this study, $n = 8$ for the AuNP group, while $n = 11$ for the AuNP-T cell group.

Results

Loading of Activated Human T Cells with AuNPs

Synthesized gold colloid was determined to be 40-45 nm in diameter by transmission electron microscopy (TEM) (**Figure 5-1**). Activated and expanded human T cells were cultured in the presence of AuNPs for a period of 1 to 24 h to permit AuNP internalization. AuNP loading was confirmed using bright field and dark field microscopy demonstrating that T cells co-localize with AuNPs (**Figure 5-2**). We further optimized loading conditions by altering AuNP concentration To determine the number of nanoparticles present per T cell, an inductively coupled plasma optical emission spectrometry (ICP-OES) analysis was used. T cells from three different human donors were first cultured with concentrations of AuNPs ranging from 0.05 to 0.5 nM for a period of 24 h to evaluate for variability in gold nanoparticle loading due to differences in T cells from different donors (Figure 1c). A maximum of 14,900 ± 2,400 AuNPs was internalized per T cell using a AuNP loading concentration of 0.5 nM (**Figure 5-3**).

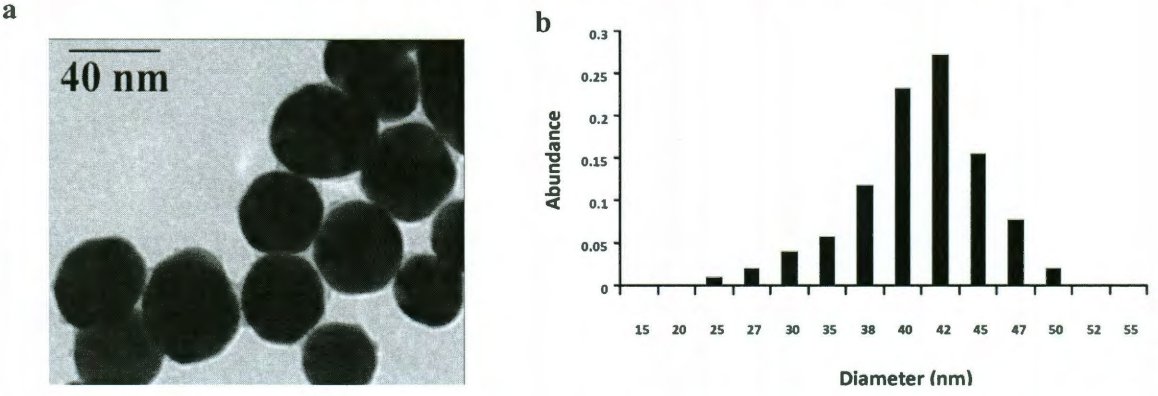

Figure 5-1. Gold nanoparticle characterization. a) TEM imaging of gold colloid (diameter = 40-45 nm). b) Gold colloid size distribution. Particle sizes were determined using TEM. A total of 585 particles were examined over multiple images to generate the histogram.

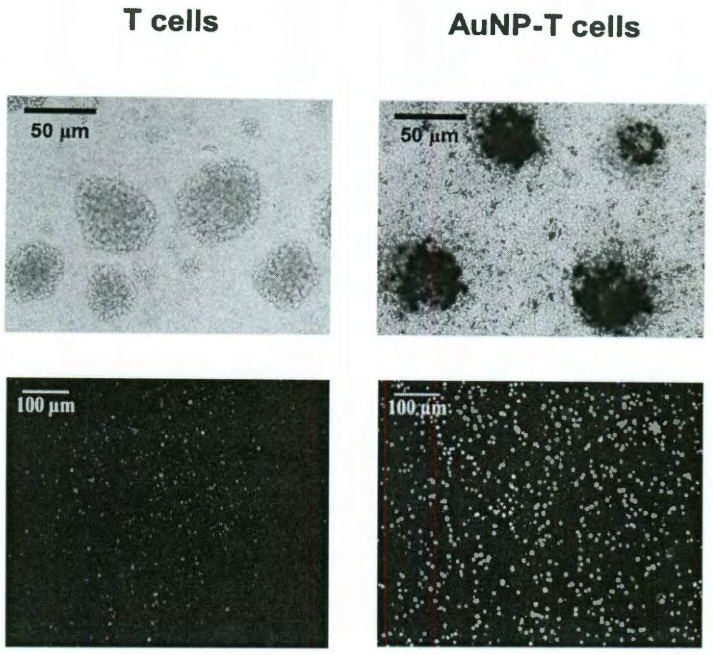

Figure 5-2. Brightfield (upper) and darkfield (lower) images of human T cells demonstrate gold nanoparticle uptake by the increased light scattering seen in the AuNP-T cell group compared to T cells alone.

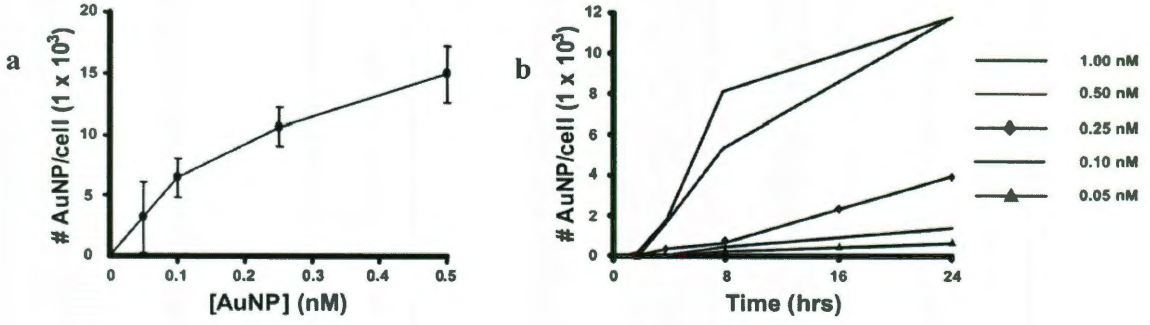

Figure 5-3. a) ICP-OES analysis of T cell gold content at 24 h using different nanoparticle loading concentrations. Each point is a composite of data acquired from three different T cell donors. b) Time course data for T cells from a single donor loaded with different concentrations of gold nanoparticles. Optimal loading occurred after 24 h at a concentration between 0.5 and 1.0 nM.

We then performed a time course study using T cells from a single donor to determine the minimum amount of time required to load the T cells with the maximum number of AuNPs (**Figure 5-3**). For this study, we incubated T cells with nanoparticle concentrations ranging from 0.05 to 1 nM. At 24 h, the 0.5 and 1 nM groups have similar

gold content, suggesting that there is a maximum amount of AuNPs that can be internalized by T cells. These results demonstrate that maximal AuNP loading of T cells can be achieved using a concentration of 0.5 nM AuNP and an incubation period of 24 h.

AuNP-Loading Does Not Affect T cell Viability or Function

We next measured T cell viability and function post-AuNP loading to assess potential toxicity that may inhibit T cell performance as an *in vivo* delivery vehicle. Loading T cells with AuNPs had no immediate effect on T cell viability as determined by Annexin-V/7-AAD staining (**Figure 5-4**) and did not alter the phenotype of the cells

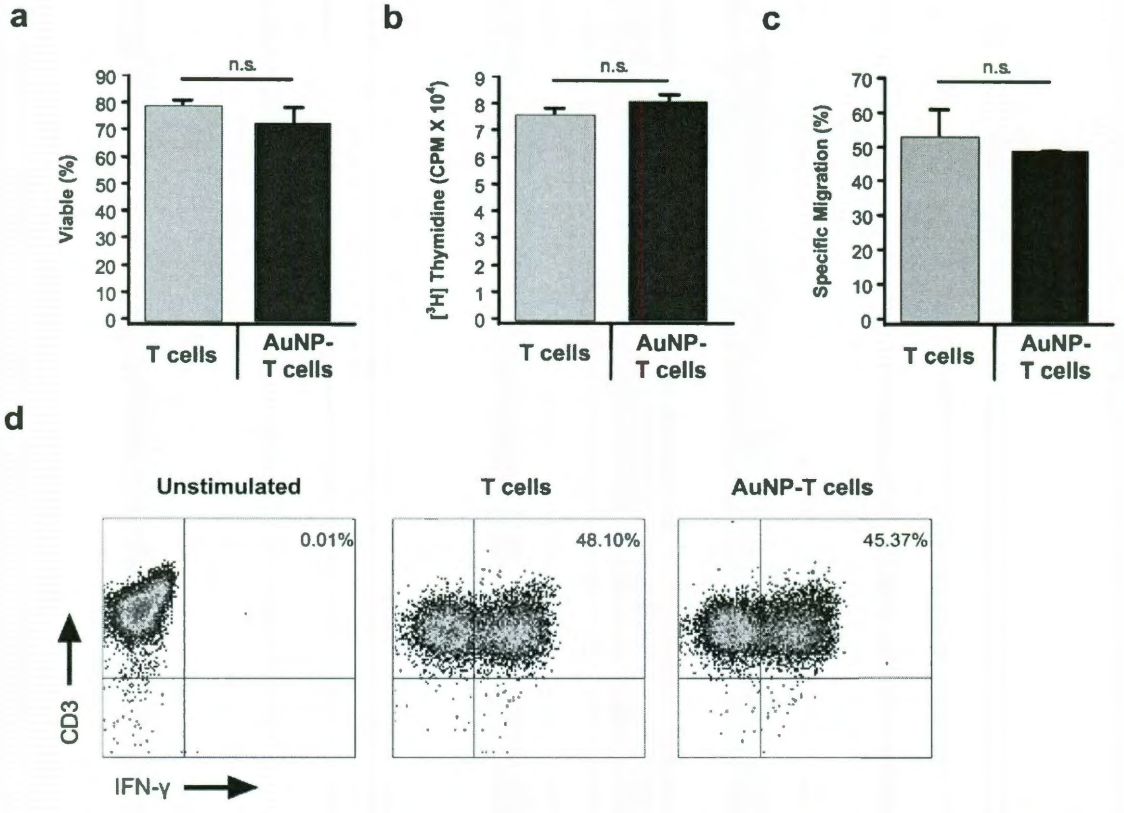

Figure 5-4. AuNP loading has no significant effect on T cell viability or function. T cells were loaded in the presence of 0.5 nM AuNPs for 24 h or cultured in medium alone and then measured for viability using Annexin-V/PI staining, b) proliferation using thymidine incorporation, c) migration through a transwell membrane in response to tumor (LCL) produced supernatant, and d) intracellular analysis of IFN-γ cytokine production following mitogen stimulation.

(**Figure 5-5**). Furthermore, there were no prolonged effects on T cell proliferation as measured by thymidine incorporation (**Figure 5-4**). Importantly, AuNPs did not affect migration when tested in a transwell chemotaxis assay against supernatant produced from human LCL tumors, suggesting that T cells retain their migratory behavior post-AuNP loading (**Figure 5-4**). Finally, production of IFN-γ following mitogen activation (PMA-I) was not impaired by AuNPs (**Figure 5-4**). These results show that AuNPs have no detrimental effects on T cell viability and function *in vitro* and indicate that T cell migration *in vivo* will likely be retained following loading.

T Cells Migrate and Transport AuNPs to Tumors *in vivo*

In vivo AuNP-T cell migration to tumor sites was first examined using bioluminescent imaging and histology. T cells were first genetically modified to express

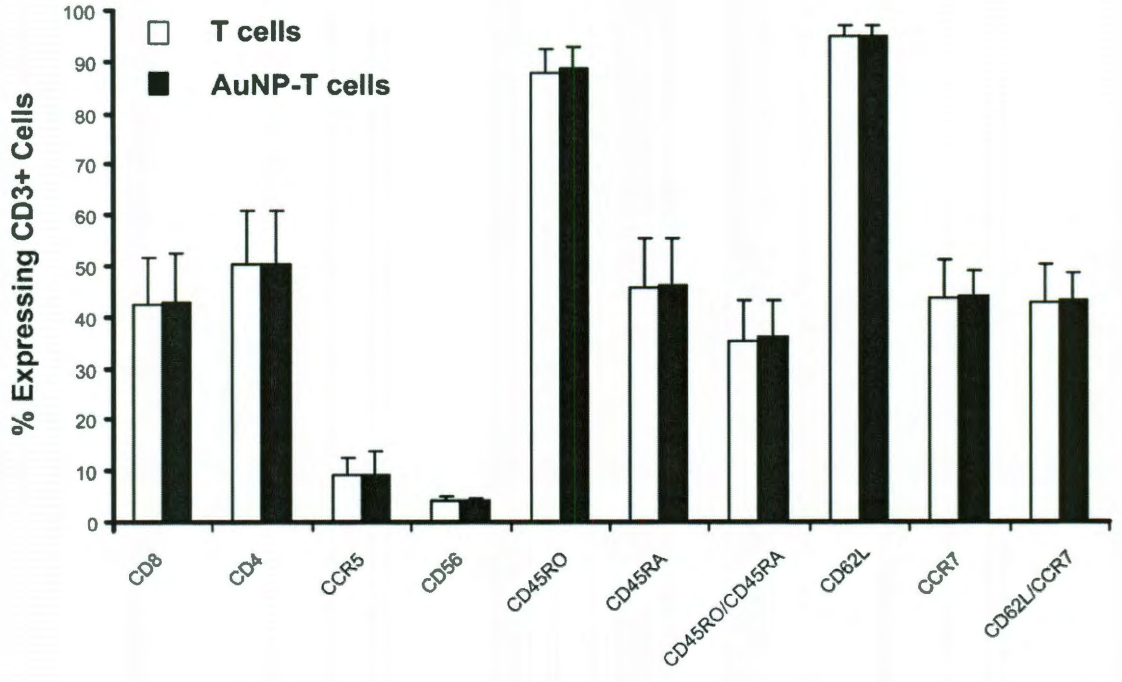

Figure 5-5. AuNP-loading does not affect T cell phenotype. T cells were loaded in the presence of 0.5 nM AuNP for 24 h and subsequently stained with a panel of antibodies and analyzed by flow cytometry.

firefly luciferase and then subsequently loaded with AuNPs. Bioluminescent imaging 48 h post-intravenous injection of AuNP-T cells demonstrate specific migration of the T cells to subcutaneous LCL tumors in immune deficient SCID mice (**Figure 5-6**). This timepoint was selected based on previous studies that have demonstrated T cell localization to tumor sites 48 h post-infusion.[168, 169] We next resected the tumors and performed histology to determine if AuNPs and T cells co-localized within the tumor. Immunohistochemical staining using CD3 antibody (a pan-T cell marker) demonstrated infiltration of T cells into the tumor (**Figure 5-6**). In addition, areas of increased scatter in the darkfield images correlated well with areas of $CD3^+$ staining. This observation demonstrates that the T cells maintain internalized AuNPs during *in vivo* migration to the tumor site.

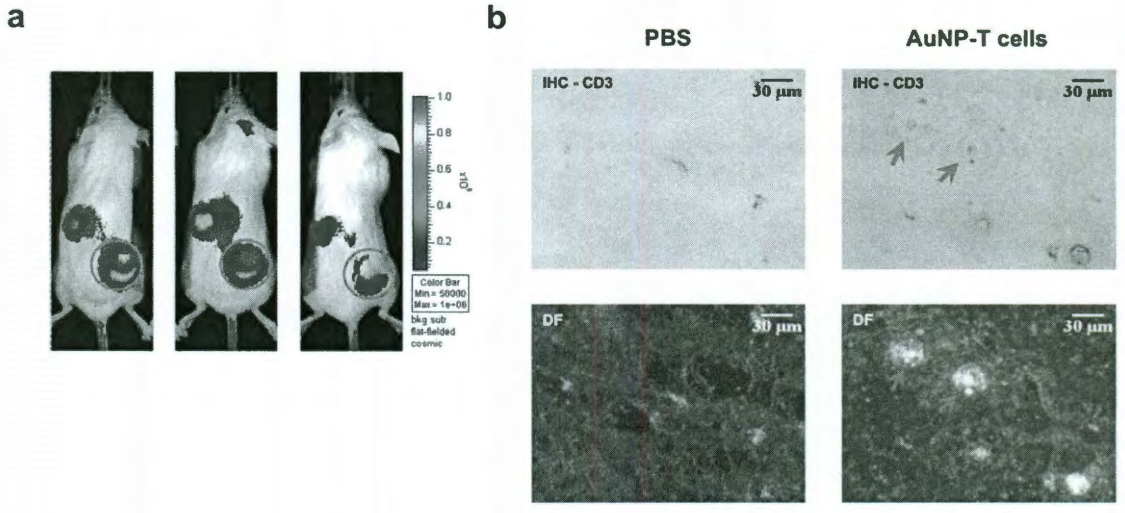

Figure 5-6. AuNP-loaded T cells migrate to tumors *in vivo*. a) T cells were retrovirally modified to express firefly luciferase then loaded in the presence of 0.5 nM AuNP for 24 h. Cells were subsequently injected intravenously into SCID mice bearing subcutaneous xenografted LCL tumors. Bioluminescent imaging of AuNP-T cell biodistribution at 48 h post-injection showing AuNP-T cell localization at the tumor site (red circle) and within the spleen. b) Resected tumors were analyzed by bright field imaging (top row) and immunohistochemistry for human CD3 expression and dark field imaging (bottom row) to indicate the presence of AuNPs. Red arrows indicate the colocalization of $CD3^+$ T cells and AuNPs within the tumor.

Delivery of AuNPs by T Cells Alters Nanoparticle Biodistribution

We next performed a comprehensive *in vivo* biodistribution study using inductively coupled plasma mass spectrometry (ICP-MS) and ICP-OES to map the location of free PEGylated AuNPs (40-45 nm gold colloid coated with 5000 MW PEG) and AuNPs delivered by T cells. Prior to injection, ICP-OES was performed to determine the absolute gold dose for PEG-AuNPs and AuNP-T cells. Following intravenous injection with PEG-AuNPs or AuNP-T cells, tumors, and organs (bone, brain, heart, intestine, kidney, liver, lungs, muscle, plasma, and spleen) were harvested and analyzed for gold levels using ICP-MS. For PEG-AuNP treated mice, organs were harvested at 4, 8, 24, and 48 h post-injection, while for AuNP-T cell treated mice, organs were harvested at 24 and 48 h (**Figure 5-7**). Predictably, the biodistribution of AuNP-T cells is altered when compared to that of the PEG-AuNPs. As observed in previous studies,[107, 170] the highest percentages of AuNPs using PEG coating were delivered to the liver and spleen (5.65 and 17.03% of the injected dose, respectively, at 48 h, **Figure 5-7**). In comparison, T cells delivered AuNPs to the lung, liver, and spleen, which received 4.76, 33.5, and 2.69% of the injected dose at 48 h, respectively (**Figure 5-7**). The plasma half-life of the PEG-AuNPs was calculated to be 6.05 h, and no gold was detected in the plasma for the AuNP-T cell group, suggesting no significant AuNP leakage from the T cells during *in vivo* migration. The AuNP-T cell biodistribution over time correlates with the normal biodistribution of human T cells, suggesting that the presence of internalized AuNPs does not significantly change the T cell biodistribution.[168] These data suggest that cellular delivery of AuNP will result in a unique biodistribution pattern that is dependent on the cell type used for delivery.

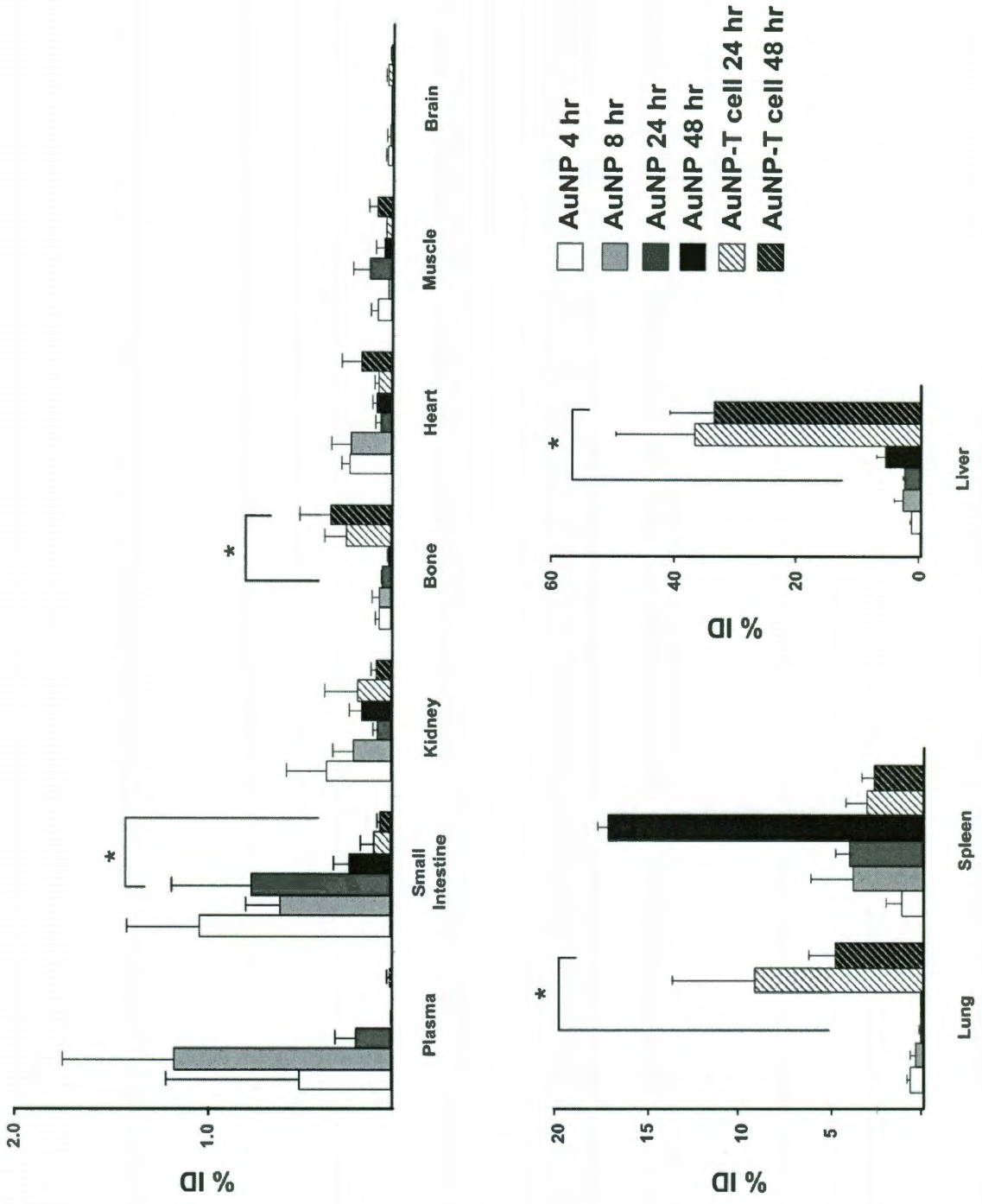

Figure 5-7. Biodistribution comparison of AuNPs and AuNP-T cells in mice. Mice were injected with PEG-AuNPs (60-65 nm hydrodynamic diameter), AuNP-T cells, or PBS and subsequently sacrificed at various time points to determine biodistribution. PBS gold levels were negligible in comparison to AuNP and AuNP-T cell groups for all organs. Values are percentage of the injected gold dose (%ID) were calculated from ICP-MS and are normalized for dry weight differences. The AuNP-T cell group exhibited significantly higher gold delivery to the lungs, liver, and bone, while the AuNP group demonstrated higher gold levels within the small intestine. No significant differences were seen in the spleen, kidney, muscle, or brain. An asterisk indicates statistically significant ($P < 0.05$) differences.

T Cell Delivery Increases Tumor Accumulation of AuNPs

Closer examination of LCL tumors following treatment with either PEG-AuNPs or AuNP-T cells showed an increase in AuNP delivery to tumors following cellular transport. For PEG-AuNPs, the highest level of accumulation in tumors was observed at 24 h post-injection, while peak tumor gold accumulation following T cell delivery was seen at 48 h. Using PEG-AuNP, ICP-MS analysis of gold content of excised tumor tissue showed that $0.39 \pm 0.33\%$ of the injected dose reached the tumor at 24 h. Whereas, using AuNP-T cells, $1.55 \pm 0.72\%$ of the injected dose localized to the tumor at 48 h ($P < 0.01$) (**Figure 5-8**). This represents a four-fold increase in the efficiency of AuNP delivery to the tumor site using T cells as vehicles.

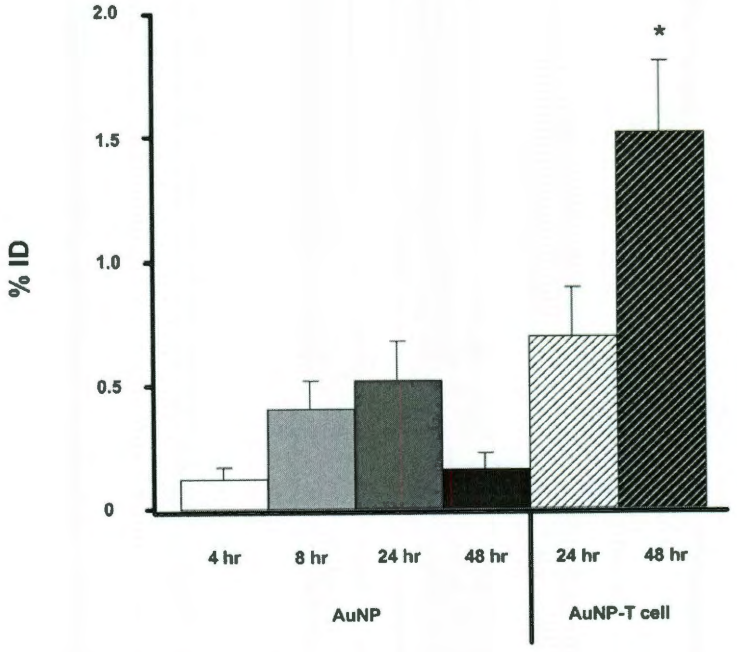

Figure 5-8. AuNP-T cells enhance the delivery of gold nanoparticles to the tumor site *in vivo*. Tumor-bearing mice were injected i.v. with PEG-AuNPs or AuNP-T cells. Tumors were subsequently resected at various time points and measured for AuNP content using ICP-MS. Values displayed represent the percentage of injected gold normalized for tumor dry weight differences (mean ± SEM). The percentage of gold delivered by the AuNP-T cells at 48 h represents a significant, four-fold increase over the PEG-AuNP group at 24 h ($P < 0.01$).

Discussion

One of the greatest challenges of translating nanotechnologies to the clinical realm is optimizing *in vivo* delivery. Maximizing AuNP accumulation at the tumor site has the potential to enhance photothermal cancer therapy, as well as other applications such as optical imaging. In this study, we show that human T cells can be used to transport AuNPs to distant tumor sites following intravenous administration. Following short term incubation with AuNPs, T cells can be efficiently loaded with over 14,000 AuNPs per cell without affecting cell viability, proliferation, and cytokine production. Importantly, T cells loaded with AuNPs retain their ability to migrate *in vitro*, and demonstrate tumor-specific homing in mice. Using T cells as a vehicle to deliver AuNPs resulted in a four-fold increase in the efficiency of AuNP tumor accumulation, demonstrating that active transport of AuNPs by cellular chaperones is superior to that of passive accumulation through the EPR effect.

Stephan et al. recently demonstrated that synthetic drug-carrier nanoparticles could be stably conjugated to the surface of immune cells, including T cells, for delivery of therapeutic molecules.[169] In these studies, T cells efficiently carried surface-tethered nanoparticles to tumors in mice, and when loaded with cytokines to support T cell growth, dramatically increased antitumor efficacy. However, our study conclusively demonstrates *in vivo* that internal loading of AuNPs in T cells can improve tumor localization, and thus may be a useful technology for a variety of nanoparticle based therapies.

In this study, we elect to use AuNPs. AuNPs are known to have low cytotoxicity, and gold has been used in humans for the treatment of arthritis for over 50 years,[171]

which makes AuNPs a logical choice in the pursuit of clinical applications. For this study, 40-45 nm gold colloidal nanospheres were selected for internalization by activated human T cells. The internalization of nanoparticles by cells is believed to be accomplished predominantly by receptor-mediated endocytosis, and particle size is an important variable in determining the kinetics of cellular uptake, with maximal uptake in a size range of 40-50 nm.[98, 172] We selected the size of our AuNPs for this proof-of-concept delivery study to optimize nanoparticle cellular uptake. We modulated the degree of nanoparticle internalization by altering the concentration of nanoparticles incubated with the T cells (**Figure 5-3**). We also evaluated nanoparticle uptake using T cells isolated from three different human donors (**Figure 5-3**) and saw only small variation, suggesting that this technique could be extrapolated to the T cells of any patient.

The internalized gold colloid used in this study also had no detrimental impact on the viability or function of activated human T cells *in vitro* (**Figure 5-4** and **Figure 5-5**), and the T cells were able to migrate to tumors *in vivo* while maintaining their AuNP payload (**Figure 5-6**). In addition to their ability to carry AuNPs to tumors, T cells can be selected for tumor-specificity for adoptive immunotherapy studies.[9, 173, 174] Furthermore, T cells may be genetically engineered to improve their function [10, 175] or enhance their ability to migrate to tumors *in vivo*[142, 176]. It has been demonstrated that systemically administered AuNPs tend to accumulate mainly in the perivascular regions of the tumor,[96] limiting passive accumulation of nanoparticles by the EPR effect to well-vascularized regions of the tumor. T cells may naturally localize to tumors, and tumor-specific T cell clones have been demonstrated to penetrate into the hypoxic cores of the tumors *in vivo*.[177] The more extensive infiltration of tumor sites by

antigen-specific T cells may permit enhanced penetration of the tumor when compared to freely-injected nanoparticles, potentially augmenting therapeutic efficacy.

The use of T cell vehicles also significantly affects nanoparticle biodistribution (**Figure 5-7**). Freely injected nanoparticles (40-45 nm gold colloidal nanospheres coated with 5000 MW PEG) accumulate most significantly in well-vascularized organs such as the liver, spleen, kidney, and gut (**Figure 5-7**). Maximal AuNP tumor accumulation for the freely injected PEG-AuNP group is seen at 24 h (**Figure 5-8**). After 24 h, increased gold content for the PEG-AuNP group is seen in the spleen, liver, and kidney with a corresponding decrease in gold content within the tumor and other organs, which represents a shift towards AuNP clearance.

AuNP-T cells present a much different biodistribution from the systemically administered nanoparticles that correlates with the expected biodistribution of T cells. After adoptive transfer of AuNP-T cells, a large percentage of the ID is seen within the liver and lungs at 24 h. T cells are known to accumulate within the liver and lungs after administration due to the vascularity and number of adhesion molecules present in these organs.[178] This pattern of T cell migration is consistent with the biodistribution of adoptively transferred T cells seen in previous studies.[169, 178] AuNP-T cells are also seen accumulating in the spleen and bone of the mice; these locations are also normal reservoirs of T cells.[179] The large number of AuNP-T cells seen in the liver likely represents apoptotic T cells. This large accumulation is not observed by bioluminescence imaging in Figure 3, and the liver is a known site where apoptotic T cells are entrapped.[180] Tumor accumulation of AuNP-T cells increases from 24 to 48 h as T cells escape from the lungs and migrate to the tumor (**Figure 5-8**). The biodistribution of

AuNP-T cells matches the expected biodistribution of normal activated T cells, suggesting that AuNP biodistribution can be modulated based on the selection of the cellular vehicle. In the case of T cells, it is possible that the biodistribution may be altered to to further favor tumor accumulation and persistence by manipulating cell culture conditions [178] or by genetic modification of T cells.[142]

Using T cells as cellular vehicles for AuNP delivery, we achieve a four-fold increase in tumor delivery efficiency at 48 h when compared to freely injected PEG-coated AuNPs at 24 h (**Figure 5-8**). This represents a significant increase in delivery efficiency ($P < 0.01$, Student's *t*-test) using T cells. These results demonstrate for the first time that T cells can be used to enhance AuNP delivery to a tumor *in vivo*. The use of AuNPs and T cells together combines the photothermal therapy and imaging advantages of AuNPs with the immunotherapy and biodistribution advantages of T cells. Future directions will focus on utilizing the AuNP-T cell system for cancer therapy by modifying the T cells to further enrich AuNP tumor accumulation and enhance anti-tumor effects.

Conclusions

In this study we demonstrate the internalization of AuNPs into activated human T cells for the delivery of nanoparticles *in vivo*. AuNP uptake has no negative impact on T cell viability, proliferation, or immune function, and T cells are able to transport the AuNP payload to tumor sites *in vivo*. Furthermore, the use of T cells as a AuNP vehicle enhances *in vivo* delivery efficiency by four-fold. This delivery method alters the biodistribution of gold compared to freely injected AuNPs, and demonstrates that the selection of a particular cellular vehicle may dictate AuNP biodistribution.

CHAPTER 6

TUMOR-SPECIFIC DELIVERY OF HOLLOW GOLD NANOSHELLS FOR PHOTOTHERMAL THERAPY USING ANTIGEN-SPECIFIC T CELLS

Introduction

In Chapter 5, we demonstrated the ability of human T cells to bear gold colloidal nanospheres to a xenografted lymphoblastoid cell line (LCL) tumor in an immunocomproomised mouse model. This proof of principle study opened up a range of opportunities for the combination of gold nanoparticles and immunotherapy for disease treatment and imaging. However, the Chapter 5 study was also limited in that a) the gold nanoparticles used did not have near-infrared (NIR) resonance and b) the T cells tested were xenogeneic to the host. The next steps towards developing this delivery system for photothermal therapy include using NIR-resonant gold nanoparticles and allogeneic T cells.

With this in mind, we elected to use the B16F10 melanoma tumor model. These tumors express the mouse homologue of gp100, a known human melanoma antigen. A transgenic mouse line, strain B6.Cg-*Thy1*^{a}/Cy Tg(TcraTcrb)8Rest/J, has been developed to express CD8+ T cells with T cell receptors specific to the mouse homologue of gp100. We hypothesized the use of antigen-specific T cells would increase gold nanoparticle delivery and penetration into the tumor. The use of these T cells has an added benefit in that they are murine T cells, not human T cells, which should reduce liver sequestration

of the T cells. These transgenic mice and their gp100-targeting T cells will subsequently be referred to as pmel mice and pmel T cells respectively.

There are many choices for NIR-resonant gold nanoparticles that can be used for photothermal therapy. For the initial testing of the AuNP-T cell delivery system, gold colloidal nanospheres around 45 nm in diameter were chosen because of their similarity in size to the second generation of NIR-resonant gold nanoparticles, which range from 25-60 nm in diameter. This size range has also been shown to be within the ideal range for the uptake of gold nanoparticles by cells.[98] Although gold-gold sulfide nanoparticles (GGS NPs), hollow gold nanoshells (HAuNS), and gold nanocages were all possible choices for this study, I chose to use hollow gold nanoshells because these nanoparticles have been previously used in the literature to ablate melanoma tumors.[6] In fact, these nanoparticles to date have the best tumor accumulation in the literature of ~12.6 % of the injected dose per gram of tissue at the 4 hour timepoint post-injection.[6] They are also very close in size to the gold colloid used in Chapter 5 (~40-45 nm diameter) when tuned to the NIR.

There are two methods used to synthesize HAuNS. Although mechanistically similar because both methods use a core template nanoparticle that is oxidized while the gold shell is forming, one method uses a silver-template nanoparticle while the other uses a cobalt-template nanoparticle. Both of these methods have previously synthesized hollow gold nanoshells with NIR resonance.[52, 181] However, in the experience of my lab, the cobalt-template method does not easily produce NIR-resonant HAuNS. For this reason, I chose the silver-template HAuNS for these experiments.

One challenge in the choice of these silver-based gold nanoparticles is the risk of cytotoxicity. Although the template core nanoparticle is oxidized during the reduction of the gold shell, leaving a hollow spherical nanoparticle, this does not mean that the template materials are removed from the nanoparticle solution. In the case of silver-nanoparticle based hollow gold nanoshells, the likely source of toxicity would be residual silver salt remaining from the synthesis. Silver salts are known to be toxic and have been employed in the past as antiseptics due to their ability to inhibit microbial growth.[182] Because hollow gold nanoshells tend to be porous,[53] any residual silver salt in the hollow core could leach and kill surrounding cells. To circumvent this toxicity for T cell loading, a heating and salting step was added after HAuNS synthesis to remove the remaining silver salt from the solution.

In this chapter, we will demonstrate the loading and *in vivo* delivery of silver-based HAuNS to gp100-expressing melanoma tumors using transgenic pmel T cells. We will compare the pmel T cell delivery of HAuNS to the HAuNS delivery of wild type T cells that have no antigen-specificity. These experiments will evaluate the translation of the AuNP-T cell delivery system to a more realistic tumor and T cell model, and will allow us to determine if the gold nanoparticle biodistribution and tumor delivery is enhanced by the use of allogeneic and antigen-specific T cells.

Methods

Silver-Based Hollow Gold Nanoshell Synthesis

Silver Nanoparticle Synthesis

Silver nanoparticles (AgNPs) were prepared at 60°C in a well-stirred solution of 0.2mM silver nitrate solution (50mL, $AgNO_3$) in the presence of sodium citrate (0.5mM) following an injection of 100 sodium borohydride solution (1mL, $NaBH_4$), which produces a yellow color. The silver colloid was allowed to stir at 60°C for a minimum of two hours.

Increasing Core Size

The Ag core solutions were then allowed to cool to room temperature. AgNP growth was initiated by adding a 200mM hydroxylamine hydrochloride solution (1mL, NH_2OH-HCL) to the silver colloid, followed by stirring for a minimum of 5 minutes. An additional 200μL $AgNO_3$ (0.1M) solution was injected, and the solution was allowed to age for a minimum of 24 hours with stirring. Growth was confirmed by the solution changing to a dark yellow or orange color based on the amount of $AgNO_3$ added.

Gold Shell Growth

The aged silver core solutions were then heated to 80°C and stirred at a rate of 900 RPM. A 1 mL $HAuCl_4$ (25mM) solution bolus was injected into the silver core solution. The solution immediately changed color from the yellow-orange of the cores to a dark blue-black. The blue-black solution was allowed to stir for an additional 10 minutes. Each 50mL Ag core solution with 1mL 25mM $HAuCl_4$ addition generated a final HAuNS solution with an OD between ~2.5 to 3.

Removal of Excess Ag and AgCl

During the formation of the gold shell, each Au atom that reduces to the surface of the core particle oxidizes 3 Ag atoms. These Ag atoms bind with free Cl^- ions in the solution to form AgCl, which is insoluble in water at room temperature. To remove as much silver as possible from the HAuNS solution, the solubility of the AgCl must be increased by heating and the AgCl adsorbed to the surfaces of the HAuNS must be released.

To achieve these goals, 3 grams of NaCl crystals and 1 mL of 1% tween solution were added to every 50mL of HAuNS solution. The 1% tween solution was added to help stabilize the HAuNS during the salting steps. After the addition of the NaCl and Tween, the solutions were heated to 80°C, probe sonicated, and pelleted using centrifugation at 2500g for 5 minutes. The supernatant was removed, the pellets were combined, and the washed HAuNS concentrate was resuspended in 30mL of water. The addition of salt, tween, and heat was repeated as before, and the solution was once again probe sonicated. The solution was then split into 3 equal volumes of 10mL and diluted to 30mL with water. The solutions were heated to 80°C and probe sonicated again. The solutions were then pelleted at 2500g for 5 minutes, the supernatant discarded, and the centrifugation step repeated twice more. After washing, the pellets were recombined into a single tube and 100uL of 1% tween was added as a stabilizer for storage at 4°C.

Removal of Tween

Prior to use with cell, the Tween stabilizer must be removed. The HAuNS were heated to 80°C and 3 grams of NaCl were added to the solution as before. After salting and heating, the solution was split into 3 tubes of equal volume and diluted to 30mL

using water. The solution was then washed 5 times at 2500g for 5 minutes, the pellets recombined, and 200μL of 0.1mM citrate added as a stabilizing agent. The concentration of the nanoparticles was then determined using a combination of Mie Theory and the nanoparticle extinction spectra.

PEGylation of Hollow Gold Nanoshells for Injection

For free nanoparticle injection, hollow gold nanoshells prepared without the additional silver removal steps were used. The day prior to the mouse study, particles were coated with sterile polyethylene glycol (PEG MW 5000) by adding an optimized amount of 1 mM PEG solution. The optimized ratio of PEG molecules to gold nanoparticles was determined using a salt stability assay as described previously in Chapters 4 and 5. The nanoparticles and PEG were incubated overnight at 4°C. Excess PEG molecules were then removed by centrifuging the nanoparticles and removing the supernatant. The nanoparticles were then resuspended in sterile 1x PBS immediately prior to mouse injection.

Cell Lines and Culture

Both SK-BR-3, a breast cancer cell line, and B16F10, a melanoma cell line, were used for HAuNS toxicity testing. The SK-BR-3 was cultured in McCoy's 5A Medium supplemented with 10% fetal bovine serum (FBS) and 1% penicillin-streptomycin. The B16F10 cells were cultured in Dulbecco's Modified Essential Medium (DMEM) supplemented with 10% fetal bovine serum (FBS) and 1% penicillin-streptomycin. Cells were incubated in a humidified 37°C incubator with 5% CO_2.

Isolation and Expansion of Mouse Splenocytes

To isolate wild type and pmel splenocytes, a wild type or pmel mouse was sacrificed as per Baylor animal protocol and the spleen harvested. The spleen was then homogenized into a cell suspension using a cell strainer and phosphate buffered saline (PBS). The cells was then centrifuged at 400 rcf for 5 minutes and resuspended in 10 mL of PBS. Afterwards, the cell suspension was layered on top of 5 mL of Lympholyte FICOL buffer (2 tubes) and centrifuged at 1000 rcf for 20 minutes with acceleration = 3/9 and brake = 0/9. The interphase was then transferred to separate tube and centrifuged at 400 g for 5 minutes. The cell pellet was resuspended in 25 mL of splenocyte media (RPMI-1640 media supplemented with 10% fetal calf serum, 1% Glutamax, 1% HEPES, and 0.001% 2-B mercaptoethanol). The splenocyte mixture was then stimulated with 10 ng/mL murine interleukin-2 (IL-2) and 5 μg/mL ConA and plated in a 24 well culture plate. The splenocytes were incubated at 37°C with 5% CO_2 and the media supplemented with 10 ng/mL of murine IL-2 at each feeding.

Hollow Gold Nanoshell Toxicity Testing

MTT Assay

The cytotoxicity of HAuNS was initially evaluated using an MTT assay on SK-BR-3 and B16F10 cells. Cells were seeded at 4000 cells per well in a 96 well plate and allowed to grow for 48-72 hours. B16F10 cells were exchanged into a phenol-free DMEM media for this experiment. For initial testing of the hollow gold nanoshells, B16F10 cells were incubated with 0.1 nM and 0.5 nM of both bare and PEG-coated hollow gold nanoshells synthesized with no additional cleaning steps. For testing of the HAuNS after additional silver removal steps, SK-BR-3 and B16F10 cells were incubated

with 0.1 nM, 0.25 nM, 0.5 nM, and 1.0 nM of cleaned HAuNS overnight. After an overnight nanoparticle incubation, the cells were washed 2-3 times with fresh media to remove the nanoparticles. A dead control was created by incubating some wells with 0.1% Triton X in PBS for 10 minutes at room temperature. The 3-(4,5-Dimethylthiazol-2-yl)-2,5-diphenyltetrazolium bromide (MTT) assay was then carried out as per Vybrant MTT Cell Proliferation Assay Kit protocol (Invitrogen V-13154).

ICP-OES Testing of Hollow Gold Nanoshells for Silver

The hollow gold nanoshells were tested for silver content using inductively coupled plasma optical emission spectroscopy (ICP-OES) analysis. For this experiment, hollow gold nanoshells were synthesized as described above without additional salting steps to remove excess silver. Approximately 1 x 10^{11} hollow gold nanoshells were concentrated into a <100 microliter volume and transferred to a glass scintillation vial. The nanoshells were digested in concentrated trace metal grade nitric acid for a minimum of 12 hours to leach any silver salt from the nanoshell core. The acid digests were then digested to 5 mL in Millipore-filtered water and analyzed on the ICP-OES for silver content.

Loading and Analysis of Mouse Splenocytes with HAuNS

Splenocyte Incubation with HAuNS

On days 7-14, the splenocytes are incubated with the HAuNS at a loading concentration ranging from 0.25 nM to 1.0 nM in splenocyte media overnight. Prior to adding the nanoparticle mixture to the splenocytes, sonication was performed to disperse the nanoparticles evenly throughout the solution. After the overnight incubation at 37°C,

the loaded splenocytes were extensively washed using 1x PBS to remove excess nanoparticles.

Propidium Iodide Staining

Propidium iodide staining was performed using the FITC Annexin V Apoptosis Detection Kit I (BD Pharmingen #556547). Half a million washed T cells loaded with HAuNS were incubated with 5 mL of propidium iodide staining solution for 15 minutes at room temperature then analyzed by flow cytometry.

Darkfield Microscopy and Hyperspectral Imaging of HAuNS-T Cells

To confirm T cell loading with the HAuNS, the splenocytes were imaged using a Cytoviva® microscope and the Cytoviva® Hyperspectral Imaging System. After collecting the hyperspectral data for HAuNS-loaded and control T cells, the mean spectra of the entire cell was calculated using the ENVI software's region of interest tool. The spectral data was then normalized for a maximum intensity of 1 and divided by the lamp spectrum, also normalized for a maximum intensity of 1. The control cell spectrum was then subtracted from the HAuNS-loaded T cell spectra.

ICP-OES Analysis of HAuNS-T Cells

The number of gold nanoparticles per T cell was determined using inductively coupled plasma optical emission spectroscopy (ICP-OES). A minimum of 2×10^6 T cells loaded with HAuNS was digested using trace metal grade hydrochloric acid and trace metal grade nitric acid at a ratio of 3:1 $HCl:HNO_3$ to form aqua regia overnight. Samples diluted to 1% aqua regia by volume using Millipore-filtered water, then filtered using a polyethersulfone syringe filter to remove undigestible debris. Samples were analyzed using ICP-OES.

In vivo Delivery Analysis of HAuNS-T Cell

B16F10 Xenograft Model

In vivo migration, AuNP delivery, and biodistribution studies were performed using albino and wild type C57BL/6 mice. All mouse experiments were performed under a Baylor College of Medicine Institutional Animal Care and Use Committee (IACUC) approved protocol. 5×10^5 B16F10 tumor cells were resuspended in PBS and injected subcutaneously (s.c.) into the shaved right flanks of mice. Tumors were allowed to establish and grow to at least 0.5 mm × 0.5 mm in size (7-10 days) before beginning experiments.

Mouse Injections and Sample Collection

To prepare AuNP-T cell injections, T cells were prepared as above and incubated with 0.25-1.0 nM HAuNS for 24 h. Cells were collected and washed extensively using 1× PBS prior to injection. For delivery studies, mice received either PBS, 1×10^7 HAuNS-T cells, or 1.2×10^{12} PEGylated HAuNS via the tail vein in a 200 µL bolus. These dosages were selected based on previous *in vivo* studies using HAuNS and adoptively transferred T cells.

To determine optimal time points for delivery analysis, tumors were resected at either 6, 24, or 48 hours for the PEGylated HAuNS group and 24 or 48 h for the HAuNS-T cell group. In addition, whole blood, plasma, the spleen, left kidney, lungs, right tibia, tumor, and a portion of the liver were also collected for analysis at 6, 24, or 48 hours for the PEGylated AuNP group and 24 or 48 hours for the HAuNS-T cell group. All tissues, including tumors, were flash frozen with liquid nitrogen after collection and stored at -80°C until analysis.

Fluorescent Immunohistochemistry for CD3 and Thy1.1

Tumors treated with PBS, wild type T cells, and pmel T cells were harvested 48 hours post-injection and bisected. One half went to ICP analysis, while the other half went to immunohistochemistry analysis. To image HAuNS-T cells within the tumor, the tumors were thawed in a 37°C water bath and embedded in optimal cutting temperature (O.C.T.) compound (Sakura Finetek USA, Inc., Torrence, CA) using dry ice. The embedded tissue was then sectioned into 8 μm slices using a cryostat, dried for 30 minutes at room temperature, and stored at -80°C. When ready for staining, the slides were allowed to equilibrate with room temperature for 30 minutes prior to proceeding.

Tissue sections were fixed with ice-cold acetone for 1 minute and subsequently washed with ice-cold PBS twice. Blocking was performed used 10% goat serum (Jackson ImmunoResearch Laboratories, 005-000-121) in PBS plus 0.5% saponin for 30 minutes at room temperature followed by the blocking of endogenous mouse IgGs using Affinipure Fab fragment anti-mouse IgG (Jackson ImmunoResearch Laboratories, 115-075-144) for 1 hour at room temperature. The primary antibodies, either anti-CD3 (Abcam 19639) or anti-Thy1.1 (Abcam 65193), and anti-CD31 (Abcam 28364) were then applied to the tissue and allowed to bind overnight at 4°C in a humidified chamber.

The tissue was then washed three times in PBS to remove unbound excess primary antibody and incubated with FITC-conjugated secondary Fab fragment or antibody (FITC-anti-syrian hamster for CD3, Jackson Immunoresearch Laboratories 107-095-142, and FITC-anti-mouse Fab fragment for Thy1.1, Jackson Immunoresearch Laboratories 115-097-003) and Texas Red-anti-rabbit for CD31 (Jackson Immunoresearch Laboratories 111-075-144) for 30-60 minutes in the dark at room

temperature. The tissue was washed three times in PBS for 5 minutes after the secondary antibody incubation, then mounted with Fluoro-Gel II with Dapi mounting medium (Electron Microscopy Sciences #17985-50), coverslipped, and allowed to harden overnight in the dark at 4°C. The coverslips were then sealed with nail polish prior to imaging.

Preparation and Analysis of Tissue by ICP-MS and ICP-OES

Resected mouse tissues were prepared and analyzed for gold content using inductively coupled plasma mass spectrometry (ICP-MS) and ICP-OES. Solid tissue samples were lyophilized and weighed, then digested for 48-72 hours with trace metal grade hydrochloric acid and trace metal grade nitric acid at a ratio of 3:1 HCl:HNO_3 to form aqua regia. Samples diluted to 1% aqua regia by volume using Millipore-filtered water, then filtered using a polyethersulfone syringe filter to remove undigestible debris. Blood and plasma samples were weighed but not lyophilized, then treated in the same manner as the solid tissue samples. All samples were then analyzed on either the ICP-OES or ICP-MS for gold content. Samples of the AuNP-T cell boluses were also analyzed to confirm the amount of gold systemically administered.

Results

Hollow Gold Nanoshell Characterization

Hollow gold nanoshells were synthesized as described above. The outer diameter of the nanoshells was 40 nm, and the shell thickness was 5-7 nm by transmission electron microscopy (TEM) imaging (**Figure 6-1**). The outer surfaces of the HAuNS show signs

of stress from the silver removal steps, but the inner surfaces of the nanoshells remain spherical and hollow. In addition, the peak resonance is in the near-infrared, and remains in the near-infrared after the removal of the Tween (**Figure 6-2**).

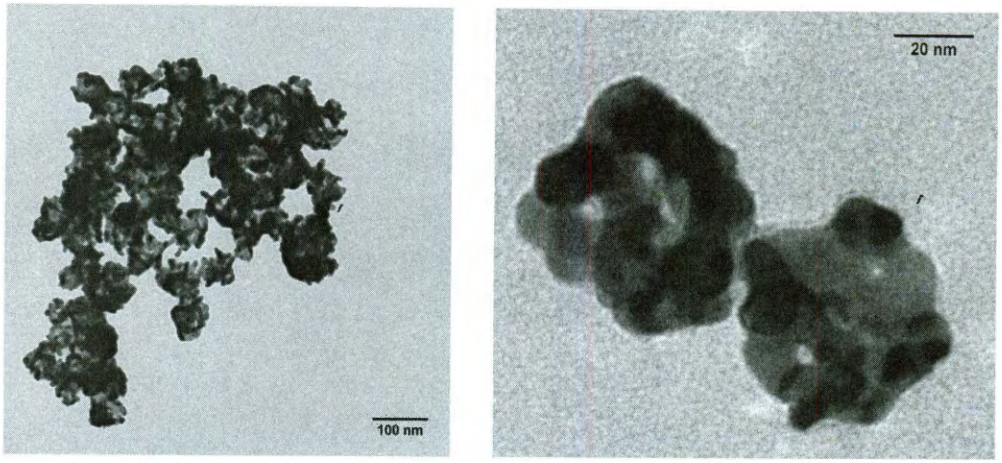

Figure 6-1. Transmission electron microscopy images of hollow gold nanoshells after synthesis, silver removal, and Tween removal.

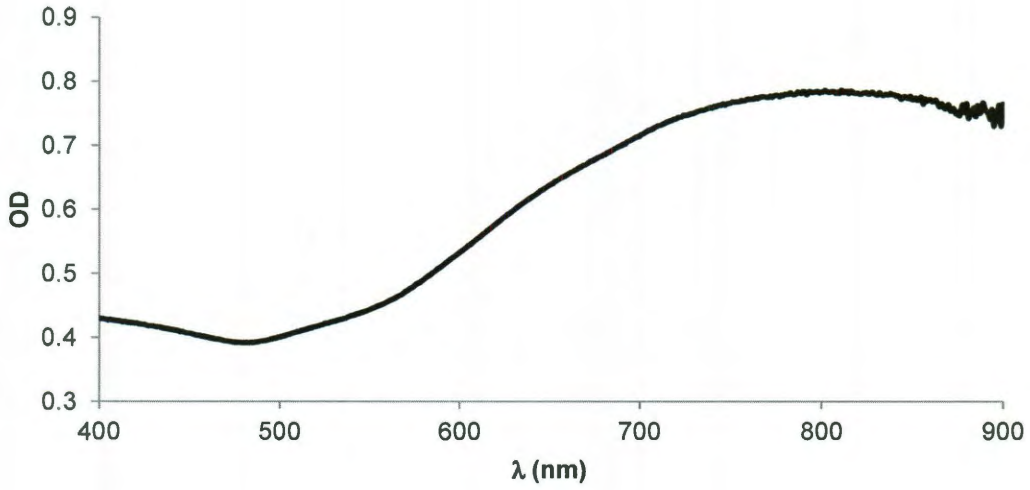

Figure 6-2. Extinction spectra of hollow gold nanoshells. Hollow gold nanoshells were stabilized with Tween and have undergone salting and heating to remove excess silver.

Hollow Gold Nanoshell Cytotoxicity Testing

Initial Cytotoxicity Evaluation of Hollow Gold Nanoshells

For initial testing, hollow gold nanoshells were synthesized as described above through the gold shell growth step, then washed using centrifugation twice. Preliminary toxicity testing was performed using an MTT assay on B16F10 cells. Both bare and PEG-coated hollow gold nanoshells were tested at two different concentrations (1 mole = 6.022 x 10^{23} HAuNS). The uncoated hollow gold nanoshells demonstrated appreciable toxicity at both the 0.1 nM and 0.5 nM concentrations compared to the control cells incubated with media alone. The 0.1 nM concentration of the PEG-coated nanoshells had better cell viability, but still showed some toxicity. The 0.5 nM concentration of the PEG-coated nanoshells, like the uncoated nanoshells, demonstrated appreciable toxicity from nanoparticle exposure (**Figure 6-3**).

ICP-OES analysis of the hollow gold nanoshells for silver revealed an average of 0.016 moles of silver present per 1 x 10^{11} HAuNS. **Table 6-1** shows the potential

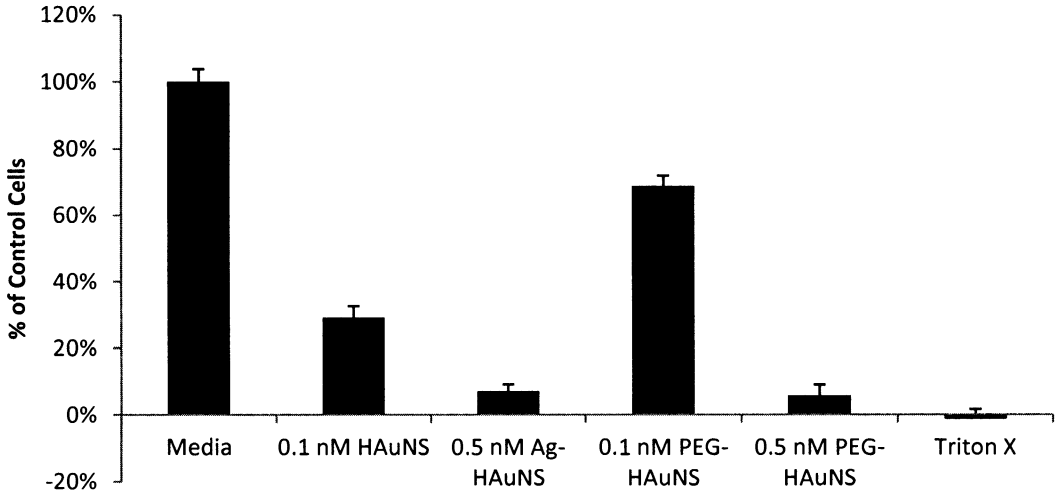

Figure 6-3. MTT assay results for hollow gold nanoshells (HAuNS) synthesized with no additional silver removal steps. Both bare and polyethylene glycol (PEG) coated nanoshells caused a decrease in cell viability after a 12 hour incubation.

Table 6-1. Potential Silver Salt Concentration for Hollow Gold Nanoshell Loading Concentrations

[HAuNS]	0.1 nM	0.25 nM	0.5 nM	1 nM
$[Ag^+]$	9.7 μM	24.2 μM	48.5 μM	96.9 μM

corresponding silver salt concentration for each concentration of the unwashed hollow gold nanoshells (Group A) tested in the MTT assay below. This concentration assumes that all silver associated with the hollow gold nanoshells leaches into the media to affect the cells. Silver-mediated cytotoxicity has been previously demonstrated at concentrations greater than 4.1 μM after a 24 hour incubation of silver nitrate with fibroblasts.[182]

The addition of the heating and salting steps described in the methods section significantly reduces cytotoxicity for all of the tested concentrations (**Figure 6-4**). This change confirms that the silver salt remaining from the synthesis causes cell death and that the removal of this silver abrogates toxicity. The lack of toxicity was further

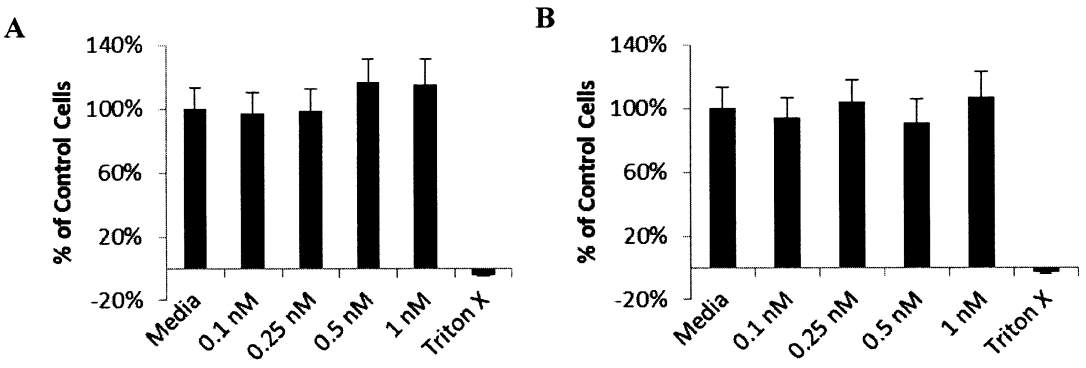

Figure 6-4. MTT Assay Results for Hollow Gold Nanoshells with Additional Silver Removal Steps. A) HAuNS incubation at different concentrations with B16F10 cells. No appreciable toxicity is seen at any concentration tested. B) HAuNS incubation at different concentrations with SK-BR-3 cells. As with the B16F10 cells, no appreciable toxicity is seen.

confirmed by testing with a different cell line (SK-BR-3 cells). Based on these results, I proceeded with hollow gold nanoshell loading into mouse T cells.

Internalization of Hollow Gold Nanoshells by Mouse T Cells

Wild type and pmel mouse splenocytes were incubated with 0.25 nM, 0.5 nM, and 1 nM of HAuNS. Propidium iodide staining was performed to confirm that the splenocytes tolerated the nanoparticle incubation well with minimal effect on cell viability. The number of hollow gold nanoshells internalized per cell was estimated using ICP-OES. The wild type T cells internalized a maximum of 14500 ± 100 nanoparticles per cell using the 1.0 nM HAuNS loading concentration, while the pmel T cells were calculated to have a maximum HAuNS of 33300 ± 300 nanoparticles per cell using the 1.0 nM HAuNS loading concentration (**Figure 6-5**). It is likely, however, that the pmel T cell gold content was artificially inflated due to the presence of visible gold

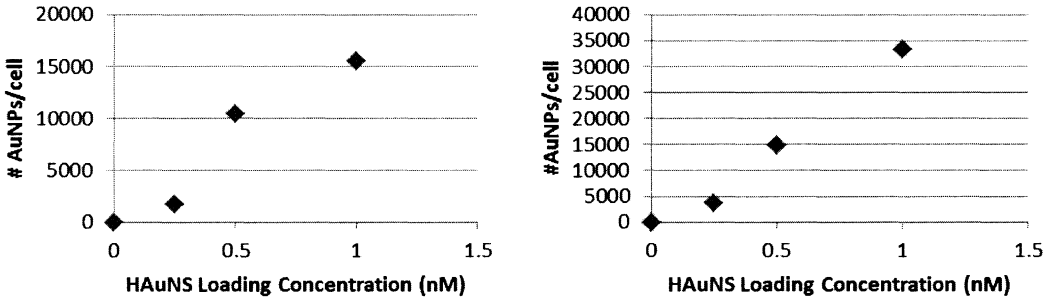

Figure 6-5. ICP-OES quantification of hollow gold nanoshell content per cell. A) Wild type T cells B) pmel T cells.

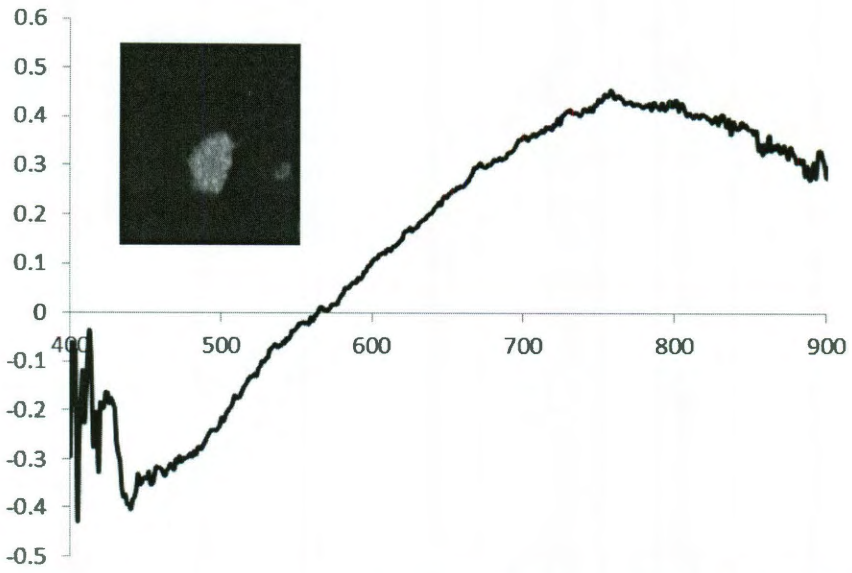

Figure 6-6. Hyperspectral imaging results for pmel T cells loaded with 0.25 nM HAuNS. The average spectra of the entire cell was normalized for the lamp spectrum and a control cell's spectrum was subtracted. The presence of the HAuNS is confirmed by the scattering peak that peaks at 760 nm. The inset image is representative of the appearance of the HAuNS-loaded T cells.

aggregates in the cell solution both during and after washing. The large size of these aggregates made separating them from the cells using centrifugation very difficult.

The loaded splenocytes were further characterized using darkfield imaging and the Hyperspectral Cytoviva® Imaging system. T cells incubated with hollow gold nanoshells exhibited a scattering spectrum that peaked around 760 nm (**Figure 6-6**). For hollow gold nanoshells tuned to the NIR, the scattering and the absorption spectra generally overlap fairly well,[183] so we assume that the HAuNS-loaded T cells will absorb well in the NIR.

In vivo Delivery of Hollow Gold Nanoshells by Mouse T Cells

After confirmation that the mouse T cells could be successfully loaded with HAuNS, *in vivo* testing was performed to confirm gold and T cell delivery to the tumor

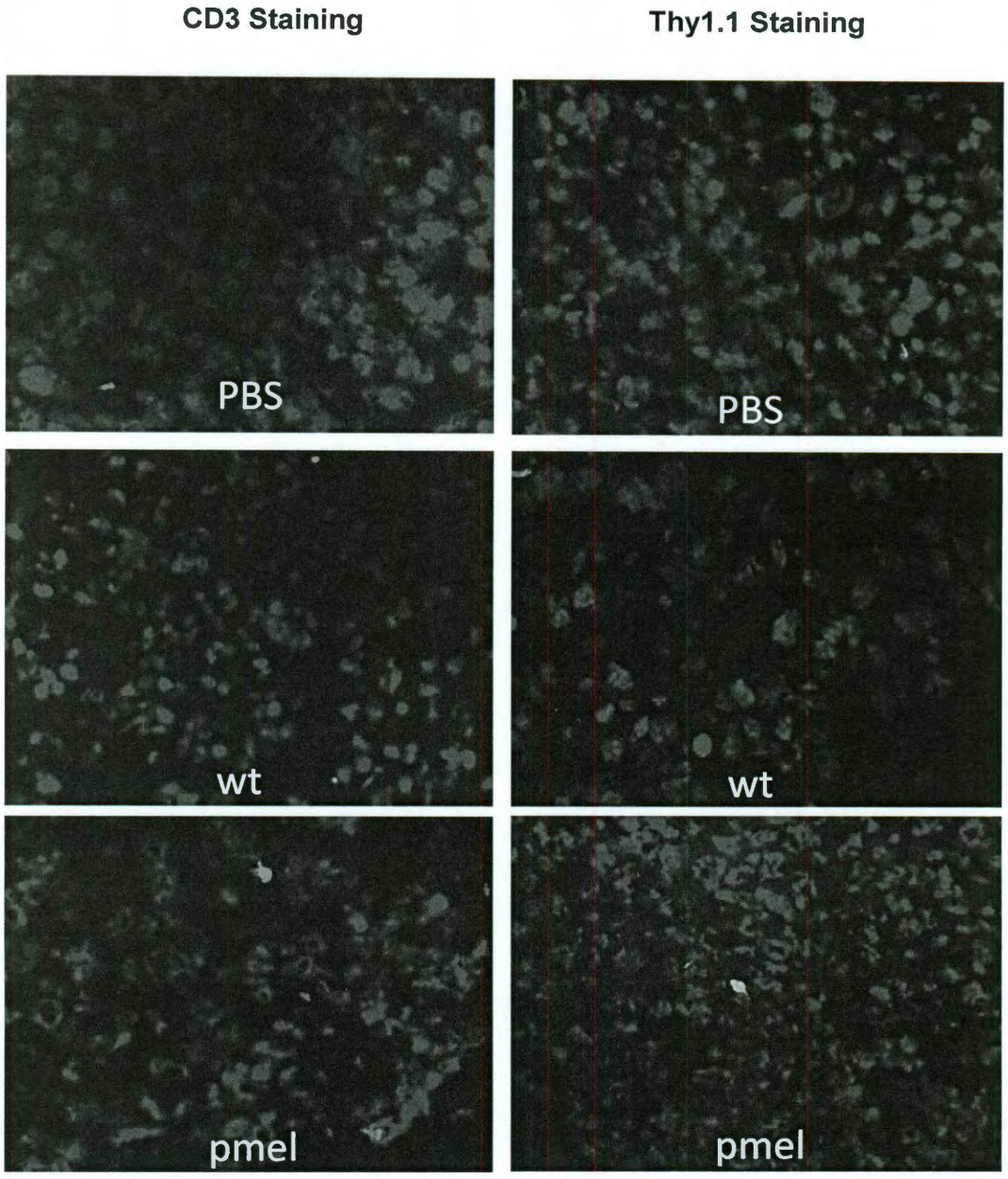

Figure 6-7. Immunohistochemistry of tumors harvested 48 hours after mice were intravenously injected with phosphate buffered saline (PBS), wild type T cells loaded with HAuNS (wt), or pmel T cells loaded with HAuNS (pmel). Left column shows staining CD3 (green) and DAPI. Right column shows staining for Thy1.1 (green), CD31 (red), and DAPI. CD3 staining shows endogenous and adoptively transferred T cell accumulation in all tumors. Thy 1.1 staining shows that the pmel treated group did have pmel T cell accumulation at the tumor site, while neither the PBS or wild type treatment groups stain for Thy1.1.

and compare the performance of the wild type T cells to the pmel T cells for tumor delivery. Immunohistochemistry of tumors harvested 48 hours post-injections revealed the presence of endogenous and adoptively transferred T cells in the PBS-, wild type T cell-, and pmel T cell-treated tumors (**Figure 6-7**, left column) by staining for CD3, a T cell marker. The presence of pmel T cells was only found in the pmel treatment group as determined by staining for Thy1.1, a glycophosphatidylinositol (GPI) membrane protein found on the surface of some murine T cells (**Figure 6-7**, right column). The wild type T cells injected in the other treatment group and the endogenous T cells have Thy1.2, not Thy1.1, and thus will not stain. Although all treatment groups show T cell accumulation, only a 3-4 T cells were seen per 8 micron tissue section. This is unlike the immunohistochemistry performed in Chapter 5, where many T cells were seen in each tissue section.

The delivery of HAuNS by the T cells was confirmed by using ICP-MS and ICP-OES analysis to quantify the delivered gold. Both the wild type and pmel T cells were able to deliver gold to the tumor. Surprisingly, the wild type T cells delivered more gold than the pmel T cells at the 48 hour timepoint (**Figure 6-8**). The T cell delivery was much lower than the freely injected nanoparticle delivery; intravenously administered PEGylated HAuNS had a tumor delivery of 27.0 ± 3.4 % of the injected dose per gram tissue (**Figure 6-9**).

The T cell biodistribution results were more promising, however. As seen in Chapter 5, the gold biodistribution follows the expected biodistribution of the T cell carrier, with large accumulations seen in the lungs, spleen, liver, and bone. The pmel T cells had less accumulation than the wild type T cells in off-target sites such as the lungs,

liver, and spleen. In addition, the liver delivery at 48 hours seen with these murine T cells (wild type = 198 ± 23 % ID/gram tissue, pmel = 108 ± 24 % ID/gram tissue) is less than the liver delivery seen with human T cells (248 ± 22 %ID/gram tissue) at 48 hours, supporting our hypothesis that the large liver accumulation seen in Chapter 5 was due to the use of human T cells in a mouse model.

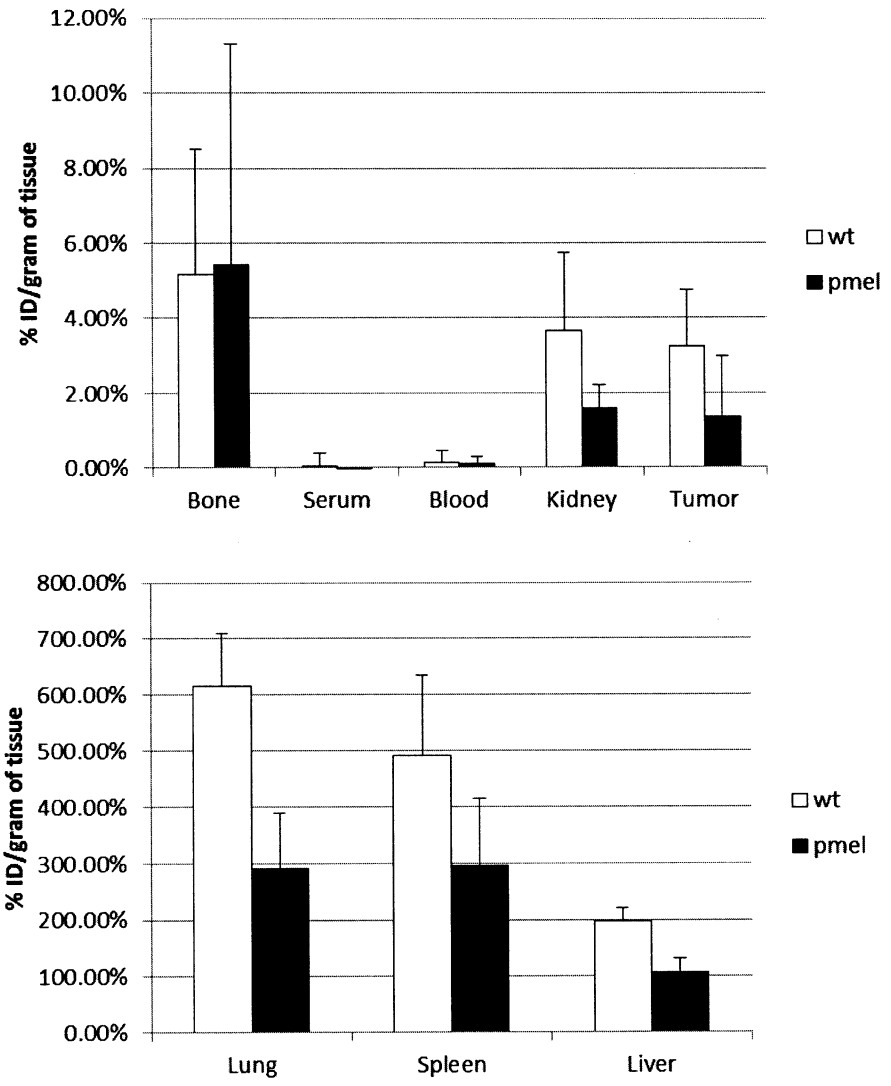

Figure 6-8. Percentage of injected dose (% ID) per gram of tissue for mice receiving either wild type T cell loaded with 0.25 nM HAuNS or pmel T cells loaded with 0.25 nM HAuNS 48 hour post-injection.

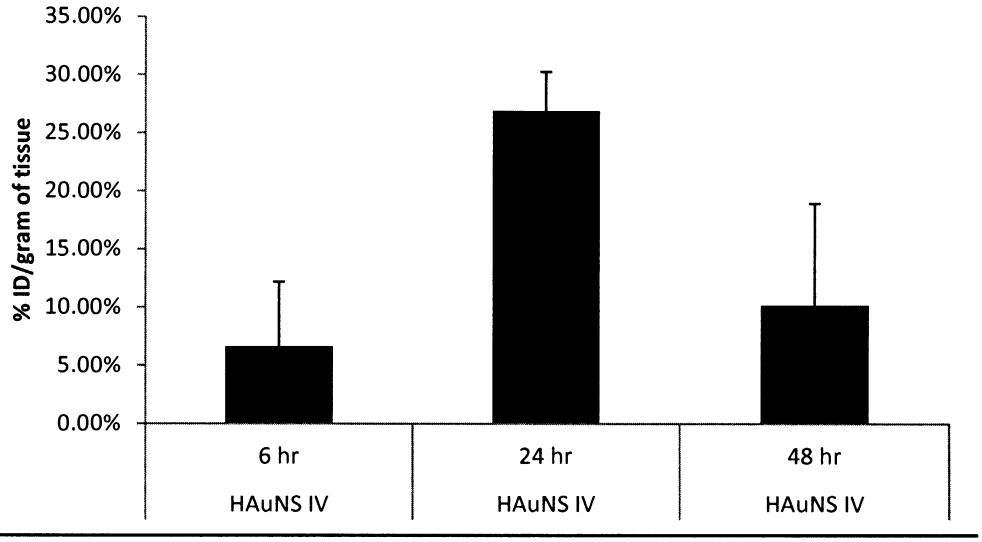

Figure 6-9. Percentage of injected dose (% ID) per gram of tissue for PEG-coated HAuNS injected via mouse tail vein at different timepoints.

When directly comparing these results to the results seen in Chapter 5, it appears that the human T cells migrated more efficiently to the LCL tumors than the pmel or wild type T cells migrated to the melanoma tumors (**Table 6-2**). However, it is important to recognize that two different tumor and mouse models were used for these two studies, which could affect the biodistribution, tumor delivery, and the ability of the T cells to localize to the tumor. The human T cells also seemed to have less retention in the lungs,

Table 6-2. Comparison of select organs from T cell and nanoparticle biodistribution studies.[e]

Treatment and Timepoint	Tumor	Bone	Kidney	Lung	Liver	Spleen
	% Injected dose of gold/gram of tissue					
wt T cells 48 hr	3.25 ± 1.51	5.17 ± 3.33	3.65 ± 2.10	615 ± 95	198 ± 23	493 ± 141
pmel T cells 48 hr	1.36 ± 1.63	5.43 ± 5.90	1.59 ± 0.64	292 ± 98	108 ± 24	294 ± 119
human T cells 48 hr	36.5 ± 12.8	7.65 ± 2.71	0.85 ± 0.26	117 ± 35	248 ± 22	148 ± 50
gold colloid 24 hr	17.0 ± 2.6	1.46 ± 0.13	1.69 ± 0.52	3.14 ± 1.29	31.1 ± 7.5	226 ± 100
HAuNS 24 hr	26.9 ± 3.4					

[e] Human T cell and gold colloid values adapted from Kennedy *et al* (2011) *Nanoscale Research Letters* 6(1):283 been converted from percentage of injected dose to percentage of injected dose per gram of tissue.

spleen, and kidneys compared to the murine T cells. It is unclear if this is a result of differences in integrins on the human versus murine T cells, or if this is a reflection of the human T cells being healthier than the murine T cells prior to injection.

Discussion

Intravenously injected gold nanoparticles for cancer imaging and therapy accumulate within the tumor by the non-specific enhanced permeability and retention (EPR) effect. Although many studies have demonstrated that gold nanoparticle tumor accumulation is sufficient for therapy using intravenous injection,[6, 7, 47] maximizing tumor accumulation also maximizes the liklihood that the ablated tumor will not return. In addition, freely injected gold nanoparticles accumulate in high concentrations in organs such as the liver and spleen, which is undesirable. We hypothesized that the use of the T cell delivery system with antigen-specific murine T cells would increase gold nanoparticle tumor accumulation and decrease off-target delivery to organs such as the liver and spleen. In this study, we demonstrate the ability of gp100-targeting murine T cells to carry hollow gold nanoshells to gp100-positive melanoma tumors xenografted in immunocompetant mice.

Although the hollow gold nanoshells loaded well into the murine T cells, the pmel T cells did not home well to the melanoma tumor. This is reflected in the immunohistochemistry and ICP-MS data. The wild type T cells actually accumulate in the tumor more efficiently based on the quantitative gold data. It is possible that this is a reflection of low level toxicity on the T cells from the hollow gold nanoshells. However, bioluminescent imaging done on unloaded wild type and pmel T cells shows that the wild

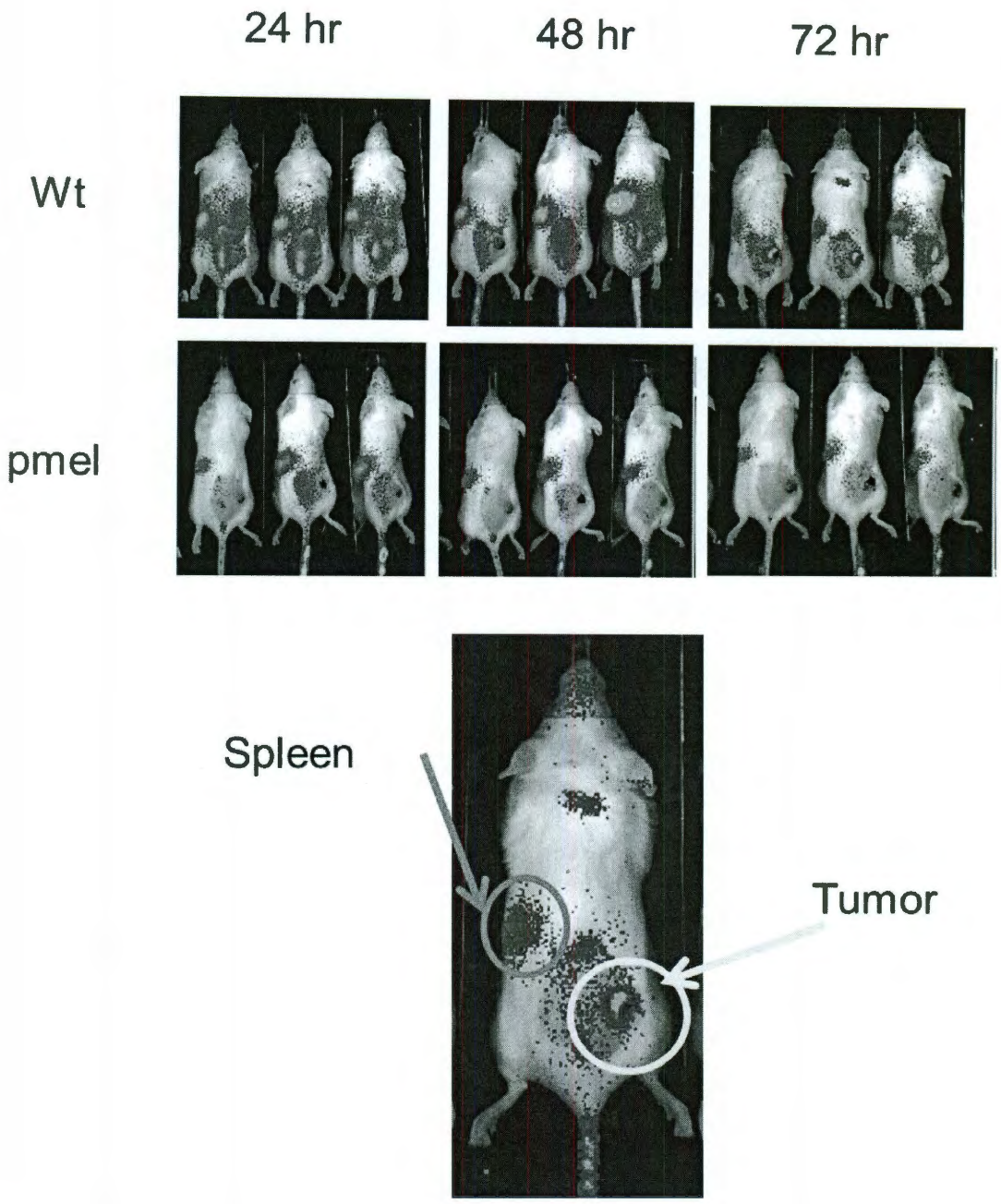

Figure 6-10. Bioluminescent imaging showing the migration of wild type and pmel T cells to B16F10 tumors seeded on the right flank. Signal is seen in both the spleen and tumor. The wild type T cells have stronger signal in the tumor and spleen than the pmel T cells.

type T cells accumulate at the tumor site better than the pmel T cells, and neither T cell has very high signal at the tumor site (**Figure 6-10**). In addition, it can be seen from the bioluminescent imaging data of the unloaded T cells that 72 hours has a stronger signal at the tumor for the wild type T cells. The pmel T cells do not have sufficient signal to make an evaluation of tumor accumulation at 72 hours. We based our timepoints on the previous study in Chapter 5, where 48 hours was the best timepoint, but perhaps a later timepoint for these T cells would yield better results.

Regardless, the freely injected PEG-coated HAuNS demonstrate significantly better tumor accumulation than the T cell-based delivery. In fact, the delivery of the hollow gold nanoshells for this tumor model is better than the previously reported highest value for hollow gold nanoshells with melanoma tumors.[6] In that previous study, a timepoint of 4 hours was selected for the quantitation of gold in the tumor. Lu et al report a tumor concentration of 12.6 ± 3.1 % injected dose of gold per gram of tissue. However, it would seem that 24 hours is the optimal timepoint based on **Figure 6-9**, where we are able to deliver 26.9 ± 3.4 % injected dose of gold per gram of tissue.

The T cell-based delivery method may still have an advantage in terms of modulating biodistribution and targeting organs where gold nanoparticle do not accumulate well. Based on the biodistribution performed by Melancon et al, the majority of injected hollow gold nanoshells accumulate in the liver and spleen, while a smaller percentage goes to the tumor and other organs.[7] Using the murine T cells as delivery vectors, the distribution of the gold nanoparticles followed the expected biodistribution of the T cells, seen in **Figure 6-10**. The murine T cells also decreased the percentage of the injected dose being sequestered in the liver when compared to the percentage of the

injected dose in the liver with the human T cells. It is also notable that T cells accumulate well in bone compared to freely injected gold nanoparticles due to their affinity for the bone marrow space, and HAuNS-T cells could function as possible vectors for gold nanoparticle PTT of bone tumors.

While the use of antigen-specific T cells did not increase gold nanoparticle tumor accumulation in this case, it is clear that the gold nanoparticle biodistribution can be altered by the selection of cellular vehicle. Although the lack of tumor delivery enhancement using pmel T cells was disappointing, it does not invalidate the previous success seen in Chapter 5. It is possible that the T cell delivery system would function more efficiently with a different tumor model that attracts T cells with higher avidity. Alternatively, perhaps a targeting a different melanoma tumor antigen, such as MART-1 or Trp2, with the antigen-specific T cells would yield better results. The T cells could also be genetically engineered to increase tumor homing, retention, and persistence through the addition of chemokine receptors.[142, 184] There are many potential avenues that could be explored for augmenting gold nanoparticle delivery using antigen-specific T cells. However, even if improved delivery is not possible, the ability to load gold nanoparticles into the T cell without detriment to viability or migration function opens a realm of possibilities for the combination of gold nanoparticles and immunotherapy.

CHAPTER 7

HYPERTHERMIA-ENHANCED IMMUNOTHERAPY FOR THE TREATMENT OF DISTANT SECONDARY TUMORS

Introduction

Gold nanoparticle photothermal therapy (AuNP PTT) improves the survival and decreases the tumor progression of mice bearing a variety of subcutaneous xenografted tumors [6, 34, 38]. Although this treatment demonstrates efficacy against localized tumors, it does not address metastatic cancers, which continue to present a clinical challenge. The primary difficulty in using AuNP PTT against metastatic cancers is the source of irradiating energy, which is typically a near-infrared (NIR) laser. As discussed in Chapter 2, NIR light is advantageous for *in vivo* applications because of its low absorption by tissue chromophores, permitting maximum transmissivity of light. However, the penetration depth of NIR light into tissue is still limited to less than 1 cm under ideal conditions. This limitation impairs the use of AuNP PTT against cancerous lesions in solid organs, such as the liver or lung, which are common locations of secondary cancer spread. Therefore, we must consider complementary therapies that will benefit from the use of AuNP PTT as an adjuvant. We hypothesize that the combination of AuNP PTT with adoptive T cell transfer, or hyperthermia-enhanced immunotherapy (HIT), has the potential to combat metastatic cancer by enhancing T cell expansion and infiltration into distant secondary tumors.

As discussed in Chapter 3, adoptive T cell transfer has previously demonstrated efficacy in patients with metastatic melanoma. Despite its successes, enhancing adoptively transferred cell expansion and tumor infiltration *in vivo* would most likely improve clinical tumor response. HIT could achieve these goals by inducing heat shock protein expression in the tumor, which has been associated with improved dendritic cell activation and cross-presentation.

Heat shock proteins (HSPs) are a family of chaperone molecules that have been implicated in maintaining the progression of cancers and in promoting an inflammatory response by the adaptive immune system [185]. HSPs complex with tumor peptides and will couple with toll-like receptors (TLRs) and CD91 to activate dendritic cells [186-188]. Activated dendritic cells then express higher levels of co-stimulatory molecules

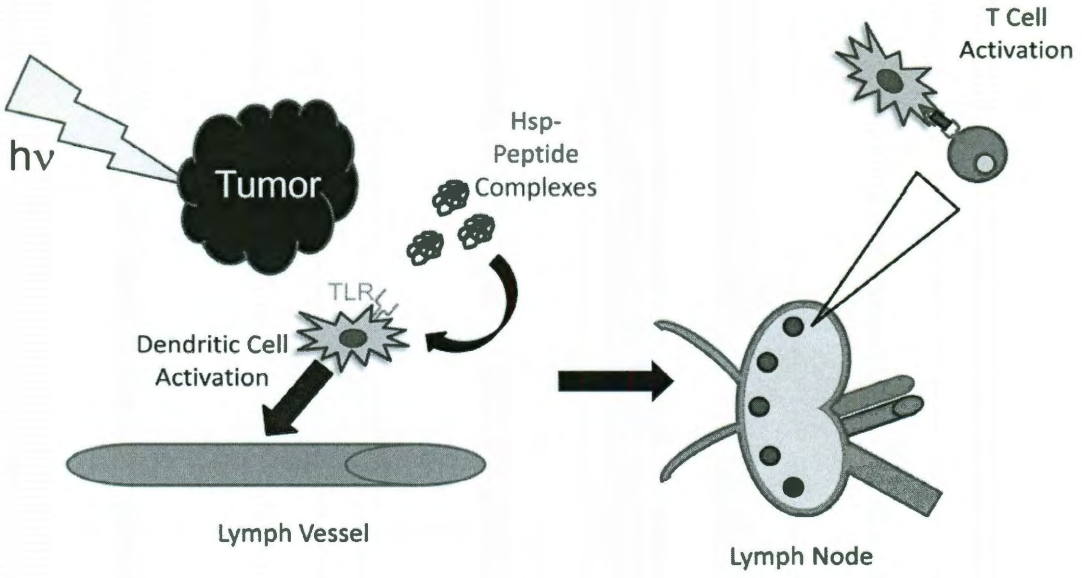

Figure 7-1. Heat shock protein-peptide (Hsp-peptide) complexes activate dendritic cells and ultimately T cells against the tumor. After hyperthermia, the tumor produces heat shock proteins that complex with peptides released by necrotic or apoptotic cells. These Hsp-peptide complexes are endocytosed and processed by professional antigen presenting cells such as dendritic cells (DCs). In addition, the Hsp-peptide complexes provide the second signal needed for complete DC activation by activating toll-like receptors (TLRs) on the DC surface. The DC then travels to the tumor draining lymph nodes where it presents the tumor antigens to lymphocytes such as T cells.

and major histocompatibility complexes (MHC), becoming mature, and will ultimately present the processed tumor peptides on a MHC molecule to activate tumor-peptide specific T cells or B cells (**Figure 7-1**). Somersan et. al. demonstrated that dendritic cell (DC) maturation was proportional to the concentration of heat shock proteins present in tumor lysates [189]. HSP-peptide complexes also enhance cross-presentation [187, 188, 190], which, as discussed in Chapter 3, is important for an effective immune response against tumor cells. The discovery of HSP-peptide complexes' role in triggering an immune response against tumors has spawned the development of HSP pharmaceuticals, including Vitespin®.

Vitespin® (Oncophage, Antigenetics, Inc.) consists of autologous HSP gp-96-peptide complexes extracted and purified from an individual patient's tumor. These complexes are reinjected into the patient subdermally and should bind CD91 on dendritic cells [187]. This approach has an advantage in that the tumor antigen does not have to be specifically selected, but may be tailored to the individual patient. Two disadvantages are the preparation of Vitespin®, which requires the patient's tumor to have sufficient non-necrotic tissue, and variations in the immunogenicity of an individual patient's gp96 peptides, which may influence cancer response to treatment. In pilot studies, Vitespin® increased the number of T cells recognizing a tumor-specific antigen in metastatic melanoma patients [191], while a study with metastatic colon cancer patients saw a general increased T cell response to the cancer cells [192]. However, subsequent Phase II/III clinical trials in patients with metastatic renal clear cell carcinoma did not see appreciable clinical gains in time to progression or in survival with the use of Vitespin®, possibly due to insufficient immune response or continued suppression of the immune

response by the tumor microenvironment [193, 194]. An alternative means of producing hsp-complexes would be to use hyperthermia against an easily accessible tumor lesion.

Hyperthermia, or raising the temperature of cells to trigger cell death, has been utilized previously in cancer therapy to sensitize malignant cells to chemotherapy and radiation [152, 158]. The relationship of HSPs with inducing dendritic cell maturation made the extension of hyperthermia as an adjuvant for immunotherapies natural. Shi and colleagues confirmed that melanoma cells heated to 42°C for a minimum of 2 hours had increased HSP70 expression compared to control cells, and demonstrated that heat-treated melanoma cells excited a stronger melanoma-specific CTL response than the control [190]. In addition, Shi et. al. also discovered that melanoma cells treated with hyperthermia had increased expression of tumor antigens than the control cells, suggesting the possibility that the improved specific CTL response could also be due to enhanced antigen expression by the cancer cells [190].

Subsequent studies expanded on this idea by treating tumors with hyperthermia, then injecting immature dendritic cells cultured *ex vivo* directly into the tumor. Intratumoral dendritic cells are thought to modulate the tumor microenvironment by secreting immune response-amplifying cytokines and reducing the number of regulatory T cells [195]. Mukhopadhaya et. al. performed a study in mice bearing xenografted prostate adenocarcinoma [196]. Hyperthermia was performed by placing the tumor-bearing extremity in a warm water bath at 43.7°C for 1 hour; control mice received no hyperthermia treatment. One day after hyperthermia treatment, mice received nothing, granulocyte-macrophage colony stimulating factor (GM-CSF), dendritic cells, or dendritic cells plus GM-CSF. GM-CSF is a cytokine known to stimulate dendritic cell

persistence. Hyperthermia-treated tumors demonstrated primarily apoptotic cell death *in vivo* and had increased levels of HSP70. The combination of hyperthermia, dendritic cell injection, and GM-CSF elevated the number of prostate cancer-specific effector T cells when compared to the other treatment groups and had the smallest amount of tumor volume growth over 22 days. Guo et. al. translated this to humans, performing a pilot study with 9 patients diagnosed with metastatic melanoma [197]. The hyperthermia treatment group received radiofrequency ablation of a single metastatic lesion plus direct injection of immature dendritic cells into the heated lesion, while the non-hyperthermia group received dendritic cell injection alone into a metastatic lesion. Patients treated with hyperthermia demonstrated expression of HSP70, HSP90, and gp96 in the heat-treated tumor lysates, greater expression of T_H1 versus T_H2 cytokines, decreased levels of regulatory T cells in the treated tumor, and migration of dendritic cells to the local lymph nodes. Both treatment groups saw increased levels of activated T cells. Clinically, hyperthermia treated patients had better local response than the control patients, but overall survival was the same.

These studies show promising early results when hyperthermia is combined with the transfer of immune cells. However, the hyperthermia techniques employed above are disadvantaged because of concerns about damaging normal tissue. The addition of a mediating agent, such as gold nanoparticles, would permit localization of the thermal treatment, increase patient tolerance for the hyperthermia treatments, and minimize damage to normal tissues by reducing irradiation power requirements. Several groups have already begun to approach combined hyperthermia and immunotherapy this way. In a study on human metastatic breast cancer patients, Li et. al. administered indocyanine

green (ICG), a NIR-absorbing dye, into the tumor, then heat the tumor using a NIR laser, and finally inject glycated chitosan into the tumor to stimulate an immune response [198]. Kobayashi and colleagues have utilized magnetite liposomes and an alternating magnetic field to induce hyperthermia in rats and mice for their immunotherapy studies[199, 200]. The use of gold nanoparticles instead of a dye or other type of nanoparticle would enhance these types of therapies because of the low toxicity, enhanced NIR absorbance per particle, and simple conjugation of the gold nanoparticle surface to drugs or other molecules.

We propose using AuNP PTT as our hyperthermia modality and adoptively transferring tumor-specific T cells post-ablation. To our knowledge, no previous studies have combined hyperthermia with adoptive T cell transfer. As opposed to using a dendritic cell-based vaccine, the use of adoptive T cell transfer in human patients with metastatic melanoma in clinical trials has shown greater objective clinical response [137, 139], and we hypothesize that a T cell-based immunotherapy will have a greater effect when combined with photothermal ablation. The use of gold nanoparticles for tumor ablation has the added benefit of protecting healthy tissue from thermal damage. We will subcutaneously xenograft two opposing melanoma tumors in immunocompetent C57BL/6 mice. One tumor will serve as the primary tumor, which will be treated with PTT. The other tumor will serve as a secondary tumor and will be monitored for changes in growth secondary to immunotherapy (**Figure 7-2**). Hollow gold nanoshells will be injected intratumorally into the primary tumor and ablated using a NIR laser. One day post nanoparticle injection, tumor-specific T cells will be administered intravenously. The HSP-peptide complexes generated in the primary tumor by the PTT will activate

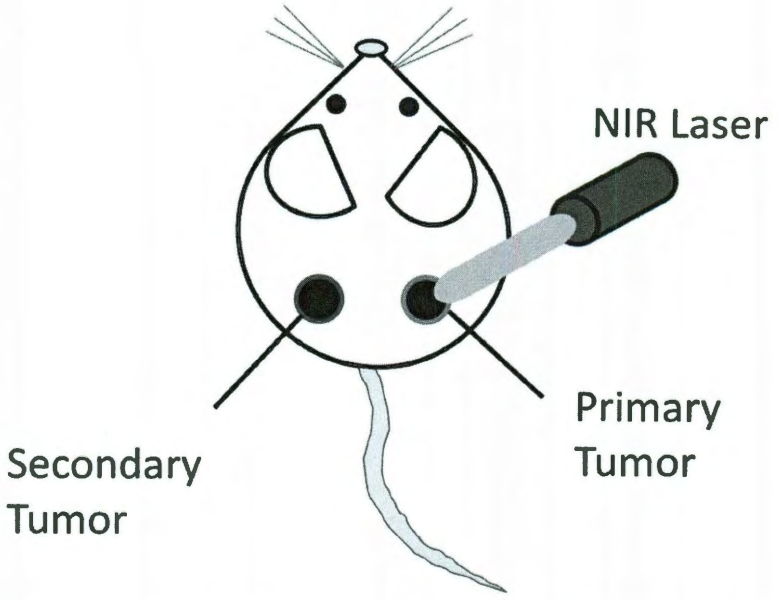

Figure 7-2. Schematic of basic experimental layout. C57BL/6 mice will be seeded with adjacent melanoma tumors. The primary tumor will be injected with HAuNS and treated with a NIR laser to ablate the tumor. One day post-ablation, T cells specific for melanoma will be injected via tail vein. We hypothesize that these cells will be activated and expand in the tumor draining lymph nodes of the primary tumor. The T cells will then suppress growth of the secondary, non-ablated tumor.

dendritic cells and stimulate cross-presentation of tumor antigens to the injected CD8+ T cells. We hypothesize that the tumor ablation will result in increased T cell proliferation, tumor infiltration, and decrease the growth rate of the secondary tumor. Ultimately, we hope that this method will enhance the objective clinical benefits of adoptive T cell transfer in metastatic melanoma and extend patient survival.

Methods

Hollow Gold Nanoshell Synthesis and PEGylation

Silver Nanoparticle Synthesis

Silver nanoparticles (AgNPs) were prepared at 60°C in a well-stirred solution of 0.2mM silver nitrate solution (50mL, $AgNO_3$) in the presence of sodium citrate (0.5mM)

following an injection of 100 sodium borohydride solution (1mL, $NaBH_4$), which produces a yellow color. The silver colloid was allowed to stir at 60°C for a minimum of two hours.

Increasing Core Size

The Ag core solutions were then allowed to cool to room temperature. AgNP growth was initiated by adding a 200mM hydroxylamine hydrochloride solution (1mL, NH_2OH-HCL) to the silver colloid, followed by stirring for a minimum of 5 minutes. An additional 200μL $AgNO_3$ (0.1M) solution was injected, and the solution was allowed to age for a minimum of 24 hours with stirring. Growth was confirmed by the solution changing to a dark yellow or orange color based on the amount of $AgNO_3$ added.

Gold Shell Growth

The aged silver core solutions were then heated to 80°C and stirred at a rate of 900 RPM. A 1 mL $HAuCl_4$ (25mM) solution bolus was injected into the silver core solution. The solution immediately changed color from the yellow-orange of the cores to a dark blue-black. The blue-black solution was allowed to stir for an additional 10 minutes. Each 50mL Ag core solution with 1mL 25mM $HAuCl_4$ addition generated a final HAuNS solution with an OD between ~2.5 to 3.

The gold nanoparticles were centrifuged at 2500 g for 30 minutes and the supernatant removed. The pelleted nanoparticles were resuspended in in MQ water. The washing step was repeated 2-3 times. Nanoparticles were sterilized by passing the solution through a 0.22 μm polyethylsulfone syringe filter. The concentration of the nanoparticles was determined after sterilization using a combination of Mie Theory and the nanoparticle extinction spectra.

PEGylation of Hollow Gold Nanoshells for Injection

The day prior to the mouse study, particles were coated with sterile polyethylene glycol (PEG MW 5000) by adding an optimized amount of 1 mM PEG solution. The optimized ratio of PEG molecules to gold nanoparticles was determined using a salt stability assay as described previously in Chapters 4 and 5. The nanoparticles and PEG were incubated overnight at 4°C. Excess PEG molecules were then removed by centrifuging the nanoparticles and removing the supernatant. The nanoparticles were then resuspended in sterile 1x PBS immediately prior to mouse injection.

Preparation of T cells for Adoptive Transfer

To acquire murine T cells for culture, a PMEL mouse was sacrificed and the spleen resected. Pmel T cells have a TCR specific for the mouse equivalent of gp100. A single cell suspension of splenocytes was created by placing the spleen in a cell strainer, homogenizing with the end of a syringe pluger, and washing with normal phosphate buffered saline (PBS). The strainer was washed with 15 additional milliliters of PBS. Cells were pelleted by centrifugation at 400 g for 5 minutes and the supernatant removed. Cells were resuspended in 10 milliliters of fresh PBS. Red blood cells were removed and white blood cells isolated using FICOL centrifugation. Isolated leukocytes were washed twice in fresh PBS. Leukocytes were respuspended in RPMI media supplemented with 10% fetal calf serum, 1% glutamax, 1% HEPES buffer, and 0.001% 2-B mercaptoethanol. The T cells in the splenocyte resuspension were stimulated to proliferate by the addition of murine IL-2 (10 ng/mL) and ConA (5 μg/mL). The cells were seeded in a 24-well plate, placed in a 37°C incubator with 5% CO_2, and allowed to grow to confluency.

Photothermal Ablation of Tumors Using HAuNS

Two tumor models were used for this study. The first model, B16-OVA, is a melanoma cell line that has been engineered to express chicken ovalbumin, which is an antigen with excellent immunogenicity. This mouse model will be used to evaluate the endogenous response of the mouse immune system to PTT. The second model, B16F10, is a melanoma cell line that expresses the murine equivalent of gp100, a known marker of human melanoma. This group will receive PTT followed by adoptive transfer therapy of pmel T cells.

To xenograft the melanoma tumors, C57BL/6 mice were anesthetized with isoflurane and received two subcutaneous injections of 2.5 x 10^5 B16F10 or B16-OVA melanoma cells, one in each flank. Tumors were allowed to grow to 5 x 5 mm over the course of 7-10 days. To treat the primary tumor with PTT, mice were again anesthetized using isoflurane. The region around the tumor was shaved to remove excess hair, then injected with 10 microliters of PEG-coated hollow gold nanoshells (OD ~40) in the primary tumor as shown in Figure 6.1. Nanoshells were allowed to disperse throughout the tumor for 5 minutes. The tumor was then irradiated with a near-infrared laser (Coherent diode array laser, λ = 808 nm, 3 W/cm^2) for 3 minutes. In the mice with B16F10 tumors, an intravenous injection of 10 x 10^6 PMEL T cells in a 100 microliter bolus was administered one day after PTT. Tumors were monitored for volume changes using digital calipers and mouse survival was recorded.

Bioluminescent Imaging for T Cell Expansion

To visualize the T cell biodistribution and expansion, T cells were transduced with retrovirus encoding GFP*luc* as previously described [167]. Forty-eight hours post-T cell infusion, the biodistribution of T cells was visualized using the *In Vivo* Imaging System (IVIS; Xenogen) following intraperitoneal (i.p.) injection of 150 mg/kg D-luciferin (Xenogen, Alameda, CA). The biodistribution was evaluated at a minimum of three timepoints: 24 hours, 48 hours, and 96 hours.

Analysis of Immunological Response to Ablation

Immune Cell Phenotyping

One week post-ablation, mice were sacrificed and the tumor, tumor-draining lymph nodes, and spleen were resected. The tumor, lymph nodes, and spleen were homogenized through a cell strainer and washed using complete splenocyte media. To look at the phenotype of the immune cells present in each tissue, we used the following monoclonal antibodies conjugated to FITC, PE, PerCP, or APC (BD Biosciences): CD4, CD8, CD25, Thy1.1, CD11c, CD80, CD86, I-A/I-E, CD11b, GR-1, and Thy1.1. Cells were analyzed using a FACSCalibur flow cytometer (BD Biosciences) and FCSExpress software (De Novo Software, Los Angeles, CA).

ELISPOT

ELISPOT was performed on the extracted spleen and lymph node cells to evaluate IFN-γ expression of the T cells in response to melanoma tumor antigens OT-1, Trp-2, and gp100. The ELISPOT plate was prepared with anti-IFN-γ antibody and blocked with complete RPMI media to prevent non-specific binding. Cells were seeded into the wells (1×10^6 cells/well from the spleen and 2×10^5 cells/well for the lymph

nodes) and the tumor antigen peptides were added (final concentration in well = 5 μM). Cells were incubated with the peptide for 20 hours at 37°C. Cells are then decanted and the ELISPOT plate is washed using PBS and 0.05% Tween 20. A biotinylated secondary antibody is then added for 2 hours at 37°C and followed by a 1 hour room temperature incubation with Vectastain, an avidin-peroxidase complex. The ELISPOT plate is then thoroughly washed using 0.05% Tween 20 in PBS and developed by incubating each well with AEC chromogen for 4 minutes at room temperature. The color development is stopped by rinsing the plate thoroughly in tap water. After overnight drying of the plate in the dark, the membrane is removed and counted for IFN-γ signal.

32 plex Cytokine Kit

Ablation study was performed on mice having a single tumor in the right flank. After ablation, peripheral blood was collected by retroorbital bleed at the 24 and 96 hour timepoint post-ablation. A 32-plex Milliplex MAP Mouse Cytokine/Chemokine panel kit (Millipore # MPXMCYTO-70K) was used to quantify cytokine and chemokine levels.

Results

Characterization of Hollow Gold Nanoshells

Synthesized hollow gold nanoshells had a final outer diameter of 40-42 nm with a shell thickness of 5-7 nm. The extinction peak maximum was at 780 nm (**Figure 7-3**).

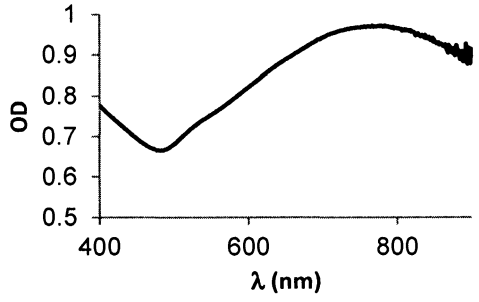

Figure 7-3. Extinction spectra of hollow gold nanoshells used for photothermal ablation.

Endogenous T Cell Response to Gold Nanoparticle PTT

The first studies performed looked at endogenous T cell response after ablation of B16-OVA primary tumors using hollow gold nanoshells. A B16F10 cell line with engineered expression of chicken ovalbumin (OVA) was used for these studies because the OVA protein is perceived as foreign and has excellent immunogenicity. These initial studies were designed to evaluate the immunological benefits of gold nanoparticle PTT

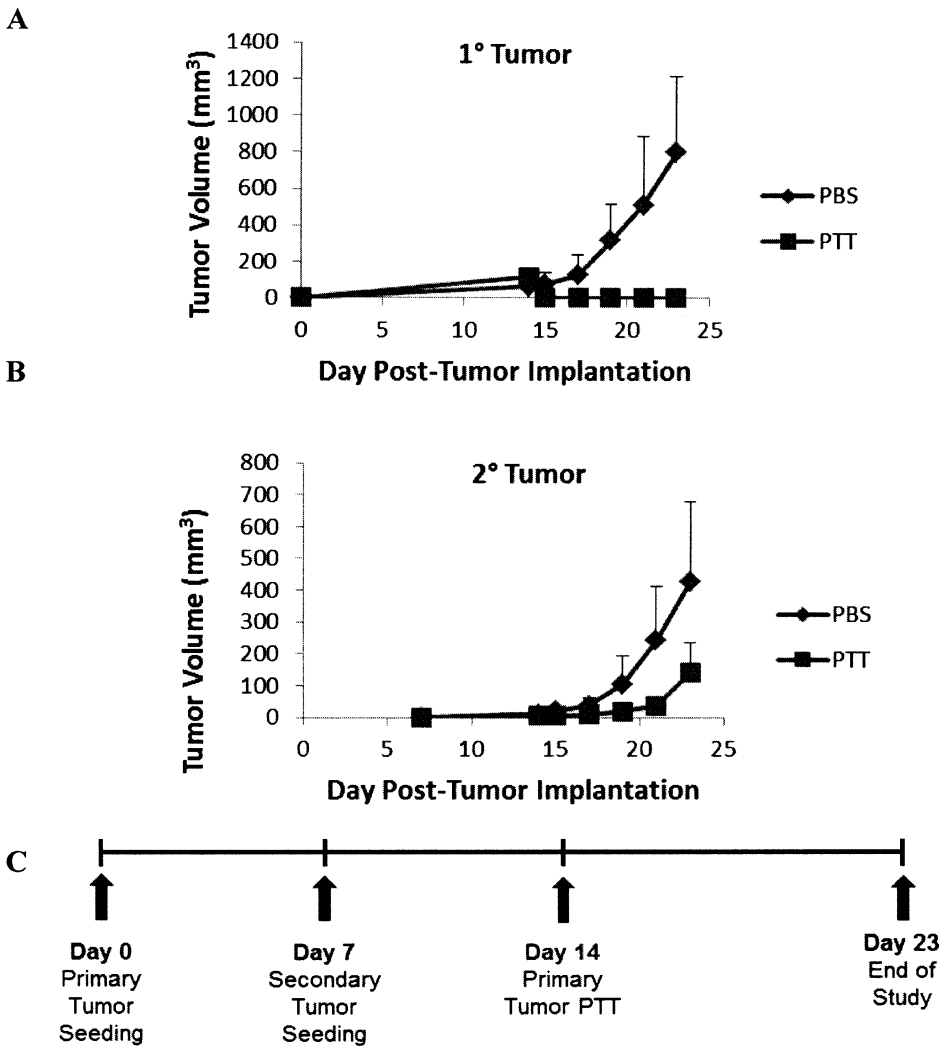

Figure 7-4. Tumor volume changes after PTT treatment of primary B16-OVA tumors. A) The PTT-treated primary tumor volume goes to 0 mm^3 and remains at 0 mm^3 for the remainder of the study. B) The secondary tumor in the PTT-treated mice has suppressed growth when compared to the secondary tumor of the PBS-treated mice. C) Timeline for tumor seeding and treatment.

and the impact of PTT on T cell activation and tumor response. Mice were xenografted with bilateral B16-OVA tumors, and one of the two tumors was treated using PTT on day 14 post-primary tumor seeding. After ablation, tumor volume was monitored using digital calipers for 9 additional days (**Figure 7-4**). The ablated tumors collapse to a tumor volume of 0 mm^3, and remain 0 mm^3 for the remainder of the study. The secondary or distant tumor growth appears suppressed when compared to PBS-treated mice.

To evaluate the immune system's role in the tumor suppression, a second study was performed where the secondary or distant tumors of PTT-treated and PBS mice were resected 7-8 days post-ablation. The number of viable tumor cells was evaluated by using flow cytometry and looking at at the forward and side scattering of the cells (**Figure 7-5**). The secondary tumors in the PTT-treated mice trended towards having a smaller number of viable cells than the secondary tumors in the PBS-treated mice, but this difference was not statistically significant ($p = 0.06$).

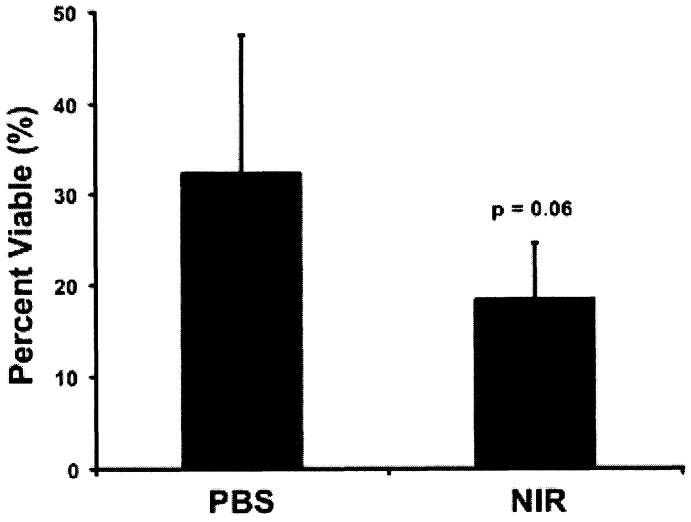

Figure 7-5. B16-OVA distant tumor cell viability by flow cytometry after treatment with PBS (PBS) or PTT (NIR). The secondary tumor cells were less viable in the group where the primary tumor was treated with PTT versus PBS.

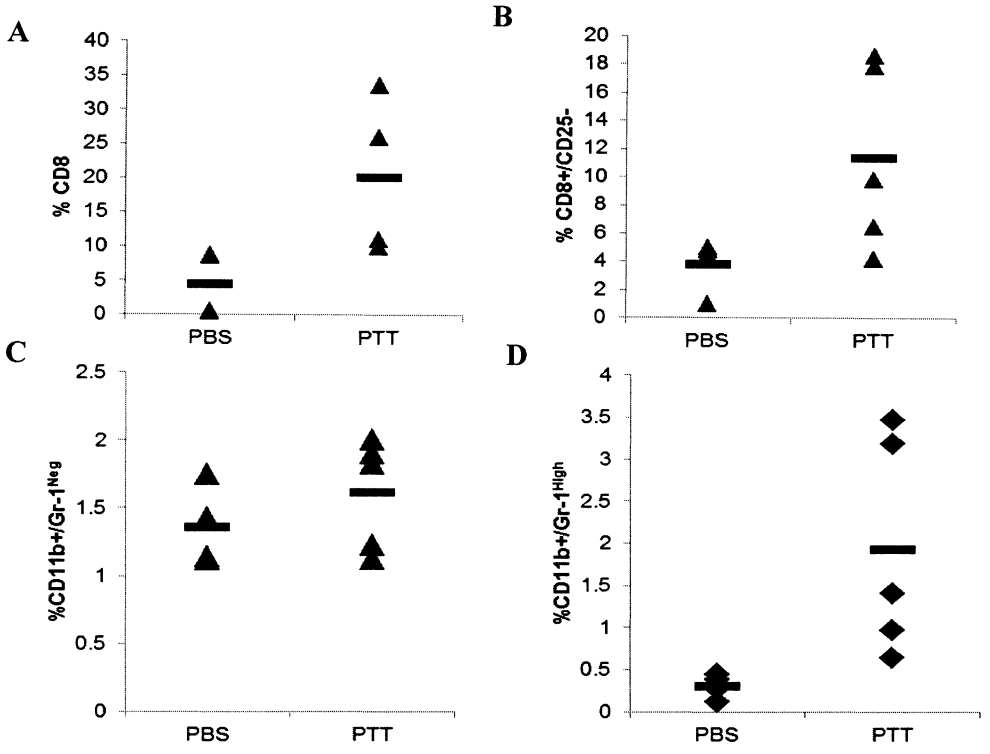

Figure 7-6. Flow cytometry analysis of tumor microenvironment. A) Percentage of cytotoxic T cells (CTLs) present in the tumor. B) Percentage of activated CTLs within the tumor. C) Percentage of tumor infiltrate that is made up of macrophages. D) Percentage of the tumor infiltrate that is composed of myeloderived suppressor cells.

Further evaluation of the tumor cell content reveals that the PTT-treated mice had a larger number of $CD8^+$ T cells ($p < 0.05$) infiltrating the tumor (**Figure 7-6**). The PTT-treated mice did not have significantly larger macrophage population than the PBS-treated mice, but did have a significantly larger ($p < 0.05$) infiltrate of myeloderived suppressor cells (MDSCs). While macrophages are capable of suppressing tumor growth, MDSCs are cells that participate in the anti-immunity response of the tumor. The PTT-treated mice also have a higher concentration of activated T cells ($CD8^+/CD25^+$) ($p < 0.05$) than the PBS-treated mice. CD25 is a marker of T cell activation. Activated CTLs secrete IFN-γ, a cytokine that attracts macrophages, and the secondary tumors in the PTT-treated mice also show a higher tumor infiltration of macrophages. This result is highly promising for

PTT being able to stimulate adoptively transferred T cell effector function against the tumor.

An ELISPOT for IFN-γ expression was also performed on the tumor-draining lymph nodes extracted from the mice. Although changes in the T cell and macrophage populations of the secondary tumor were seen in the PTT-treated mice, no significant differences in IFN-γ expression were seen between the PBS-treated and PTT-treated mice in response to ovalbumin, Trp-2, or gp100. However, because no booster, i.e. second

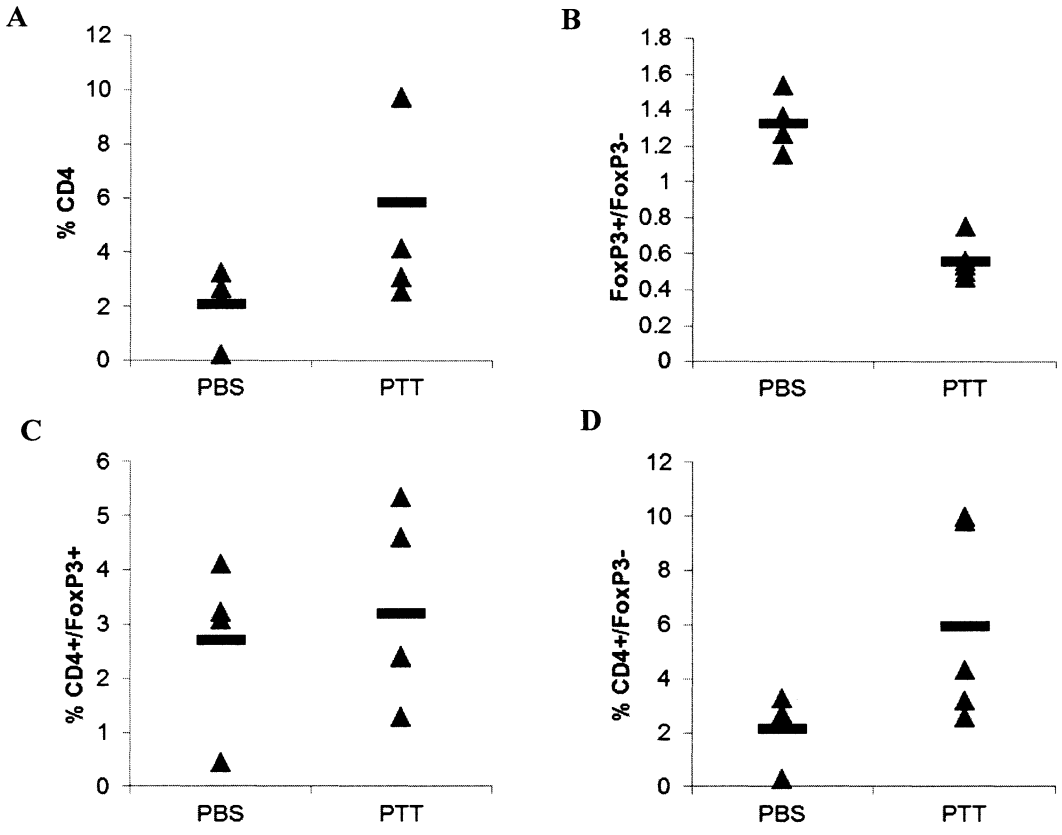

Figure 7-7. Flow cytometry analysis of tumor microenvironment. A) Percentage of helper T cells present in the tumor. B) Ratio of regulatory to non-regulatory helper T cells. C) Percentage of tumor infiltrate that is regulatory helper T cells D) Percentage of the tumor infiltrate that is non-regulatory helper T cells.

ablation, was performed on these mice, that result was not surprising.

The PTT-treated mice also had an increased percentage of helper T cells infiltrating the tumor compared to the control mice (**Figure 7-7**). Helper T cells are important for complete activation of CTLs against tumor cells. We also evaluated the ratio of FoxP3+ helper T cells to FoxP3- helper T cells. FoxP3 is a marker of regulatory T cells, which have a role in suppressing the immune response against the tumor. The ratio of regulatory T cells in the secondary tumor was lower in the PTT-treated mice than the PBS-treated mice. Although the percentage of regulatory T cells in both the PBS and PTT mice was about the same, the percentage of non-regulatory T cells in the PTT mice was significantly higher ($p = 0.029$).

Based on these results, we have established that PTT does increase T cell activation and proliferation against distant tumors. Increased tumor infiltration by CD8+ and CD4+ T cells was seen in the secondary tumor of the PTT-treated mice with a corresponding increase in CD8+ T cell activation. The next experiments focus on treating melanoma tumors with PTT that are not engineered with an immunogenic foreign protein. For this set of experiments, we will use adoptively transferred pmel T cells that target gp100, an endogenous melanoma antigen.

Hyperthermia-Enhanced Immunotherapy of Melanoma

The combination of PTT with pmel T cells is envisioned to combine the benefits of tumor debulking given by PTT with the ability of pmel T cells to localize and destroy tumor cells in distant lesions. Based on the results in the previous section, we hypothesize that PTT will stimulate an augmented pmel T cell response to the secondary

melanoma tumor that has not been directly treated via ablation. The experimental set-up was the same bilateral tumor design described in **Figure 7-2**. Melanoma-bearing mice were treated with PBS or PTT in the primary tumor on day 10 post-tumor challenge. Mice then received either PBS or pmel T cells by tail vein injection 24 hours after ablation, giving a total of 5 treatment groups: PBS alone, PTT alone, pmel T cells alone, pmel T cells plus a direct injection of HAuNS with no laser irradiation, or combined PTT and pmel T cells.

Tumor volume was monitored using digital calipers (**Figure 7-8**) for approximately a week after treatment. The two groups that received PTT had primary tumor volumes of 0 mm^3 one day post-treatment. Primary tumors that did not receive PTT continued to grow. The secondary tumors that received pmel or pmel+PTT treatment seem to have a slower rate of growth when compared to the PBS, PTT, or pmel+HAuNS group secondary tumors. This supports our assertion that adding adoptively transferred T cells to therapy could have benefits for treating distant or metastatic lesions.

We next looked at the overall tumor burden of each treatment group by adding the primary and secondary tumor volumes together (**Figure 7-9**). As expected, mice receiving PTT of the primary tumor had lower tumor burden than mice that did not receive PTT ($p < 0.05$, Tukey-Kramer comparison). The ablation of the primary tumor serves as a debulking agent. As established in the previous section, it also has effects on the tumor microenvironment that extend to the secondary, untreated tumor. Although there is no statistically significant difference between the total tumor burden of the PTT-

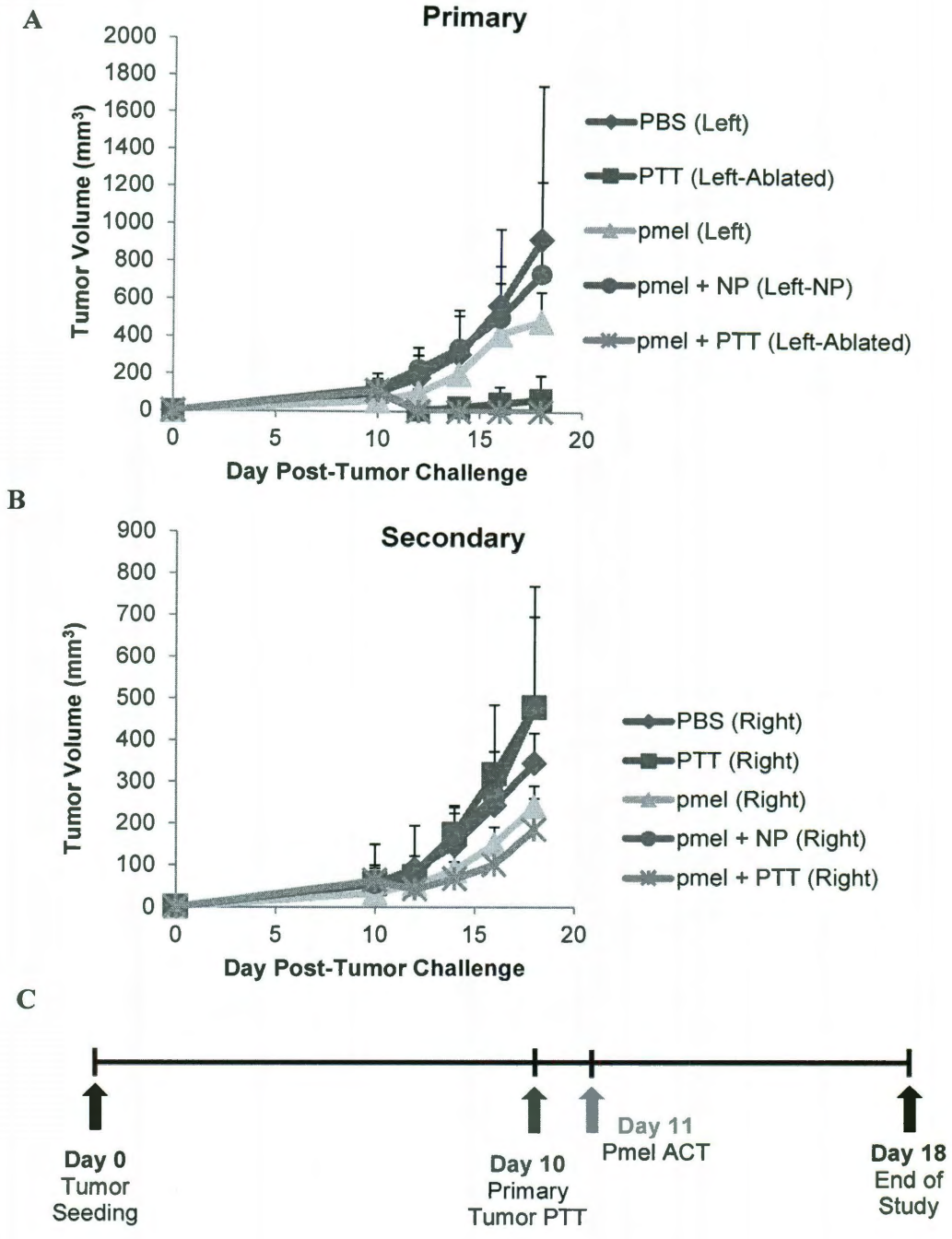

Figure 7-8. Tumor volume data for B16F10 tumors treated with a combination of PTT and pmel T cell adoptive transfer. The primary tumor received a direct injection of either PBS, ablation, or nanoparticles alone. Twenty-four hours post-primary tumor treatment, mice received either an intravenous injection of PBS or of pmel T cells. A) Primary tumor (left flank) tumor volume data. B) Secondary tumor (right flank) tumor volume data. C) Timeline of the study.

treated and pmel+PTT-treated mice ($p = 0.115$, Tukey-Kramer comparison), there does seem to be a difference in the rate of secondary tumor growth between the two groups (**Figure 7-10**). The secondary tumors in the pmel+PTT group had a slower rate of growth than the secondary tumors of the PTT group ($p < 0.05$, Tukey-Kramer comparison), strongly suggesting that the combination of PTT and adoptive transfer of pmel T cells may have some benefit in treating patients with distant lesions such as metastases. The reduced tumor burden provided by the PTT and the reduced distant lesion growth provided by the pmel T cells has the potential to prolong survival.

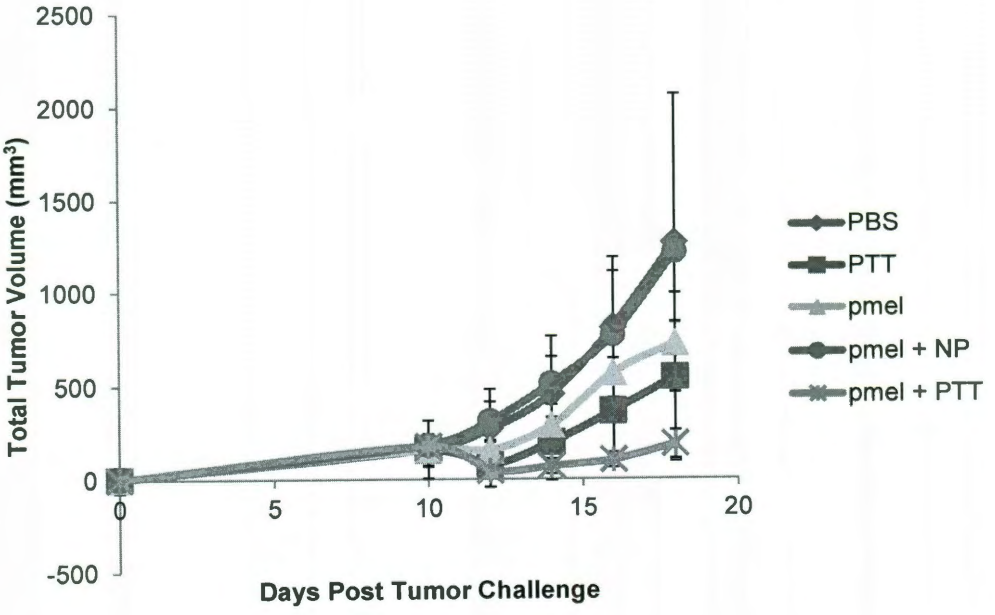

Figure 7-9. Total Tumor Burden for mice seeded with B16F10 tumors and treated with a combination of PTT and pmel adoptive transfer. Total tumor burden is significantly lower in mice treated with PTT or pmel+PTT ($p < 0.05$).

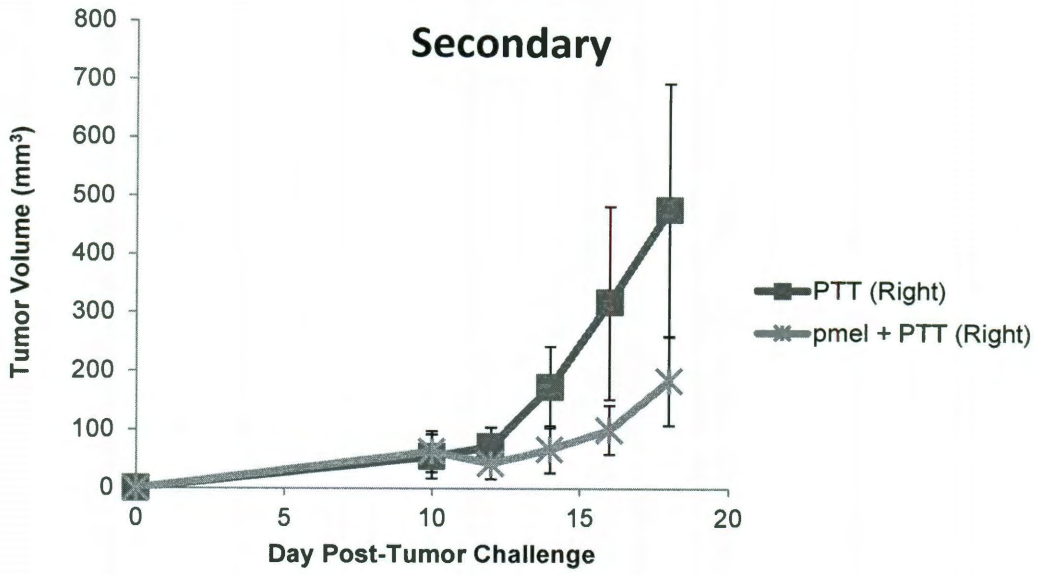

Figure 7-10. Detail from **Figure 7-7** showing secondary tumor growth of the PTT treated group versus the pmel+PTT group.

Based on the tumor growth data shown in **Figure 7-8**, **Figure 7-9**, and **Figure 7-10**, we expect to see increased expansion and tumor infiltration of pmel T cells into the secondary, non-ablated tumor of the pmel+PTT mice. Bioluminescent imaging was used to evaluate T cell expansion *in vivo* by modifying the pmel T cells with firefly luciferase. **Figure 7-11** shows the pmel and pmel+PTT treatment groups. The maximum T cell accumulation in the secondary tumor (left flank for this study) was seen at 72 hours. Stong signal can be seen within the spleen of some mice at both 24, 72, and 144 hours. The tumor draining lymph nodes of the mice did not show significant accumulation over the course of bioluminescent imaging (data not shown). Using the bioluminescent signal as a means for comparison and normalizing the signal to the 24 hour timepoint, the pmel+PTT group demonstrated a transient T cell expansion at 72 hours ($p < 0.05$), while the pmel only group does not demonstrate a T cell expansion (**Figure 7-12**). This

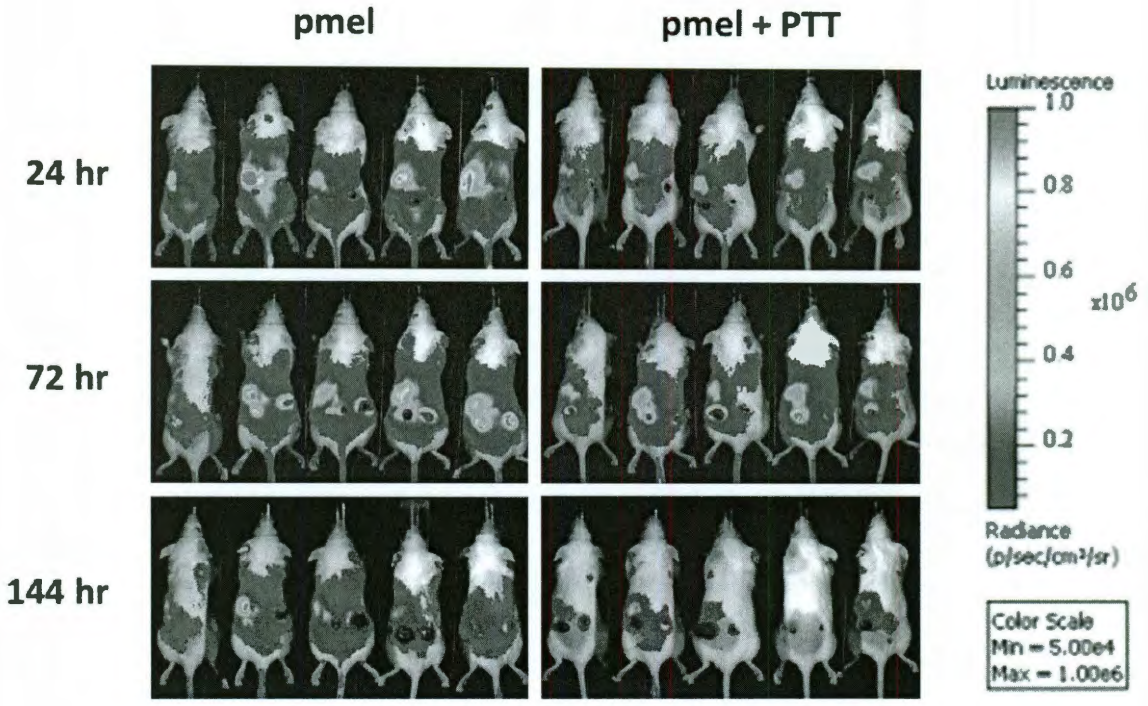

Figure 7-11. IVIS imaging data showing pmel T cell biodistribution. T cells are seen mostly in the lungs and the spleen at 24 hours, then gradually accumulate at the tumor sites over the course of the next 48 hours. At the 144 hour timepoint, the T cells have been predominantly cleared from the tumors.

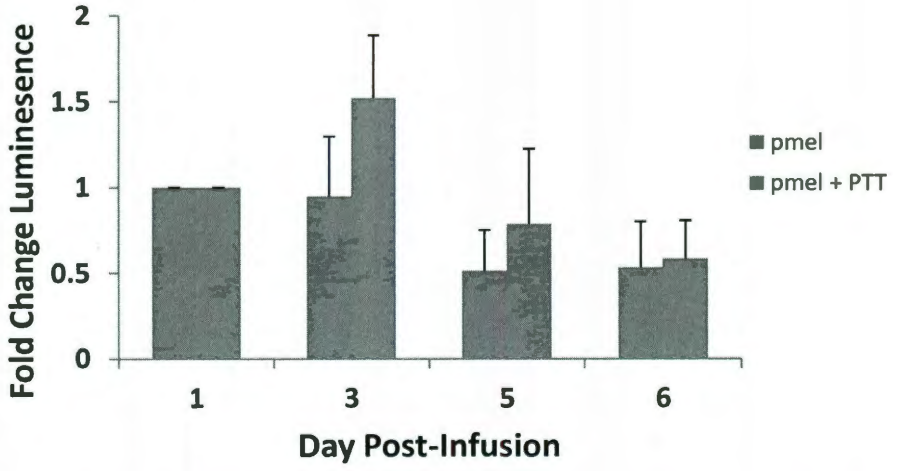

Figure 7-12. IVIS signal normalized to 24 hour timepoint. The pmel+PTT treatment group demonstrates a transient expansion at the 72 hour timepoint, while the pmel treatment group does not demonstrate any expansion.

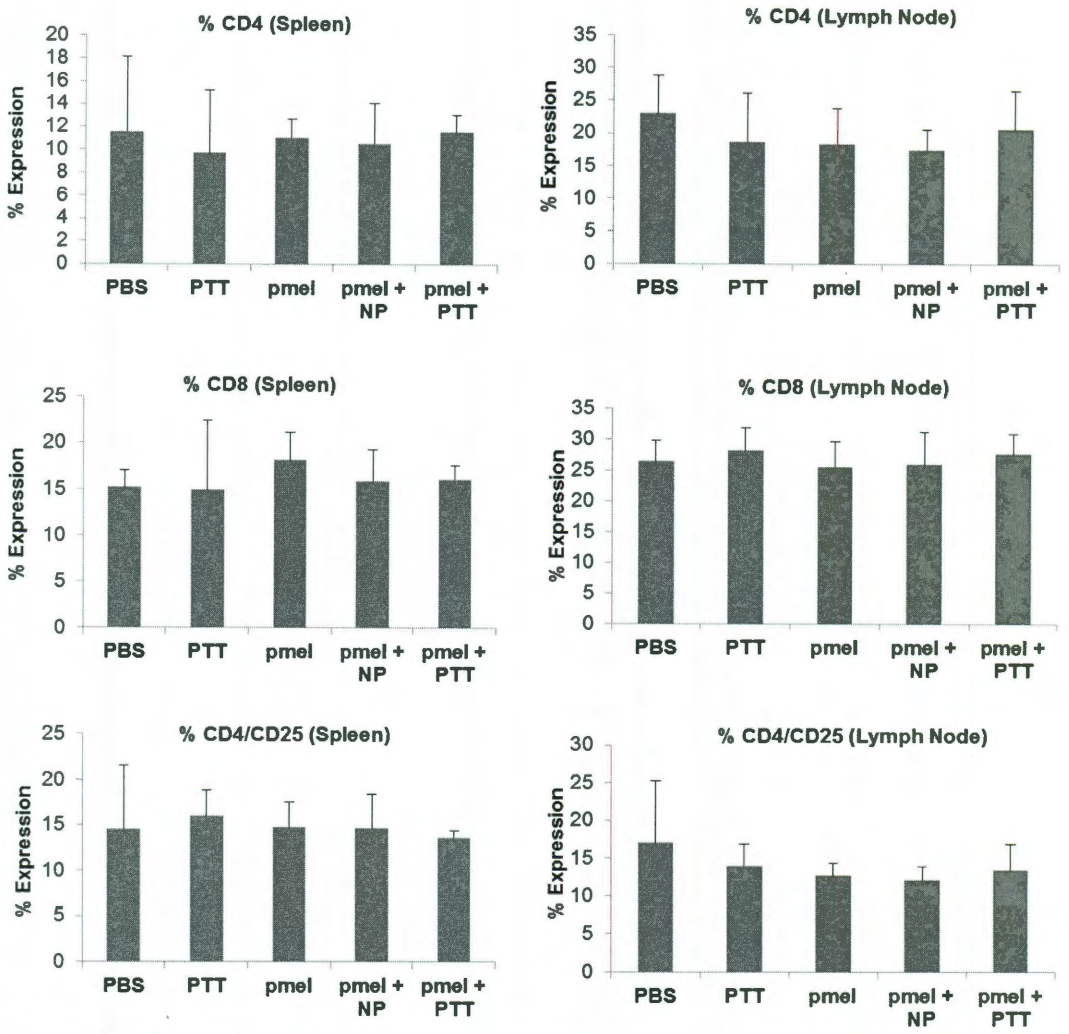

Figure 7-13. T cell phenotype in the spleen and tumor-draining lymph nodes 1 week after B16F10 ablation. No significant differences were seen in tumor-draining lymph node phenotype.

expansion suggests that the addition of PTT may have stimulatory effects on adoptively transferred T cells.

We next looked more closely at differences in cell phenotype in the spleen and tumor-draining lymph nodes between the treatment groups 1 week after ablative treatment using flow cytometry. No significant differences in T cell phenotype were seen between treatment groups in either the spleen or the tumor-draining lymph nodes (**Figure**

7-13). The lack of T cell phenotype change in the spleen simply indicates that the effects from pmel+PTT treatment are not systemic.

We next stained for Thy1.1, a pmel T cell marker. Endogenous T cells express Thy1.2, not Thy1.1, so this marker allows us to differentiate between adoptively transferred and native T cells. Using flow cytometry, pmel T cells were detected in both the spleen and the lymph nodes of mice in the pmel T cell-receiving groups (**Figure 7-14**). There was no significant difference in pmel T cell accumulation between treatment groups in the spleen, but there were differences in pmel T cell accumulation in the tumor

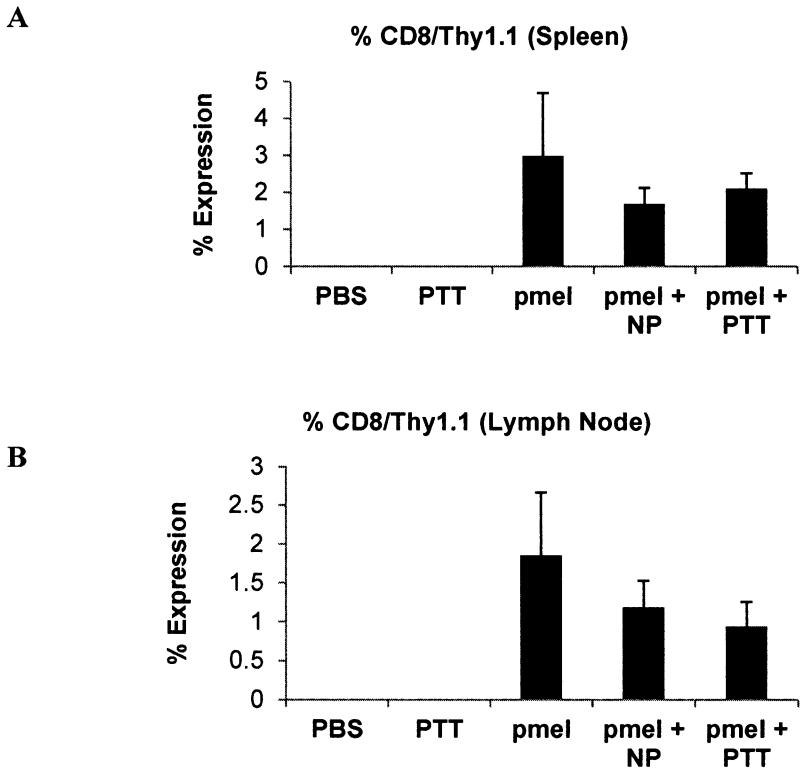

Figure 7-14. A) Spleen pmel expression one week after B16F10 tumor ablation. No significant differences are seen between the pmel, pmel+NP, and pmel+PTT treatment groups in the spleen. B) pmel T cell accumulation in the lymph nodes one week after B16F10 ablation. Quantified average Thy1.1 expression for different treatment groups. The pmel+PTT treatment group has lower accumulation of pmel T cells in the tumor draining lymph nodes than the pmel treatment group.

draining lymph nodes (**Figure 7-14**). While the pmel only treatment group had the most accumulation of pmel T cells in the tumor-draining lymph nodes, the pmel + PTT group had the least accumulation of pmel T cells in the tumor draining lymph nodes.

Despite the pmel+PTT treatment group's lower pmel T cell lymph node accumulation, the ELISPOT performed on the tumor draining lymph nodes for IFN-γ secretion shows that the pmel+PTT group has higher IFN-γ secretion in response to gp100 than the pmel only treatment group ($p < 0.05$, **Figure 7-15**). This correlates to a higher IFN-γ secretion per T cell in the pmel+PTT group than in the pmel only group. No difference is seen between the pmel and pmel+PTT treatment groups in the spleen ELISPOT for IFN-γ production in response to gp100. PTT seems to induce an enhanced T cell response in the local environment of the tumor.

Despite these indications that the T cell response is restricted to the tumor draining lymph nodes and does not extend systemically, we did look at the peripheral blood cytokine profile mice with a single tumor receiving either PBS, PTT, pmel T cells,

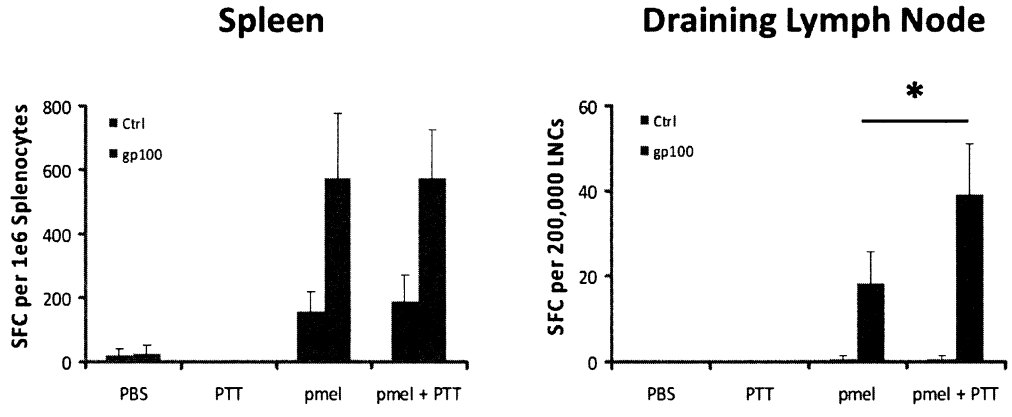

Figure 7-15. IFN-γ ELISPOT results for spleen and tumor draining lymph nodes one week after B16F10 ablation. No differences in IFN-γ response to gp100 are seen in the spleen, but in the lymph nodes the pmel+PTT treatment group has a greater IFN-γ response than the pmel alone treatment group.

or combination pmel T cell and PTT. Peripheral blood was collected 24 and 96 hours after ablation and analyzed for cytokine levels. At the 24 hour timepoint, three cytokines had statistically significant differences between PTT-treated, PBS-treated, and tumor-free mice: interleukin-6, KC, and MIP-1β **(Table 7-1)**. For each of these cytokines, there were no significant differences in expression between mice with tumors and mice without tumors. This suggests that the cytokine changes at this point are directly associated with the tissue damage or burn done by tumor ablation. Interleukin 6 is an early mediator the T_H17 inflammatory response, which is associated with burns.[201] No difference between groups was seen for interleukin-7, another T_H17 early mediator, and

Table 7-1. Significant ($p < 0.05$) Cytokine Profile Changes 24 hours After Ablation

Cytokine/Chemokine	PTT-treated vs PBS-treated Mice	PTT-treated vs Tumor-Free Mice	PBS-treated vs Tumor-Free Mice
Interleukin-6	↑	↑	Equal
KC	↑	Equal	Equal
MIP-1β	↑	↑	Equal

Table 7-2. Significant cytokine profile differences 96 hours post-ablation

Cytokine/Chemokine	PTT-treated vs PBS-treated Mice	pmel+PTT-treated vs PBS-treated Mice	PBS-treated vs Tumor-Free Mice
IL-1β	↑	↑	Equal
IP-10	↓	Equal	↑
VEGF	↓	↓	↑

TGF-β was not one an analyte on the cytoplex kit. A later mediator of the T_H17 response, interleukin-17, also was not statistically different between treatment groups. Both elevated KC and elevated MIP-1β are also associated with burn injuries.[202]

On day 4 post-ablation, three different cytokines have statistically significant differences between the PBS-treated, tumor-free, PTT-treated, pmel-treated, and pmel+PTT-treated mice: interleukin-1β, IP-10, and VEGF (**Table 7-2**). Like IL-6, KC, and MIP-1b at the 24 hour timepoint, the IL-1β increase in the mice treated with PTT is most likely associated with the burned tumor tissue, and has previously been shown to be increased in burn injuries.[202] However, the addition of pmel T cells to the PTT treatment seems to increase the amount of IL-1β present in the peripheral blood at 96 hours when compared to PTT alone. This result is encouraging, as IL-1 is produced by macrophages in response to IFN-γ stimulation by T_H1 $CD4^+$ T cells.

IFN-γ-inducible protein 10 (IP-10) secretion is also stimulated by the presence of IFN-γ. The IP-10 level is higher in mice with tumors versus mice without tumors, indicating that this cytokine is affected by the presence of the tumor. IP-10 is a chemokine that has been associated with IL-12 mediated tumor growth suppression and the attraction of T cells and NK cells to tumor sites.[203, 204] PTT reduces IP-10 levels below that of the PBS-treated control tumors to levels comparable with tumor-free mice. Because these mice only had one tumor instead of two, this could reflect complete ablation of the tumor. However, the pmel+PTT treated mice had levels of IP-10 that were comparable to the PBS control mice. The likely explanation is IFN-γ secretion by the pmel T cells in response to tumor antigen found in the tumor-draining lymph nodes, which would result in increased levels of IP-10. IP-10 is also known to be a strong

inhibitor of angiogenesis *in vivo*, and tumor progression is associated with lowered levels of IP-10.[205, 206] Although PTT alone lowered IP-10 levels, a combination of PTT+pmel resulted in IP-10 levels that were on the same level as the PBS-treated mice.

Another angiogenesis factor that had signficant changes after PTT was vascular endothelial growth factor (VEGF). While IP-10 functions as an anti-angiogenic factor, VEGF functions as a pro-angiogenic factor in the tumor. However, high levels of IP-10 are associated with lower levels of VEGF.[205] In our study, the mice with tumors had higher levels of VEGF than the tumor-free controls ($p < 0.05$). Mice receiving either pmel T cells, PTT, or combination PTT and pmel T cells all had significantly lower levels of VEGF than the PBS control mice with tumors ($p < 0.05$).

Discussion

Metastatic cancer continues to be a leading cause of cancer death. Immunotherapy has emerged as an effective treatment of metastatic melanoma and is able to produce objective clinical responses in up to 60% of clinical trial patients. However, the lymphdepletion schemes used in these trials are a risk for the patient, and many patients fail to respond to adoptive T cell transfer. The combination of gold nanoparticle PTT and adoptive T cell transfer presents a possible enhancement of immunotherapy treatment for metastatic cancer. The use of PTT as an immune system stimulant may decrease the need for lymphodepletion prior to adoptive cell transfer and increase the number of responding patients.

We have demonstrated that the combination of hollow gold nanoshell-mediated ablation and intravenous administration of T cells that specifically target gp100, a melanoma antigen, can suppress the growth of distant tumors. We initially evaluated the

response of endogenous T cells to PTT using a B16-OVA tumor model. The engineered chicken ovalbumin antigen used in this study is considered foreign by the mouse immune system, and thus stimulates a strong immune response. Using this model, we demonstrated that treatment with PTT induces distant tumor suppression and superior CTL and helper T cell infiltration of the distant tumor compared to control tumors.

We next evaluated the combination of PTT and immunotherapy using B16F10 melanoma tumors in combination with pmel T cells, which are specific for the murine gp100 that is expressed in B16F10 cells. This is a more realistic tumor model, as tumor antigens often have moderate to low immunogenicity due to their great similarity to molecules recognized as self by the immune system. In this study, we did see moderate suppression of distant tumor growth after PTT ablation and pmel T cell infusion compared to PTT ablation alone. In addition, the combination of PTT with pmel T cells resulted in a transient expansion of pmel T cells *in vivo* at the 72 hour timepoint and increased IFN-γ secretion in response to gp100 in the tumor-draining lymph nodes. These T cell effects were seen without systemic injections of IL-2 or lymphodepletion prior to T cell administration, both of which have previously been required to get the clinical response seen recently in clinical trials. These results are encouraging for PTT being able to induce a T cell response against the tumor without IL-2 or lymphodepletion.

The second study also demonstrates the additive effects of PTT and pmel T cells. When looking at the total tumor burden of the mice, mice treated with PTT had substantially lower tumor burden than non-PTT treated mice due to the ablative debulking of one of the two tumor masses. Lower tumor burden has been demonstrated in previous PTT studies to correlate with longer survival times.[34, 47, 207] However,

PTT to date has not been able to address metastatic disease because of the difficulty in targeting the NIR laser to every metastatic lesion. We have shown that the addition of pmel T cells after PTT slows distant tumor growth when compared to PTT alone. In addition, the secondary tumors that we were using to model distant lesions were comparable in size to the primary tumors. In reality, metastases are usually much smaller than the primary lesion, and the T cells would most likely be more effective. We conclude, therefore, that the combination of PTT and adoptive T cell transfer may have utility against metastatic disease.

Finally, the second study demonstrates that there may be some benefit for using combined PTT and adoptive T cell transfer in terms of chemokine profiling. Mice treated with photothermal therapy had decreased levels of VEGF when compared to the PBS-treated mice. The addition of pmel T cells to photothermal therapy resulted in a low level of VEGF and a higher level of IP-10, which has angiostatic effects, compared to PTT-alone. This profile has been shown to be favorable to preventing tumor progression and angiogenesis.[205]

Future studies could begin to apply this treatment strategy to models of melanoma with lung metastases to evaluate the impact of PTT and pmel T cell transfer on metastase progression. Studies exploring the immunological mechanisms behind the PTT enhancement of T cell response could also be performed. Because dendritic cells have previously been implicated in hyperthermia-enhanced immune responses, it would be interesting to repeat these treatments in dendritic cell knock-out mice. Future experiments could also focus on increasing the T cell response by choosing different tumor antigens to target, or by using a population of T cells that target multiple tumor

antigens to maximize response. We have demonstrated that the combination of PTT with adoptive T cell transfer, or hyperthermia-enhanced immunotherapy (HIT), has potential for suppressing metastatic cancer growth and extending patient survival.

CHAPTER 8

CONCLUSIONS AND FUTURE WORK

Conclusions

Cancer research continues to be highly funded, with the NIH estimating it spent over $5 billion dollars in cancer research in 2010.[208] This research funding reflects the impact that cancer has on the United States as one of the leading causes of death. Researchers continue to seek new ways to prevent, screen, diagnose, and treat cancer. Gold nanoparticle photothermal therapy (AuNP PTT) is one technology that has recently gone to clinical trials for the treatment of head and neck cancer. This technology has advantages in that it has high tumor specificity, low occurrence of side effects, and the ability to treat any tumor that is accessible to NIR light. This therapy is currently limited to localized tumors because of the < 1 cm depth penetration of NIR light and because of concerns about shielding the liver and other healthy organs that tend to accumulate large quantities of nanoparticles. Metastatic disease, however, is one of the major causes of cancer death, and conventional treatments such as chemotherapy and radiation have been limited in their success against widespread cancers. In this thesis, we seek to expand the realm of gold nanoparticle photothermal therapies to treatment-resistant or metastatic cancers that continue to defy conventional treatments.

In Chapter 4, we addressed a form of chemotherapy-resistant breast cancer with photothermal therapy. Using anti-HER2 conjugated gold-silica nanoshells, we demonstrated for the first time *in vitro* that HER2+ breast cancer cells that were resistant

to ther chemotherapy agents trastuzumab or lapatinib could be treated using PTT. Trastuzumab and lapatinib are both chemotherapy agents approved by the Food and Drug Administration (FDA) to treated patients with advanced or metastatic HER2+ breast cancer. A high percentage of patients' tumors are resistant to these drugs, leaving fewer potential treatment options for these patients. The success of photothermal therapy against these cancers could open another avenue for treatment of HER2+ metastatic breast cancer.

In Chapter 5, we introduced a new gold nanoparticle delivery strategy using T cells as nanoparticle vectors. When performing *in vivo* PTT studies using nanoparticles, one major difficulty is optimizing gold nanoparticle tumor accumulation while minimizing off-target delivery to the liver and spleen. Freely injected nanoparticles use the EPR effect to accumulate at the tumor site, which is passive and non-targeted. We proposed a T cell-based delivery strategy that was active and more targeted. We internalized gold nanoparticles into human T cells with no adverse effects on the viability or functionality of the T cells, then injected these AuNP-T cells into mice bearing lymphoblastoid cell line (LCL) tumors. Using this stategy, we increased gold nanoparticle delivery efficiency by a factor of 4 compared to EPR effect delivered freely-injected gold nanoparticles. We also demonstrated a shift in the biodistribution of gold; the T cell-delivered gold nanoparticles accumulated in areas that matched the normal biodistribution of T cells. Because we were using a xenogeneic model (human T cells in a mouse), we did see significant liver sequestration of T cells. However, the tumor delivery that we were able to achieve of 36.5 ± 12.8% injected dose per gram[f] of tissue

[f] This value has been converted from the % injected dose value reported in Chapter 5 for T cell delivery at 48 hours

using human T cells in Chapter 5 is 2.9 times higher than the highest tumor accumulation currently reported in the literature of 12.6 % of the injected dose per gram of tissue.[6] Therefore we have shown that the T cell delivery strategy has merits over EPR effect-based delivery and potentially could improve gold nanoparticle delivery for PTT.

In Chapter 6, we turned to using gp100-specific murine T cells to carry hollow gold nanoshells to melanoma tumors. We were able to demonstrate for the first time that NIR-resonant gold nanoparticles could be borne to the tumor by antigen-specific murine T cells. Unfortunately, the wild type T cells migrated to the tumor more efficiently than the pmel T cells, disproving our hypothesis that using antigen-specific T cells would further enhance tumor delivery. Because this was an allogeneic, not xenogeneic, model, the liver sequestration in this study was substantially improved. These negative results do not, however, disprove the overall concept of T cell-based gold nanoparticle delivery. A different antigen-specific T cell or even a different tumor model with different antigen-specific T cell may have better results. As was the case with the human T cells, the HAuNS-murine T cells followed the normal biodistribution of the murine T cells, establishing firmly that the biodistribution is decided by the cellular carrier. In addition, we found that freely injected hollow gold nanoshells had delivered 27.0 ± 3.4 % of the injected dose per gram of tissue to the tumor, which is the better than the value previously reported in the literature for hollow gold nanoshells and melanoma (12.6 ± 3.1 % injected dose per gram of tissue).[6]

In Chapter 7, we demonstrated the benefits of hyperthermia-enhanced immunotherapy (HIT) for treating distant tumors. We initally looked at the endogenous

immune effects on a secondary tumor that occurred after treating a separate primary tumor with photothermal therapy using a B16-OVA tumor model. We saw that the secondary tumor in the mouse treated with PTT had increased $CD4^+$ T cell and $CD8^+$ T cell infiltration compared to the secondary tumor in a mouse treated with PBS. In addition, the secondary tumors of a mice treated with PTT had slower growth than the secondary tumors of a mice treated with PBS. These results indicate that PTT has some immune system-boosting effects and could be used to enhance adoptive T cell transfer.

We next tried the bilateral tumor study using PBS, PTT, pmel T cells, or combined pmel T cells and PTT with B16F10 tumors. While the previous study had the advantage of using a tumor with ovalbumin (OVA), a strongly immunogenic protein, this study targeted the mouse homologue of gp100, a known melanoma antigen that is less immunogenic than OVA. Although no massive systemic T cell expansion or phenotype changes were seen, there was a transient T cell expansion seen at 72 hours in the combined PTT+pmel group and an increase in IFN-γ secretion in the tumor-draining lymph nodes of the PTT+pmel group, suggesting a localized enhancement in T cell function.

Although PTT did not significantly improve the performance of the adoptively transferred pmel T cells, the additive effects of PTT and pmel T cells on the total tumor burden were encouraging for applying this combinatorial therapy towards metastatic disease. We showed that mice receiving PTT had lower tumor burden than mice that did not receive PTT. We also showed that in mice receiving PTT alone versus PTT with pmel T cell transfer, the unablated tumor grew more slowly in the combined PTT+pmel treatment group versus PTT alone. The mice receiving PTT or PTT+pmel also had lower

vascular endothelial growth factor (VEGF) levels than mice treated with PBS, suggesting that PTT may have some angiostatic benefits. This gives hope that a mouse with a primary tumor and micrometastases could successfully be treated using HIT (combined PTT with pmel T cell transfer), ultimately giving longer survival than PTT alone or pmel T cell transfer alone.

Future Work

The combination of gold nanoparticles and T cells presents many exciting possible combinations that extend even beyond cancer. In terms of gold nanoparticle delivery, experimentation with different antigen-specific T cells and tumor models may yield certain cancers that attract T cells well and thus have improved gold nanoparticle delivery. T cells could also be genetically engineered with chemokine receptors or other factors that would improve tumor accumulation and retention. For hepatic tumors, the T cell delivery method may actually be preferable because of the altered biodistribution; there is reduced risk to healthy liver tissue.

The next step in developing this technology will be to verify that the tumors can be ablated by HAuNS-T cells. Once this is demonstrated, it may be possible to use HAuNS-T cells for HIT, which would have several advantages. For one, one injection would adminster both gold nanoparticles and antigen-specific T cells. Once the primary tumor has been ablated, there is still a reservoir of HAuNS-T cells within the spleen and tumor-draining lymph nodes that would permit a second ablation if needed. These T cells could then home to micrometastases and provide an immune response.

The use of HIT as a vaccination regimen could also be expanded to diseases other than cancer. T cell vaccines are currently being tried against a variety of infectious diseases such as HIV,[209] tuberculosis,[210] and malaria[211]. Various drugs or peptides could also be loaded into hollow gold nanoshells or nanocages that would be released upon heating and augment the activation and effector response of the T cells or dendritic cells in the local area.

This thesis had established the value of combining gold nanoparticles with T cells. We have demonstrated that T cells can function as efficient gold nanoparticle delivery vectors to tumors. We have also demonstrated that gold nanoparticle PTT can be an effective adjuvant for inducing T cell activation and effector response against distant tumors. The benefits of more efficient gold nanoparticle tumor delivery and the ability to treat distant tumor lesions using HIT have the potential to ultimately prolong cancer patient survival.

REFERENCES

1. American Cancer Society. *Cancer Facts and Figures 2010.* (American Cancer Society, Atlanta; 2010).

2. Center for Disease Control. http://www.cdc.gov/nchs/fastats/deaths.htm. Last update 6/28/10. Accessed on 7/30/2010.

3. Howlader N NA, Krapcho M, Neyman N, Aminou R, Waldron W, Altekruse SF, Kosary CL, Ruhl J, Tatalovich Z, Cho H, Mariotto A, Eisner MP, Lewis DR, Chen HS, Feuer EJ, Cronin KA, Edwards BK (eds): **SEER Cancer Statistics Review, 1975-2008.** In. Bethesda, MD: National Cancer Institute; 2010. http://seer.cancer.gov/csr/1975_2008/, based on November 2010 SEER data submission, posted to the SEER web site, 2011

4. National Institutes of Health. http://www.nlm.nih.gov/medlineplus/cancerchemotherapy.html. Last update 8/4/10. Accessed on 8/4/10.

5. National Cancer Institute. http://www.cancer.gov/cancertopics/factsheet/Therapy/radiation. Last update 6/30/2010. Accessed on 7/28/2010.

6. Lu W, Xiong C, Zhang G, Huang Q, Zhang R, Zhang JZ, Li C: **Targeted photothermal ablation of murine melanomas with melanocyte-stimulating hormone analog-conjugated hollow gold nanospheres.** *Clin Cancer Res* 2009, **15**(3):876-886.

7. Melancon MP, Lu W, Yang Z, Zhang R, Cheng Z, Elliot AM, Stafford J, Olson T, Zhang JZ, Li C: **In vitro and in vivo targeting of hollow gold nanoshells directed at epidermal growth factor receptor for photothermal ablation therapy.** *Mol Cancer Ther* 2008, 7(6):1730-1739.

8. June CH: **Adoptive T cell therapy for cancer in the clinic.** *The Journal of clinical investigation* 2007, **117**(6):1466-1476.

9. Dudley ME, Wunderlich JR, Robbins PF, Yang JC, Hwu P, Schwartzentruber DJ, Topalian SL, Sherry R, Restifo NP, Hubicki AM *et al*: **Cancer regression and autoimmunity in patients after clonal repopulation with antitumor lymphocytes.** *Science (New York, NY* 2002, **298**(5594):850-854.

10. Leen AM, Rooney CM, Foster AE: **Improving T cell therapy for cancer.** *Annual review of immunology* 2007, **25**:243-265.

11. Meropol NJ, Schrag D, Smith TJ, Mulvey TM, Langdon RM, Blum D, Ubel PA, Schnipper LE: **American Society of Clinical Oncology Guidance Statement: The Cost of Cancer Care.** *J Clin Oncol* 2009, **27**(23):3868-3874.

12. El-Sayed IH, Huang X, El-Sayed MA: **Surface plasmon resonance scattering and absorption of anti-EGFR antibody conjugated gold nanoparticles in cancer diagnostics: applications in oral cancer.** *Nano Lett* 2005, **5**(5):829-834.

13. Loo C, Hirsch L, Lee MH, Chang E, West J, Halas N, Drezek R: **Gold nanoshell bioconjugates for molecular imaging in living cells.** *Opt Lett* 2005, **30**(9):1012-1014.

14. Hirsch LR, Stafford RJ, Bankson JA, Sershen SR, Rivera B, Price RE, Hazle JD, Halas NJ, West JL: **Nanoshell-mediated near-infrared thermal therapy of tumors under magnetic resonance guidance.** *Proceedings of the National Academy of Sciences of the United States of America* 2003, **100**(23):13549-13554.

15. Gobin AM, Lee MH, Halas NJ, James WD, Drezek RA, West JL: **Near-infrared resonant nanoshells for combined optical imaging and photothermal cancer therapy.** *Nano Lett* 2007, 7(7):1929-1934.

16. Li JL, Wang L, Liu XY, Zhang ZP, Guo HC, Liu WM, Tang SH: **In vitro cancer cell imaging and therapy using transferrin-conjugated gold nanoparticles.** *Cancer Lett* 2009, **274**(2):319-326.

17. Nanospectra Biosciences, Inc. http://www.nanospectra.com/index.html, Last Update 2009. Accessed on 1/5/2010.

18. Jain RK: **Transport of molecules, particles, and cells in solid tumors.** *Annu Rev Biomed Eng* 1999, **1**:241-263.

19. Gannon CJ, Patra CR, Bhattacharya R, Mukherjee P, Curley SA: **Intracellular gold nanoparticles enhance non-invasive radiofrequency thermal destruction of human gastrointestinal cancer cells.** *J Nanobiotechnology* 2008, **6**:2.

20. Johannsen M, Gneveckow U, Eckelt L, Feussner A, Waldofner N, Scholz R, Deger S, Wust P, Loening SA, Jordan A: **Clinical hyperthermia of prostate cancer using magnetic nanoparticles: presentation of a new interstitial technique.** *Int J Hyperthermia* 2005, **21**(7):637-647.

21. Tong L, Zhao Y, Huff TB, Hansen MN, Wei A, Cheng JX: **Gold Nanorods Mediate Tumor Cell Death by Compromising Membrane Integrity.** *Adv Mater Deerfield* 2007, **19**:3136-3141.

22. Habash RW, Bansal R, Krewski D, Alhafid HT: **Thermal therapy, part 1: an introduction to thermal therapy.** *Crit Rev Biomed Eng* 2006, **34**(6):459-489.

23. Hildebrandt B, Wust P, Ahlers O, Dieing A, Sreenivasa G, Kerner T, Felix R, Riess H: **The cellular and molecular basis of hyperthermia.** *Crit Rev Oncol Hematol* 2002, **43**(1):33-56.

24. Loo C, Lowery A, Halas N, West J, Drezek R: **Immunotargeted nanoshells for integrated cancer imaging and therapy**. *Nano letters* 2005, **5**(4):709-711.

25. Bickford L, Sun, J., Fu, K., Lewinski, N., Nammalvar, V., Chang, J., Drezek, R.: **Enhanced multi-spectral imaging of live breast cancer cells using immunotargeted gold nanoshells and two-photon excitation microscopy**. *Nanotechnology* 2008, **19**(31):315102.

26. Park J, Estrada A, Sharp K, Sang K, Schwartz JA, Smith DK, Coleman C, Payne JD, Korgel BA, Dunn AK *et al*: **Two-photon-induced photoluminescence imaging of tumors using near-infrared excited gold nanoshells**. *Optics express* 2008, **16**(3):1590-1599.

27. Bickford LR, Agollah G, Drezek R, Yu TK: **Silica-gold nanoshells as potential intraoperative molecular probes for HER2-overexpression in ex vivo breast tissue using near-infrared reflectance confocal microscopy**. *Breast cancer research and treatment* 2010, **120**(3):547-555.

28. Loo C, Lin A, Hirsch L, Lee MH, Barton J, Halas N, West J, Drezek R: **Nanoshell-enabled photonics-based imaging and therapy of cancer**. *Technol Cancer Res Treat* 2004, **3**(1):33-40.

29. Lowery AR, Gobin AM, Day ES, Halas NJ, West JL: **Immunonanoshells for targeted photothermal ablation of tumor cells**. *Int J Nanomedicine* 2006, **1**(2):149-154.

30. Gobin AM, Moon JJ, West JL: **EphrinA I-targeted nanoshells for photothermal ablation of prostate cancer cells**. *International journal of nanomedicine* 2008, **3**(3):351-358.

31. Stern JM, Stanfield J, Lotan Y, Park S, Hsieh JT, Cadeddu JA: **Efficacy of laser-activated gold nanoshells in ablating prostate cancer cells in vitro**. *J Endourol* 2007, **21**(8):939-943.

32. Bernardi RJ, Lowery AR, Thompson PA, Blaney SM, West JL: **Immunonanoshells for targeted photothermal ablation in medulloblastoma and glioma: an in vitro evaluation using human cell lines**. *Journal of neuro-oncology* 2008, **86**(2):165-172.

33. Liu SY, Liang ZS, Gao F, Luo SF, Lu GQ: **In vitro photothermal study of gold nanoshells functionalized with small targeting peptides to liver cancer cells**. *Journal of materials science* 2010, **21**(2):665-674.

34. O'Neal DP, Hirsch LR, Halas NJ, Payne JD, West JL: **Photo-thermal tumor ablation in mice using near infrared-absorbing nanoparticles**. *Cancer letters* 2004, **209**(2):171-176.

35. Schwartz JA, Shetty AM, Price RE, Stafford RJ, Wang JC, Uthamanthil RK, Pham K, McNichols RJ, Coleman CL, Payne JD: **Feasibility study of particle-assisted laser ablation of brain tumors in orthotopic canine model.** *Cancer Res* 2009, **69**(4):1659-1667.

36. Huang X, El-Sayed IH, Qian W, El-Sayed MA: **Cancer cell imaging and photothermal therapy in the near-infrared region by using gold nanorods.** *Journal of the American Chemical Society* 2006, **128**(6):2115-2120.

37. Durr NJ, Larson T, Smith DK, Korgel BA, Sokolov K, Ben-Yakar A: **Two-photon luminescence imaging of cancer cells using molecularly targeted gold nanorods.** *Nano Lett* 2007, **7**(4):941-945.

38. Dickerson EB, Dreaden EC, Huang X, El-Sayed IH, Chu H, Pushpanketh S, McDonald JF, El-Sayed MA: **Gold nanorod assisted near-infrared plasmonic photothermal therapy (PPTT) of squamous cell carcinoma in mice.** *Cancer letters* 2008, **269**(1):57-66.

39. Goodrich GP, Bao L, Gill-Sharp K, Sang KL, Wang J, Payne JD: **Photothermal therapy in a murine colon cancer model using near-infrared absorbing gold nanorods.** *Journal of biomedical optics* 2010, **15**(1):018001.

40. Zijlstra P, Chon JWM, Gu M: **Effect of heat accumulation on the dynamic range of a gold nanorod doped polymer nanocomposite for optical laser writing and patterning.** *Optics Express* 2007, **15**(19):12151-12160.

41. Didychuk CL, Ephrat P, Chamson-Reig A, Jacques SL, Carson JJ: **Depth of photothermal conversion of gold nanorods embedded in a tissue-like phantom.** *Nanotechnology* 2009, **20**(19):195102.

42. Chon JWM, Bullen C, Zijlstra P, Gu M: **Spectral encoding on gold nanorods doped in a silica sol-gel matrix and its application to high-density optical data storage.** *Advanced Functional Materials* 2007, **17**(6):875-880.

43. Horiguchi Y, Honda K, Kato Y, Nakashima N, Niidome Y: **Photothermal Reshaping of Gold Nanorods Depends on the Passivating Layers of the Nanorod Surfaces.** *Langmuir* 2008, **24**(20):12026-12031.

44. Cole JR, Mirin, N. A., Knight, M. W., Goodrich, G. P., Halas, N. J.: **Photothermal Efficiencies of Nanoshells and Nanorods for Clinical Therapeutic Applications.** *J Phys Chem C* 2009, **113**:12090-12094.

45. Jain PK, Lee KS, El-Sayed IH, El-Sayed MA: **Calculated absorption and scattering properties of gold nanoparticles of different size, shape, and composition: applications in biological imaging and biomedicine.** *J Phys Chem B* 2006, **110**(14):7238-7248.

46. von Maltzahn G, Park JH, Agrawal A, Bandaru NK, Das SK, Sailor MJ, Bhatia SN: **Computationally guided photothermal tumor therapy using long-circulating gold nanorod antennas.** *Cancer Res* 2009, **69**(9):3892-3900.

47. Gobin AM, Watkins EM, Quevedo E, Colvin VL, West JL: **Near-infrared-resonant gold/gold sulfide nanoparticles as a photothermal cancer therapeutic agent.** *Small (Weinheim an der Bergstrasse, Germany)* 2010, **6**(6):745-752.

48. Raschke G, Brogl S, Susha AS, Rogach AL, Klar TA, Feldmann J, Fieres B, Petkov N, Bein T, Nichtl A *et al*: **Reply to "Comment on 'Gold Nanoshells Improve Single Nanoparticle Molecular Sensors'".** *Nano Lett* 2005, **5**(4):811-812.

49. Schwartzberg AM, Grant CD, van Buuren T, Zhang JZ: **Reduction of HAuCl4 by Na2S revisited: The case for Au nanoparticle aggregates and against Au2S/Au Core/Shell particles.** *J Phys Chem C* 2007, **111**(25):8892-8901.

50. Zhang JZ, Schwartzberg AM, Norman J, T. , Grant CD, Liu J, Bridges F, van Buuren T: **Comment on "Gold Nanoshells Improve Single Nanoparticle Molecular Sensors".** *Nano Lett* 2005, **5**(4):809-810.

51. Prevo BG, Esakoff SA, Mikhailovsky A, Zasadzinski JA: **Scalable routes to gold nanoshells with tunable sizes and response to near-infrared pulsed-laser irradiation.** *Small (Weinheim an der Bergstrasse, Germany)* 2008, **4**(8):1183-1195.

52. Schwartzberg AM, Olson TY, Talley CE, Zhang JZ: **Synthesis, characterization, and tunable optical properties of hollow gold nanospheres.** *J Phys Chem B* 2006, **110**(40):19935-19944.

53. Kumar R, Maitra AN, Patanjali PK, Sharma P: **Hollow gold nanoparticles encapsulating horseradish peroxidase.** *Biomaterials* 2005, **26**(33):6743-6753.

54. Skrabalak SE, Chen J, Sun Y, Lu X, Au L, Cobley CM, Xia Y: **Gold nanocages: synthesis, properties, and applications.** *Accounts of chemical research* 2008, **41**(12):1587-1595.

55. Chen J, Glaus C, Laforest R, Zhang Q, Yang M, Gidding M, Welch MJ, Xia Y: **Gold nanocages as photothermal transducers for cancer treatment.** *Small (Weinheim an der Bergstrasse, Germany)* 2010, **6**(7):811-817.

56. Au L, Zheng D, Zhou F, Li ZY, Li X, Xia Y: **A quantitative study on the photothermal effect of immuno gold nanocages targeted to breast cancer cells.** *ACS Nano* 2008, **2**(8):1645-1652.

57. Chen J, Wang D, Xi J, Au L, Siekkinen A, Warsen A, Li ZY, Zhang H, Xia Y, Li X: **Immuno gold nanocages with tailored optical properties for targeted photothermal destruction of cancer cells.** *Nano Lett* 2007, **7**(5):1318-1322.

58. Skrabalak SE, Chen J, Au L, Lu X, Li X, Xia Y: **Gold Nanocages for Biomedical Applications.** *Adv Mater Deerfield* 2007, **19**(20):3177-3184.

59. Boyd GT, Yu ZH, Shen YR: **Photoinduced luminescence from the noble metals and its enhancement on roughened surfaces.** *Phys Rev B Condens Matter* 1986, **33**(12):7923-7936.

60. Sokolov K, Follen M, Aaron J, Pavlova I, Malpica A, Lotan R, Richards-Kortum R: **Real-time vital optical imaging of precancer using anti-epidermal growth factor receptor antibodies conjugated to gold nanoparticles.** *Cancer Res* 2003, **63**(9):1999-2004.

61. El-Sayed IH, Huang X, El-Sayed MA: **Selective laser photo-thermal therapy of epithelial carcinoma using anti-EGFR antibody conjugated gold nanoparticles.** *Cancer Lett* 2006, **239**(1):129-135.

62. Zharov VP, Galitovskaya EN, Johnson C, Kelly T: **Synergistic enhancement of selective nanophotothermolysis with gold nanoclusters: potential for cancer therapy.** *Lasers Surg Med* 2005, **37**(3):219-226.

63. Huang X, Qian W, El-Sayed IH, El-Sayed MA: **The potential use of the enhanced nonlinear properties of gold nanospheres in photothermal cancer therapy.** *Lasers in surgery and medicine* 2007, **39**(9):747-753.

64. Lapotko D, Lukianova E, Potapnev M, Aleinikova O, Oraevsky A: **Method of laser activated nano-thermolysis for elimination of tumor cells.** *Cancer Lett* 2006, **239**(1):36-45.

65. Lapotko DO, Lukianova E, Oraevsky AA: **Selective laser nano-thermolysis of human leukemia cells with microbubbles generated around clusters of gold nanoparticles.** *Lasers Surg Med* 2006, **38**(6):631-642.

66. Lapotko DO: **Laser-induced bubbles in living cells.** *Lasers Surg Med* 2006, **38**(3):240-248.

67. Bohren CF, Huffman DR: **Absorption and scattering of light by small particles.** New York: Wiley; 1983.

68. Hulst HCvd: **Light scattering by small particles.** New York,: Wiley; 1957.

69. Jain PK, Lee KS, El-Sayed IH, El-Sayed MA: **Calculated absorption and scattering properties of gold nanoparticles of different size, shape, and composition: Applications in biological imaging and biomedicine.** *Journal of Physical Chemistry B* 2006, **110**(14):7238-7248.

70. Noguez C: **Surface plasmons on metal nanoparticles: The influence of shpae and physical environment.** *Journal of Physical Chemistry C* 2007, **111**(10):3806-3819.

71. Harris N, Ford MJ, Cortie MB: **Optimization of plasmonic heating by gold nanospheres and nanoshells.** *Journal of Physical Chemistry B* 2006, **110**(22):10701-10707.

72. Dewey WC: **Arrhenius relationships from the molecule and cell to the clinic.** *Int J Hyperthermia* 1994, **10**(4):457-483.

73. Huang X, Jain PK, El-Sayed IH, El-Sayed MA: **Determination of the minimum temperature required for selective photothermal destruction of cancer cells with the use of immunotargeted gold nanoparticles.** *Photochem Photobiol* 2006, **82**(2):412-417.

74. Weissleder R: **A clearer vision for in vivo imaging.** *Nat Biotechnol* 2001, **19**(4):316-317.

75. Weissleder R, Ntziachristos V: **Shedding light onto live molecular targets.** *Nat Med* 2003, **9**(1):123-128.

76. Vera J, Bayazitoglu Y: **Gold nanoshell density variation with laser power for induced hyperthermia.** *International Journal of Heat and Mass Transfer* 2009, **52**(3-4):564-573.

77. Elliott A, Schwartz J, Wang J, Shetty A, Hazle J, Stafford JR: **Analytical Solution to Heat Equation With Magnetic Resonance Experimental Verification for Nanoshell Enhanced Thermal Therapy.** *Lasers in Surgery and Medicine* 2008, **40**(9):660-665.

78. Elliott AM, Schwartz J, Wang J, Shetty AM, Bourgoyne C, O'Neal DP, Hazle JD, Stafford RJ: **Quantitative comparison of delta P1 versus optical diffusion approximations for modeling near-infrared gold nanoshell heating.** *Medical Physics* 2009, **36**(4):1351-1358.

79. Elliott AM, Stafford RJ, Schwartz J, Wang J, Shetty AM, Bourgoyne C, O'Neal P, Hazle JD: **Laser-induced thermal response and characterization of nanoparticles for cancer treatment using magnetic resonance thermal imaging.** *Medical Physics* 2007, **34**(7):3102-3108.

80. Puvanakrishnan P, Park J, Diagaradjane P, Schwartz JA, Coleman CL, Gill-Sharp KL, Sang KL, Payne JD, Krishnan S, Tunnell JW: **Near-infrared narrow-band imaging of gold/silica nanoshells in tumors.** *Journal of biomedical optics* 2009, **14**(2):024044.

81. McGhana JP, Dodd GD, 3rd: **Radiofrequency ablation of the liver: current status.** *AJR Am J Roentgenol* 2001, **176**(1):3-16.

82. Bernardi P, Cavagnaro M, Pisa S, Piuzzi E: **Specific absorption rate and temperature elevation in a subject exposed in the far-field of radio-frequency sources operating in the 10-900-MHz range.** *IEEE Trans Biomed Eng* 2003, **50**(3):295-304.

83. Cardinal J, Klune JR, Chory E, Jeyabalan G, Kanzius JS, Nalesnik M, Geller DA: **Noninvasive radiofrequency ablation of cancer targeted by gold nanoparticles.** *Surgery* 2008, **144**(2):125-132.

84. Gannon CJ, Cherukuri P, Yakobson BI, Cognet L, Kanzius JS, Kittrell C, Weisman RB, Pasquali M, Schmidt HK, Smalley RE *et al*: **Carbon nanotube-enhanced thermal destruction of cancer cells in a noninvasive radiofrequency field.** *Cancer* 2007, **110**(12):2654-2665.

85. Pankhurst QA, Connolly J, Jones SK, Dobson J: **Applications of magnetic nanoparticles in biomedicine.** *Journal of physics-london-d applied physics* 2003, **36**(13):167-181.

86. Maier-Hauff K, Rothe R, Scholz R, Gneveckow U, Wust P, Thiesen B, Feussner A, von Deimling A, Waldoefner N, Felix R *et al*: **Intracranial thermotherapy using magnetic nanoparticles combined with external beam radiotherapy: results of a feasibility study on patients with glioblastoma multiforme.** *Journal of neuro-oncology* 2007, **81**(1):53-60.

87. Pisanic TR, 2nd, Blackwell JD, Shubayev VI, Finones RR, Jin S: **Nanotoxicity of iron oxide nanoparticle internalization in growing neurons.** *Biomaterials* 2007, **28**(16):2572-2581.

88. Larson TA, Bankson J, Aaron J, Sokolov K: **Hybrid plasmonic magnetic nanoparticles as molecular specific agents for MRI/optical imaging and photothermal therapy of cancer cells.** *Nanotechnology* 2007, **18**(32):325101-325101.

89. Levin CS, Hofmann C, Ali TA, Kelly AT, Morosan E, Nordlander P, Whitmire KH, Halas NJ: **Magnetic-plasmonic core-shell nanoparticles.** *ACS Nano* 2009, **3**(6):1379-1388.

90. Wijaya A, Brown KA, Alper JD, Hamad-Schifferli K: **Magnetic field heating study of Fe-doped Au nanoparticles.** *Journal of Magnetism and Magnetic Materials* 2007, **309**(1):15-19.

91. Xu ZC, Hou YL, Sun SH: **Magnetic core/shell Fe3O4/Au and Fe3O4/Au/Ag nanoparticles with tunable plasmonic properties.** *Journal of the American Chemical Society* 2007, **129**(28):8698-8699.

92. Kirui DK, Rey DA, Batt CA: **Gold hybrid nanoparticles for targeted phototherapy and cancer imaging.** *Nanotechnology* 2010, **21**(10):105105.

93. Shah J, Park S, Aglyamov S, Larson T, Ma L, Sokolov K, Johnston K, Milner T, Emelianov SY: **Photoacoustic imaging and temperature measurement for photothermal cancer therapy**. *Journal of Biomedical Optics* 2008, **13**(3):034024.

94. Decuzzi P, Pasqualini R, Arap W, Ferrari M: **Intravascular delivery of particulate systems: does geometry really matter?** *Pharm Res* 2009, **26**(1):235-243.

95. Zhang GD, Yang Z, Lu W, Zhang R, Huang Q, Tian M, Li L, Liang D, Li C: **Influence of anchoring ligands and particle size on the colloidal stability and in vivo biodistribution of polyethylene glycol-coated gold nanoparticles in tumor-xenografted mice**. *Biomaterials* 2009, **30**(10):1928-1936.

96. Perrault SD, Walkey C, Jennings T, Fischer HC, Chan WC: **Mediating tumor targeting efficiency of nanoparticles through design**. *Nano Lett* 2009, **9**(5):1909-1915.

97. Terentyuk GS, Maslyakova GN, Suleymanova LV, Khlebtsov BN, Kogan BY, Akchurin GG, Shantrocha AV, Maksimova IL, Khlebtsov NG, Tuchin VV: **Circulation and distribution of gold nanoparticles and induced alterations of tissue morphology at intravenous particle delivery**. *Journal of Biophotonics* 2009, **2**(5):292-302.

98. Chithrani BD, Ghazani AA, Chan WCW: **Determining the size and shape dependence of gold nanoparticle uptake into mammalian cells**. *Nano Letters* 2006, **6**(4):662-668.

99. Jiang W, Kim BYS, Rutka JT, Chan WCW: **Nanoparticle-mediated cellular response is size-dependent**. *Nature nanotechnology* 2008, **3**(3):145-150.

100. Kim B, Han G, Toley BJ, Kim CK, Rotello VM, Forbes NS: **Tuning payload delivery in tumour cylindroids using gold nanoparticles**. *Nature nanotechnology* 2010, **5**(6):465-472.

101. Alexis F, Pridgen E, Molnar LK, Farokhzad OC: **Factors affecting the clearance and biodistribution of polymeric nanoparticles**. *Molecular pharmaceutics* 2008, **5**(4):505-515.

102. James WD, Hirsch, L. R., West, J. L., O'Neal, P. D., Payne, J. D. : **Application of INAA to the build-up and clearance of gold nanoshells in clinical studies in mice**. *Journal of Radioanalytical and Nuclear Chemistry* 2007, **271**(2):455-459.

103. Balogh L, Nigavekar SS, Nair BM, Lesniak W, Zhang C, Sung LY, Kariapper MST, El-Jawahri A, Llanes M, Bolton B *et al*: **Significant effect of size on the in vivo biodistribution of gold composite nanodevices in mouse tumor models**. *Nanomedicine-Nanotechnology Biology and Medicine* 2007, **3**(4):281-296.

104. Cho WS, Cho MJ, Jeong J, Choi M, Cho HY, Han BS, Kim SH, Kim HO, Lim YT, Chung BH *et al*: **Acute toxicity and pharmacokinetics of 13 nm-sized PEG-coated gold nanoparticles.** *Toxicology and Applied Pharmacology* 2009, **236**(1):16-24.

105. De Jong WH, Hagens WI, Krystek P, Burger MC, Sips AJAM, Geertsma RE: **Particle size-dependent organ distribution of gold nanoparticles after intravenous administration.** *Biomaterials* 2008, **29**(12):1912-1919.

106. Huang XL, Zhang B, Ren L, Ye SF, Sun LP, Zhang QQ, Tan MC, Chow GM: **In vivo toxic studies and biodistribution of near infrared sensitive Au-Au2S nanoparticles as potential drug delivery carriers.** *Journal of Materials Science-Materials in Medicine* 2008, **19**(7):2581-2588.

107. Niidome T, Yamagata M, Okamoto Y, Akiyama Y, Takahashi H, Kawano T, Katayama Y, Niidome Y: **PEG-modified gold nanorods with a stealth character for in vivo applications.** *J Control Release* 2006, **114**(3):343-347.

108. Sadauskas E, Danscher G, Stoltenberg M, Vogel U, Larsen A, Wallin H: **Protracted elimination of gold nanoparticles from mouse liver.** *Nanomedicine* 2009, **5**(2):162-169.

109. Stern JM, Stanfield J, Kabbani W, Hsieh JT, Cadeddu JRA: **Selective prostate cancer thermal ablation with laser activated gold nanoshells.** *Journal of Urology* 2008, **179**(2):748-753.

110. Sadauskas E, Wallin H, Stoltenberg M, Vogel U, Doering P, Larsen A, Danscher G: **Kupffer cells are central in the removal of nanoparticles from the organism.** *Part Fibre Toxicol* 2007, **4**:10.

111. Norman RS, Stone JW, Gole A, Murphy CJ, Sabo-Attwood TL: **Targeted photothermal lysis of the pathogenic bacteria, Pseudomonas aeruginosa, with gold nanorods.** *Nano Lett* 2008, **8**(1):302-306.

112. Black KC, Kirkpatrick ND, Troutman TS, Xu L, Vagner J, Gillies RJ, Barton JK, Utzinger U, Romanowski M: **Gold nanorods targeted to delta opioid receptor: plasmon-resonant contrast and photothermal agents.** *Mol Imaging* 2008, 7(1):50-57.

113. Chanda N, Shukla R, Katti KV, Kannan R: **Gastrin releasing protein receptor specific gold nanorods: breast and prostate tumor avid nanovectors for molecular imaging.** *Nano Lett* 2009, **9**(5):1798-1805.

114. Sun L, Liu D, Wang Z: **Functional gold nanoparticle-peptide complexes as cell-targeting agents.** *Langmuir* 2008, **24**(18):10293-10297.

115. Eghtedari M, Liopo AV, Copland JA, Oraevslty AA, Motamedi M: **Engineering of Hetero-Functional Gold Nanorods for the in vivo Molecular Targeting of Breast Cancer Cells.** *Nano Letters* 2009, **9**(1):287-291.

116. Li PC, Wang CR, Shieh DB, Wei CW, Liao CK, Poe C, Jhan S, Ding AA, Wu YN: **In vivo photoacoustic molecular imaging with simultaneous multiple selective targeting using antibody-conjugated gold nanorods.** *Opt Express* 2008, **16**(23):18605-18615.

117. Ruoslahti E: **Targeting tumor vasculature with homing peptides from phage display.** *Semin Cancer Biol* 2000, **10**(6):435-442.

118. Tasciotti E, Liu X, Bhavane R, Plant K, Leonard AD, Price BK, Cheng MM, Decuzzi P, Tour JM, Robertson F *et al*: **Mesoporous silicon particles as a multistage delivery system for imaging and therapeutic applications.** *Nature nanotechnology* 2008, **3**(3):151-157.

119. Choi MR, Stanton-Maxey KJ, Stanley JK, Levin CS, Bardhan R, Akin D, Badve S, Sturgis J, Robinson JP, Bashir R *et al*: **A cellular Trojan Horse for delivery of therapeutic nanoparticles into tumors.** *Nano Lett* 2007, **7**(12):3759-3765.

120. Abbas A, Lichtman A: **Basic Immunology**, 2nd edn. Philadelphia: Saunders, 2006.

121. Abbas AK: **Diseases of Immunity.** In: *Robbins and Cotran Pathological Basis of Disease.* Edited by Kumar V, Abbas AK, Fausto FN, 7th edn. St. Louis, MO: Saunders; 2004: 193-268.

122. Vyas JM, Van der Veen AG, Ploegh HL: **The known unknowns of antigen processing and presentation.** *Nature reviews* 2008, **8**(8):607-618.

123. Pazos MDC, Nader HB: **Effect of photodynamic therapy on the extracellular matrix and associated components.** *Braz J Med Biol Res* 2007, **40**(8):1025-1035.

124. McCarter M, Clarke J, Richter D, Wilson C: **Melanoma skews dendritic cells to facilitate a T helper 2 profile.** *Surgery* 2005, **138**(2):321-328.

125. Swann JB, Smyth MJ: **Immune surveillance of tumors.** *The Journal of clinical investigation* 2007, **117**(5):1137-1146.

126. Whiteside TL: **The tumor microenvironment and its role in promoting tumor growth.** *Oncogene* 2008, **27**(45):5904-5912.

127. Breart B, Lemaitre F, Celli S, Bousso P: **Two-photon imaging of intratumoral CD8+ T cell cytotoxic activity during adoptive T cell therapy in mice.** *The Journal of clinical investigation* 2008, **118**(4):1390-1397.

128. Frey AB, Monu N: **Signaling defects in anti-tumor T cells.** *Immunological reviews* 2008, **222**:192-205.

129. Zippelius A, Batard P, Rubio-Godoy V, Bioley G, Lienard D, Lejeune F, Rimoldi D, Guillaume P, Meidenbauer N, Mackensen A *et al*: **Effector function of human tumor-specific CD8 T cells in melanoma lesions: a state of local functional tolerance.** *Cancer research* 2004, **64**(8):2865-2873.

130. Pittet MJ: **Behavior of immune players in the tumor microenvironment.** *Current opinion in oncology* 2009, **21**(1):53-59.

131. Tiemessen MM, Jagger AL, Evans HG, van Herwijnen MJ, John S, Taams LS: **CD4+CD25+Foxp3+ regulatory T cells induce alternative activation of human monocytes/macrophages.** *Proceedings of the National Academy of Sciences of the United States of America* 2007, **104**(49):19446-19451.

132. Jensen TO, Schmidt H, Moller HJ, Hoyer M, Maniecki MB, Sjoegren P, Christensen IJ, Steiniche T: **Macrophage markers in serum and tumor have prognostic impact in American Joint Committee on Cancer stage I/II melanoma.** *J Clin Oncol* 2009, **27**(20):3330-3337.

133. Schmid MC, Varner JA: **Myeloid cells in the tumor microenvironment: modulation of tumor angiogenesis and tumor inflammation.** *Journal of oncology* 2010, **2010**:201026.

134. Dudley ME, Wunderlich JR, Yang JC, Sherry RM, Topalian SL, Restifo NP, Royal RE, Kammula U, White DE, Mavroukakis SA *et al*: **Adoptive cell transfer therapy following non-myeloablative but lymphodepleting chemotherapy for the treatment of patients with refractory metastatic melanoma.** *J Clin Oncol* 2005, **23**(10):2346-2357.

135. Weber J, Atkins M, Hwu P, Radvanyi L, Sznol M, Yee C: **White paper on adoptive cell therapy for cancer with tumor-infiltrating lymphocytes: a report of the CTEP subcommittee on adoptive cell therapy.** *Clin Cancer Res* 2011, **17**(7):1664-1673.

136. Sosman J: **Immunotherapy for advanced Melanoma.** In: *UpToDate.* Edited by Atkins M, Ross M: UpToDate, Inc.; 2011.

137. Hong JJ, Rosenberg SA, Dudley ME, Yang JC, White DE, Butman JA, Sherry RM: **Successful treatment of melanoma brain metastases with adoptive cell therapy.** *Clin Cancer Res* 2011, **16**(19):4892-4898.

138. Morgan RA, Dudley ME, Wunderlich JR, Hughes MS, Yang JC, Sherry RM, Royal RE, Topalian SL, Kammula US, Restifo NP *et al*: **Cancer regression in patients after transfer of genetically engineered lymphocytes.** *Science (New York, NY* 2006, **314**(5796):126-129.

139. Robbins PF, Morgan RA, Feldman SA, Yang JC, Sherry RM, Dudley ME, Wunderlich JR, Nahvi AV, Helman LJ, Mackall CL *et al*: **Tumor regression in patients with metastatic synovial cell sarcoma and melanoma using genetically engineered lymphocytes reactive with NY-ESO-1**. *J Clin Oncol* 2011, **29**(7):917-924.

140. Parkhurst MR, Yang JC, Langan RC, Dudley ME, Nathan DA, Feldman SA, Davis JL, Morgan RA, Merino MJ, Sherry RM *et al*: **T cells targeting carcinoembryonic antigen can mediate regression of metastatic colorectal cancer but induce severe transient colitis**. *Mol Ther* 2011, **19**(3):620-626.

141. Brenner M: **T cell receptors and cancer: gain gives pain**. *Nature medicine* 2010, **16**(5):520-521.

142. Di Stasi A, De Angelis B, Rooney CM, Zhang L, Mahendravada A, Foster AE, Heslop HE, Brenner MK, Dotti G, Savoldo B: **T lymphocytes coexpressing CCR4 and a chimeric antigen receptor targeting CD30 have improved homing and antitumor activity in a Hodgkin tumor model**. *Blood* 2009, **113**(25):6392-6402.

143. Nahta R, Yu D, Hung MC, Hortobagyi GN, Esteva FJ: **Mechanisms of disease: understanding resistance to HER2-targeted therapy in human breast cancer**. *Nature clinical practice* 2006, **3**(5):269-280.

144. Slamon DJ, Clark GM, Wong SG, Levin WJ, Ullrich A, McGuire WL: **Human breast cancer: correlation of relapse and survival with amplification of the HER-2/neu oncogene**. *Science (New York, NY* 1987, **235**(4785):177-182.

145. Cobleigh MA, Vogel CL, Tripathy D, Robert NJ, Scholl S, Fehrenbacher L, Wolter JM, Paton V, Shak S, Lieberman G *et al*: **Multinational study of the efficacy and safety of humanized anti-HER2 monoclonal antibody in women who have HER2-overexpressing metastatic breast cancer that has progressed after chemotherapy for metastatic disease**. *J Clin Oncol* 1999, **17**(9):2639-2648.

146. Vogel CL, Cobleigh MA, Tripathy D, Gutheil JC, Harris LN, Fehrenbacher L, Slamon DJ, Murphy M, Novotny WF, Burchmore M *et al*: **Efficacy and safety of trastuzumab as a single agent in first-line treatment of HER2-overexpressing metastatic breast cancer**. *J Clin Oncol* 2002, **20**(3):719-726.

147. Nahta R, Esteva FJ: **HER2 therapy: molecular mechanisms of trastuzumab resistance**. *Breast Cancer Res* 2006, **8**(6):215-.

148. Nagy P, Friedlander E, Tanner M, Kapanen AI, Carraway KL, Isola J, Jovin TM: **Decreased accessibility and lack of activation of ErbB2 in JIMT-1, a herceptin-resistant, MUC4-expressing breast cancer cell line**. *Cancer research* 2005, **65**(2):473-482.

149. Lu Y, Zi X, Zhao Y, Mascarenhas D, Pollak M: **Insulin-like growth factor-I receptor signaling and resistance to trastuzumab (Herceptin).** *Journal of the National Cancer Institute* 2001, **93**(24):1852-1857.

150. Yakes FM, Chinratanalab W, Ritter CA, King W, Seelig S, Arteaga CL: **Herceptin-induced inhibition of phosphatidylinositol-3 kinase and Akt Is required for antibody-mediated effects on p27, cyclin D1, and antitumor action.** *Cancer research* 2002, **62**(14):4132-4141.

151. Elghanian R, Storhoff JJ, Mucic RC, Letsinger RL, Mirkin CA: **Selective colorimetric detection of polynucleotides based on the distance-dependent optical properties of gold nanoparticles.** *Science (New York, NY* 1997, **277**(5329):1078-1081.

152. Hauck TS, Jennings TL, Yatsenko T, Kumaradas JC, Chan WCW: **Enhancing the Toxicity of Cancer Chemotherapeutics with Gold Nanorod Hyperthermia.** *Advanced Materials* 2008, **20**(20):3832-3838.

153. Stober W, Fink A, Bohn E: **Controlled Growth of Monodisperse Silica Spheres in Micron Size Range.** *J Colloid Interf Sci* 1968, **26**(1):62-69.

154. Carpin LB, Bickford LR, Agollah G, Yu TK, Schiff R, Li Y, Drezek RA: **Immunoconjugated gold nanoshell-mediated photothermal ablation of trastuzumab-resistant breast cancer cells.** *Breast cancer research and treatment* 2011, **125**(1):27-34.

155. Cheong SK, Krishnan S, Cho SH: **Modeling of plasmonic heating from individual gold nanoshells for near-infrared laser-induced thermal therapy.** *Medical physics* 2009, **36**(10):4664-4671.

156. de Lange DF, Hofman, J.T., Meijer, J.: **Influence of intensity distribution on the meltpool and clad shape for laser cladding.** In: *Third International WLT-Conference on Lasers in Manufacturing: 2005; Munich, Germany*; 2005.

157. Rofstad EK: **Heat sensitivity and thermotolerance in vitro of human breast carcinoma, malignant melanoma and squamous cell carcinoma of the head and neck.** *British journal of cancer* 1990, **61**(1):22-28.

158. Diagaradjane P, Shetty A, Wang JC, Elliott AM, Schwartz J, Shentu S, Park HC, Deorukhkar A, Stafford RJ, Cho SH *et al*: **Modulation of in vivo tumor radiation response via gold nanoshell-mediated vascular-focused hyperthermia: characterizing an integrated antihypoxic and localized vascular disrupting targeting strategy.** *Nano letters* 2008, **8**(5):1492-1500.

159. Cole C, Qiao J, Kottke T, Diaz RM, Ahmed A, Sanchez-Perez L, Brunn G, Thompson J, Chester J, Vile RG: **Tumor-targeted, systemic delivery of therapeutic viral vectors using hitchhiking on antigen-specific T cells.** *Nature medicine* 2005, **11**(10):1073-1081.

160. Harrington K, Alvarez-Vallina L, Crittenden M, Gough M, Chong H, Diaz RM, Vassaux G, Lemoine N, Vile R: **Cells as vehicles for cancer gene therapy: the missing link between targeted vectors and systemic delivery?** *Human gene therapy* 2002, **13**(11):1263-1280.

161. Qiao J, Kottke T, Willmon C, Galivo F, Wongthida P, Diaz RM, Thompson J, Ryno P, Barber GN, Chester J *et al*: **Purging metastases in lymphoid organs using a combination of antigen-nonspecific adoptive T cell therapy, oncolytic virotherapy and immunotherapy**. *Nature medicine* 2008, **14**(1):37-44.

162. Yotnda P, Savoldo B, Charlet-Berguerand N, Rooney C, Brenner M: **Targeted delivery of adenoviral vectors by cytotoxic T cells**. *Blood* 2004, **104**(8):2272-2280.

163. Mortensen MW, Kahns L, Hansen T, Sorensen PG, Bjorkdahl O, Jensen MR, Gundersen HJ, Bjornholm T: **Next generation adoptive immunotherapy--human T cells as carriers of therapeutic nanoparticles**. *Journal of nanoscience and nanotechnology* 2007, 7(12):4575-4580.

164. Steinfeld U, Pauli C, Kaltz N, Bergemann C, Lee HH: **T lymphocytes as potential therapeutic drug carrier for cancer treatment**. *International journal of pharmaceutics* 2006, **311**(1-2):229-236.

165. Kennedy LC, Bickford LR, Lewinski NA, Coughlin AJ, Hu Y, Day ES, West JL, Drezek RA: **A New Era for Cancer Treatment: Gold-Nanoparticle-Mediated Thermal Therapies**. *Small (Weinheim an der Bergstrasse, Germany)* 2011, 7(2):169-183.

166. Han G, Ghosh P, Rotello VM: **Functionalized gold nanoparticles for drug delivery**. *Nanomedicine (London, England)* 2007, **2**(1):113-123.

167. Vera J, Savoldo B, Vigouroux S, Biagi E, Pule M, Rossig C, Wu J, Heslop HE, Rooney CM, Brenner MK *et al*: **T lymphocytes redirected against the kappa light chain of human immunoglobulin efficiently kill mature B lymphocyte-derived malignant cells**. *Blood* 2006, **108**(12):3890-3897.

168. Foster AE, Dotti G, Lu A, Khalil M, Brenner MK, Heslop HE, Rooney CM, Bollard CM: **Antitumor activity of EBV-specific T lymphocytes transduced with a dominant negative TGF-beta receptor**. *J Immunother* 2008, **31**(5):500-505.

169. Stephan MT, Moon JJ, Um SH, Bershteyn A, Irvine DJ: **Therapeutic cell engineering with surface-conjugated synthetic nanoparticles**. *Nature medicine* 2010, **16**(9):1035-1041.

170. James W, Hirsch L, West J, O'Neal P, Payne J: **Application of INAA to the build-up and clearance of gold nanoshells in clinical studies in mice**. *Journal of Radioanalytical and Nuclear Chemistry* 2007, **271**(2):455-459.

171. Lewinski N, Colvin V, Drezek R: **Cytotoxicity of nanoparticles.** *Small (Weinheim an der Bergstrasse, Germany)* 2008, **4**(1):26-49.

172. Jiang W, Kim BY, Rutka JT, Chan WC: **Nanoparticle-mediated cellular response is size-dependent.** *Nature nanotechnology* 2008, **3**(3):145-150.

173. Bollard CM, Aguilar L, Straathof KC, Gahn B, Huls MH, Rousseau A, Sixbey J, Gresik MV, Carrum G, Hudson M *et al*: **Cytotoxic T lymphocyte therapy for Epstein-Barr virus+ Hodgkin's disease.** *The Journal of experimental medicine* 2004, **200**(12):1623-1633.

174. Rooney CM, Smith CA, Ng CY, Loftin SK, Sixbey JW, Gan Y, Srivastava DK, Bowman LC, Krance RA, Brenner MK *et al*: **Infusion of cytotoxic T cells for the prevention and treatment of Epstein-Barr virus-induced lymphoma in allogeneic transplant recipients.** *Blood* 1998, **92**(5):1549-1555.

175. Pule MA, Savoldo B, Myers GD, Rossig C, Russell HV, Dotti G, Huls MH, Liu E, Gee AP, Mei Z *et al*: **Virus-specific T cells engineered to coexpress tumor-specific receptors: persistence and antitumor activity in individuals with neuroblastoma.** *Nature medicine* 2008, **14**(11):1264-1270.

176. Craddock JA, Lu A, Bear A, Pule M, Brenner MK, Rooney CM, Foster AE: **Enhanced tumor trafficking of GD2 chimeric antigen receptor T cells by expression of the chemokine receptor CCR2b.** *J Immunother* 2010, **33**(8):780-788.

177. Boissonnas A, Fetler L, Zeelenberg IS, Hugues S, Amigorena S: **In vivo imaging of cytotoxic T cell infiltration and elimination of a solid tumor.** *The Journal of experimental medicine* 2007, **204**(2):345-356.

178. Kolen S, Dolstra H, van de Locht L, Braakman E, Schattenberg A, de Witte T, van de Wiel-van Kemenade E: **Biodistribution and retention time of retrovirally labeled T lymphocytes in mice is strongly influenced by the culture period before infusion.** *J Immunother* 2002, **25**(5):385-395.

179. Beck BH, Kim HG, Kim H, Samuel S, Liu Z, Shrestha R, Haines H, Zinn K, Lopez RD: **Adoptively transferred ex vivo expanded gammadelta-T cells mediate in vivo antitumor activity in preclinical mouse models of breast cancer.** *Breast cancer research and treatment* 2010, **122**(1):135-144.

180. Crispe IN, Dao T, Klugewitz K, Mehal WZ, Metz DP: **The liver as a site of T-cell apoptosis: graveyard, or killing field?** *Immunological reviews* 2000, **174**:47-62.

181. Liu ZX, Song HW, Yu LX, Yang LM: **Fabrication and near-infrared photothermal conversion characteristics of Au nanoshells.** *Appl Phys Lett* 2005, **86**(11):113109-113109-3.

182. Hidalgo E, Dominguez C: **Study of cytotoxicity mechanisms of silver nitrate in human dermal fibroblasts.** *Toxicology letters* 1998, **98**(3):169-179.

183. Lu W, Huang Q, Ku G, Wen X, Zhou M, Guzatov D, Brecht P, Su R, Oraevsky A, Wang LV *et al*: **Photoacoustic imaging of living mouse brain vasculature using hollow gold nanospheres.** *Biomaterials* 2010, **31**(9):2617-2626.

184. Moon EK, Carpenito C, Sun J, Wang LC, Kapoor V, Predina J, Powell DJ, Jr., Riley JL, June CH, Albelda SM: **Expression of a Functional CCR2 Receptor Enhances Tumor Localization and Tumor Eradication by Retargeted Human T cells Expressing a Mesothelin-Specific Chimeric Antibody Receptor.** *Clin Cancer Res*, **17**(14):4719-4730.

185. Calderwood SK, Khaleque MA, Sawyer DB, Ciocca DR: **Heat shock proteins in cancer: chaperones of tumorigenesis.** *Trends in biochemical sciences* 2006, **31**(3):164-172.

186. Bachleitner-Hofmann T, Strohschneider M, Krieger P, Sachet M, Dubsky P, Hayden H, Schoppmann SF, Pfragner R, Gnant M, Friedl J *et al*: **Heat shock treatment of tumor lysate-pulsed dendritic cells enhances their capacity to elicit antitumor T cell responses against medullary thyroid carcinoma.** *The Journal of clinical endocrinology and metabolism* 2006, **91**(11):4571-4577.

187. Binder RJ, Han DK, Srivastava PK: **CD91: a receptor for heat shock protein gp96.** *Nature immunology* 2000, **1**(2):151-155.

188. Srivastava PK: **Immunotherapy for human cancer using heat shock protein-peptide complexes.** *Current oncology reports* 2005, **7**(2):104-108.

189. Somersan S, Larsson M, Fonteneau JF, Basu S, Srivastava P, Bhardwaj N: **Primary tumor tissue lysates are enriched in heat shock proteins and induce the maturation of human dendritic cells.** *J Immunol* 2001, **167**(9):4844-4852.

190. Shi H, Cao T, Connolly JE, Monnet L, Bennett L, Chapel S, Bagnis C, Mannoni P, Davoust J, Palucka AK *et al*: **Hyperthermia enhances CTL cross-priming.** *J Immunol* 2006, **176**(4):2134-2141.

191. Belli F, Testori A, Rivoltini L, Maio M, Andreola G, Sertoli MR, Gallino G, Piris A, Cattelan A, Lazzari I *et al*: **Vaccination of metastatic melanoma patients with autologous tumor-derived heat shock protein gp96-peptide complexes: clinical and immunologic findings.** *J Clin Oncol* 2002, **20**(20):4169-4180.

192. Mazzaferro V, Coppa J, Carrabba MG, Rivoltini L, Schiavo M, Regalia E, Mariani L, Camerini T, Marchiano A, Andreola S *et al*: **Vaccination with autologous tumor-derived heat-shock protein gp96 after liver resection for metastatic colorectal cancer.** *Clin Cancer Res* 2003, **9**(9):3235-3245.

193. Jonasch E, Wood C, Tamboli P, Pagliaro LC, Tu SM, Kim J, Srivastava P, Perez C, Isakov L, Tannir N: **Vaccination of metastatic renal cell carcinoma patients with autologous tumour-derived vitespen vaccine: clinical findings**. *British journal of cancer* 2008, **98**(8):1336-1341.

194. Wood C, Srivastava P, Bukowski R, Lacombe L, Gorelov AI, Gorelov S, Mulders P, Zielinski H, Hoos A, Teofilovici F *et al*: **An adjuvant autologous therapeutic vaccine (HSPPC-96; vitespen) versus observation alone for patients at high risk of recurrence after nephrectomy for renal cell carcinoma: a multicentre, open-label, randomised phase III trial**. *Lancet* 2008, **372**(9633):145-154.

195. Pellegatta S, Poliani PL, Stucchi E, Corno D, Colombo CA, Orzan F, Ravanini M, Finocchiaro G: **Intra-tumoral dendritic cells increase efficacy of peripheral vaccination by modulation of glioma microenvironment**. *Neuro-oncology* 2010, **12**(4):377-388.

196. Mukhopadhaya A, Mendecki J, Dong X, Liu L, Kalnicki S, Garg M, Alfieri A, Guha C: **Localized hyperthermia combined with intratumoral dendritic cells induces systemic antitumor immunity**. *Cancer research* 2007, **67**(16):7798-7806.

197. Guo J, Zhu J, Sheng X, Wang X, Qu L, Han Y, Liu Y, Zhang H, Huo L, Zhang S *et al*: **Intratumoral injection of dendritic cells in combination with local hyperthermia induces systemic antitumor effect in patients with advanced melanoma**. *International journal of cancer* 2007, **120**(11):2418-2425.

198. Li X, Ferrel GL, Guerra MC, Hode T, Lunn JA, Adalsteinsson O, Nordquist RE, Liu H, Chen WR: **Preliminary safety and efficacy results of laser immunotherapy for the treatment of metastatic breast cancer patients**. *Photochem Photobiol Sci* 2011, **10**(5):817-821.

199. Ito A, Matsuoka F, Honda H, Kobayashi T: **Heat shock protein 70 gene therapy combined with hyperthermia using magnetic nanoparticles**. *Cancer gene therapy* 2003, **10**(12):918-925.

200. Ito A, Shinkai M, Honda H, Yoshikawa K, Saga S, Wakabayashi T, Yoshida J, Kobayashi T: **Heat shock protein 70 expression induces antitumor immunity during intracellular hyperthermia using magnetite nanoparticles**. *Cancer Immunol Immunother* 2003, **52**(2):80-88.

201. Sasaki JR, Zhang Q, Schwacha MG: **Burn induces a Th-17 inflammatory response at the injury site**. *Burns* 2011, **37**(4):646-651.

202. Finnerty CC, Przkora R, Herndon DN, Jeschke MG: **Cytokine expression profile over time in burned mice**. *Cytokine* 2009, **45**(1):20-25.

203. Kanegane C, Sgadari C, Kanegane H, Teruya-Feldstein J, Yao L, Gupta G, Farber JM, Liao F, Liu L, Tosato G: **Contribution of the CXC chemokines IP-10 and**

Mig to the antitumor effects of IL-12. *Journal of leukocyte biology* 1998, **64**(3):384-392.

204. Gorbachev AV, Kobayashi H, Kudo D, Tannenbaum CS, Finke JH, Shu S, Farber JM, Fairchild RL: **CXC chemokine ligand 9/monokine induced by IFN-gamma production by tumor cells is critical for T cell-mediated suppression of cutaneous tumors.** *J Immunol* 2007, **178**(4):2278-2286.

205. Sato E, Fujimoto J, Toyoki H, Sakaguchi H, Alam SM, Jahan I, Tamaya T: **Expression of IP-10 related to angiogenesis in uterine cervical cancers.** *British journal of cancer* 2007, **96**(11):1735-1739.

206. Angiolillo AL, Sgadari C, Taub DD, Liao F, Farber JM, Maheshwari S, Kleinman HK, Reaman GH, Tosato G: **Human interferon-inducible protein 10 is a potent inhibitor of angiogenesis in vivo.** *The Journal of experimental medicine* 1995, **182**(1):155-162.

207. Day ES, Thompson PA, Zhang L, Lewinski NA, Ahmed N, Drezek RA, Blaney SM, West JL: **Nanoshell-mediated photothermal therapy improves survival in a murine glioma model.** *Journal of neuro-oncology* 2011, **104**(1):55-63.

208. National Institutes of Health: **Estimates of Funding for Various Research, Condition, and Disease Categories (RCDC).** Bethesda, MD: National Institutes of Health; 2011. http://report.nih.gov/rcdc/categories/Default.aspx#bpopup

209. Robinson HL, Amara RR: **T cell vaccines for microbial infections.** *Nature medicine* 2005, **11**(4 Suppl):S25-32.

210. Behar SM, Woodworth JS, Wu Y: **Next generation: tuberculosis vaccines that elicit protective CD8+ T cells.** *Expert review of vaccines* 2007, **6**(3):441-456.

211. Todryk SM, Walther M: **Building better T-cell-inducing malaria vaccines.** *Immunology* 2005, **115**(2):163-169.